UNIVERSITÀ DEGLI STUDI DELL'INSUBRIA

SAN RAFFAELE SCIENTIFIC INSTITUTE

PhD THESIS

DISSECTING AND TARGETING THE PATHOGENETIC CASCADE OF AUTOSOMAL RECESSIVE SPASTIC ATAXIA OF CHARLEVOIX-SAGUENAY (ARSACS)

Candidate: **Andrea Del Bondio**

Supervisor: **Dott. Francesca Maltecca**

Tutor: **Prof.ssa Lia Forti**

DOTTORATO IN MEDICINA SPERIMENTALE E TRASLAZIONALE

XXXIII ciclo

Academic year 2020/2021

A te…

“If you can meet with Triumph and Disaster

And treat those two impostors just the same”

[Rudyard Kipling]

Table of contents

Table of contents **5**

Acknowledgements **8**

Abbreviations **10**

Abstract **14**

I. Introduction **17**

1. The cerebellum 17

1.1 Cerebellar gross anatomy and its neuroanatomic connections 17

1.2 The cerebellar cortex organization and microcircuits 21

1.3 The function of the cerebellum 27

2. The ataxias 29

2.1 Cerebellar ataxias 29

2.2 Autosomal Recessive Ataxias (ARCAs) 34

2.3 The deregulation of Ca^{2+} homeostasis as a common signature for most ataxias 36

3. Autosomal Recessive Spastic Ataxia of Charlevoix-Saguenay 41

3.1 Autosomal Recessive Spastic Ataxia of Charlevoix-Saguenay is caused by mutations in the *SACS* gene 41

3.2 ARSACS clinical manifestations 43

4. *SACS* gene expression and sacsin protein architecture and function 44

4.1 Characterization of *SACS* gene 44

4.2 Expression of *SACS* gene in mammalian tissues 44

4.3 Subcellular localization of sacsin protein 46

4.4 Sacsin protein domains and structure 48

4.5 Functional studies of ARSACS pathophysiology in cellular models 49

5. Mouse models of ARSACS pathophysiology 53

5.1 $Sacs^{-/-}$ mouse model 53

5.2 $Sacs^{R272C/R272C}$ KI mouse model 59

II. Aim of the work **61**

III. Material & Methods **63**

Declaration 63

Animals and drug administration 63

Behavioural tests 63

Histological analyses 64
Electron Microscopy analysis 64
SDS-PAGE and WB analysis 65
Co-immunoprecipitation 65
Proteomics analysis: Mass Spectrometry 65
Transcriptomics analysis: RNA sequencing 66
Primary PC cultures 67
Immunofluorescence assays 67
Morphometric analyses of primary PCs 68
Ca^{2+} imaging 68
Measurement of $\Delta\Psi_{mito}$ 69
In vivo ATP assay 69
Statistical analyses 69
IV. Results 70
1. NFH accumulation is an early event in ARSACS pathogenesis and causes defective mitochondrial distribution in *Sacs*$^{-/-}$ PCs 70
1.1 npNFH accumulation occurs perinatally in the Sacs$^{-/-}$ mouse 70
1.2 SH-SY5Y cells differentiated into neurons and primary *Sacs*$^{-/-}$ PCs recapitulate npNFH accumulation in their neurites 73
1.3 *Sacs*$^{-/-}$ primary PCs show defective distribution of mitochondria 76
1.4 Mitochondrial structure and functionality are not altered in *Sacs*$^{-/-}$ cerebella 78
1.5 Sacsin physically interacts with plectin, a cytoskeletal linker involved also in mitochondrial transport 80
2. Alteration of mitochondrial trafficking due to cytoskeleton remodeling leads to the deregulation of Ca^{2+} homeostasis in PC distal dendrites 83
2.1 Integrated OMICS approaches disclose deregulation of Ca^{2+} homeostasis in *Sacs*$^{-/-}$ cerebella 83
2.2 *Sacs*$^{-/-}$ primary PCs show defective cytosolic Ca^{2+} handling 88
3. A pre-clinical pharmacological treatment with Ceftriaxone in ARSACS 89
3.1 Long-term Ceftriaxone treatment has no major toxic side effects in wild-type mice 89
3.2 Post-symptomatic Ceftriaxone administration in *Sacs*$^{-/-}$ mice ameliorates motor ability, delays PC loss and improves Ca^{2+} homeostasis 91
3.3 *Sacs*$^{-/-}$ mice treated with Ceftriaxone at pre-symptomatic stage (1 month of age) show a delay in motor incoordination and PC degeneration 94

3.4 Ceftriaxone acts modulating transcription of genes related to synapse and neuroinflammation 97

4. *Sacs*$^{-/-}$ cerebellum manifests a strong neuroinflammatory response 98

4.1 Gene expression profile of *Sacs*$^{-/-}$ cerebellum underlines microglia and astrocyte activation 98

4.2 Astrocytosis and microgliosis appear at early stages of disease in *Sacs*$^{-/-}$ mice ... 101

V. Discussion 103

1. NFH accumulation is an early event in ARSACS pathogenesis and causes defective mitochondrial distribution in *Sacs*$^{-/-}$ PCs 103

2. Alteration of mitochondrial trafficking due to cytoskeleton remodeling leads to the deregulation of Ca^{2+} homeostasis in PC distal dendrites 108

3. A pre-clinical pharmacological treatment with Ceftriaxone in ARSACS 109

VI. Conclusions 115

References 117

Appendix 128

Publications 128

Acknowledgements

I would like to thank people having shared with me personal and professional time during these three years.

Firstly, I want to thank **Francesca** to give me the chance to attend your laboratory for this important step of my professional journey. I learnt a lot from you, dedication and passion for this fantastic and hard job, attitude and critical approach to scientific discussion, and determination to achieve a goal. I am grateful for your active support, educational mentoring and many professional opportunities you granted me. I thank you also for esteem and confidence in my abilities.

I thank **Lia** to accept to be my tutor of Università degli Studi dell'Insubria, and for many days spent at the electrophysiology setup teaching me the tricks to be a good electrophysiologist. I am not sure I was a good learner, however, I appreciated your patience and dedication.

A special thanks to my colleagues, who made better also the most difficult and busy days in the lab. Without you it would not have been the same. In particular **Fabiana**, with whom I shared the entire journey. I thank you for your valuable scientific advices and discussions, but most of all for the nice personal friendship. **Daniele** and **Valentina**, two talented (former) students, for your practical helps and brilliant scientific suggestions. **Martina**, a promising colleague, for the "bravery" to work on my beloved SCA28 project. And **Erica** and **Camilla**, the new-entries of the lab, for your skilful practical support. Finally, I want to thank all the people, who, even with a little help, contributed to my work.

I want to thank also **Laura**, **Alice** and **Matteo**, three master's thesis colleagues but most of all three fantastic friends. I will be forever grateful for the support and for sharing with me both scientific happiness and frustration. Science brought us together and personal passions let us to live unforgettable moments.

Un ringraziamento speciale ai **miei genitori** perché se ho raggiunto questo traguardo è grazie ai vostri insegnamenti, ai valori che mi avete trasmesso e al continuo e importante sostegno che mi avete sempre dimostrato in tutte le scelte che ho fatto. Grazie a mio fratello **Alieg** per

la stima e per le tue provocazioni scientifiche che hanno affinato le mie capacità di sostenere una tesi con valide argomentazioni. Grazie ai **miei nonni** per l'enorme stima che avete sempre nutrito nei miei confronti. Un ringraziamento doveroso a **zio Paolo** perché grazie alle tue doti manuali ed artistiche hai creato un apparato da Beam Walking professionale senza il quale non avrei potuto ottenere i promettenti risultati sui topolini. Infine voglio ringraziare tutti i **miei amici** per il supporto e la considerazione che mi avete dimostrato.

I love you. My most sincere thanks,
GRAZIE,
Andrea

Abbreviations

AD	Alzheimer's Disease
ALS	Amyotrophic Lateral Sclerosis
AMPA	α-amino-3-hydroxy-5-methyl-4-isoxazolepropionic acid receptor
ARCA	Autosomal Recessive Cerebellar Ataxia
ARSACS	Autosomal Recessive Spastic Ataxia of Charlevoix-Saguenay
ATP	Adenosine Triphosphate
ATXN	Ataxin
AZ	Anterior Zone
BDNF	Brain-Derived Neurotrophic Factor
BW	Beam Walking test
Ca^{2+}	Calcium ion
CaM	Calmodulin
CNS	Central Nervous System
CZ	Central Zone
DAM	Disease-Associated Microglia
DCN	Deep Cerebellar Nuclei
DEG	Differentially Expressed Genes
DIV	Day In Vitro
DNA	Deoxyribonucleic acid
DRG	Dorsal Root Ganglion
DSB	Double-Strand break (DNA)
EAAT2	Excitatory Amino Acid Transporter
EM	Electron Microscopy
ER	Endoplasmic Reticulum
FA	Friedreich Ataxia
FCCP	Carbonyl cyanide-4-(trifluoromethoxy)phenylhydrazone
FRAP	Fluorescence Recovery After Photobleaching
FXN	Frataxin

GABA	Gamma-Aminobutyric acid
GFAP	Glial Fibrillary Acidic Protein
GFP	Green Fluorescence Protein
GLT1	Glutamate Transporter 1
GO	Geno Ontology
GSH	Glutathione
GTP	Guanosine Triphosphate
HBSS	Hank's Balanced Salt Solution
Hsp	Heat Shock Protein
IF	Intermediate Filament
IMM	Inner Mitochondrial membrane
i.p.	Intraperitoneal (injection)
IP3	Inositol trisphosphate
IP3R	Inositol trisphosphate receptor
i.v.	Intravenous (injection)
KEGG	Kegg Pathway database
KI	Knock In
KCl	Potassium Chloride
LCN2	Lipocalin 2
LFQ	Label-Free Quantitation
LTD	Long-Term Depression
LTP	Long-Term Potentiation
***m*-AAA**	ATPases associated with various cellular activities
MAM	Mitochondria-Associated Membranes
MCU	Mitochondrial Calcium Unipoter
mEPSC	Excitatory Post-Synaptic Current
mGluR	Metabotropic Glutamate Receptor
MRI	Magnetic Resonance Imaging
MS	Mass Spectrometry
MTCO	Microtubule-Organizing Center
NF-kB	Nuclear Factor kB
NF	Neurofilament
NFH	Neurofilament-High molecular weight subunit

NFL	Neurofilament-Light molecular weight subunit
NFM	Neurofilament-Medium molecular weight subunit
NGS	Next Generation Sequencing
NORT	Novel Object Recognition Test
npNFH	Non-phosphorylated Neurofilament-High molecular weight subunit
NRF2	Nuclear Factor Erythroid 2-Related Factor
NZ	Nodular Zone
OCT	Optical Coherence Tomography
OMM	Outer Mitochondrial membrane
OXPHOS	Oxidative Phosphorylation
PBS	Phosphate-Buffered Saline
PC	Purkinje Cell
PD	Parkinson's Disease
PIC	Protease Inhibitor Cocktail
PZ	Posterior Zone
qRT-PCR	Quantitative Real-Time PCR
REAC	Reactome database
RNA	Ribonucleic acid
RNAseq	RNA sequencing
RNFL	Retinal Nerve Fiber Layer
ROI	Region Of Interest
ROS	Reactive Oxigen Species
RPKM	Reads Per Kilobase of exon per Million mapped reads
SCA	Spinocerebellar Ataxia
SDS-PAGE	Sodium Dodecyl Sulphate - PolyAcrylamide Gel Electrophoresis
SERCA	Sarcoplasmic-Endoreticulum Ca2+ ATPase
SIRPT	Sacsin Internal RePeaTs
SMA	Spinal Muscular Atrophy
TBP	TATA Binding Protein
TMRM	Tetramethylrhodamine methyl ester
TEM	Transmission Electron Microscope
TOM	Translocase of the Outer Mitochondrial membrane
UbL	Ubiquitin-like domain

VDAC	Voltage-Dependent Anion Channel
VGCC	Voltage-Gated Calcium Channel
WB	Western Blot
WP	WikiPathway database
$\Delta\Psi_{mito}$	Mitochondrial Membrane Potential

Abstract

Autosomal Recessive Spastic Ataxia of Charlevoix-Saguenay (ARSACS) is a childhood-onset cerebellar ataxia associated with lower limb spasticity and peripheral neuropathy. ARSACS is caused by loss-of-function mutations in *SACS* gene, which encodes for sacsin, a huge cytosolic protein mainly expressed in neurons with the highest levels in Purkinje cells (PCs). Loss of PCs is indeed the most prominent feature of ARSACS patients and mouse models (both *Sacs*$^{-/-}$ and *Sacs*$^{R272C/R272C}$ mice). In the last years several studies in cell models have been performed to understand sacsin function, that however remains largely unknown so far.

We and others have identified the remodeling of the intermediate filament (IF) cytoskeleton as one of the earliest consequences of the absence of sacsin. Both vimentin (in ARSACS patient fibroblasts, *SACS*$^{-/-}$ HEK293T and SH-SY5Y cells) and neurofilaments (NFs, in different types of neurons) accumulate in the absence of sacsin, forming aberrant dense bundles. However, in the mouse models only PCs were found degenerating and, thus, causing motor abnormalities typical of ARSACS clinical spectrum. To date, no more information is known about ARSACS pathogenetic cascade and, thus, no treatments are available for ARSACS.

My PhD project aimed at dissecting ARSACS pathogenesis, by studying the effects of NF accumulation specifically in PCs and how this phenotype causes degeneration. Based on the knowledge derived from these studies, we designed and carried out a pharmacological treatment in *Sacs*$^{-/-}$ mice.

We demonstrated that the accumulation of non-phosphorylated NFH (npNFH) bundles in PCs is an early event in *Sacs*$^{-/-}$ mice, appearing just after birth and characterizing mainly the anterior lobules of cerebellum. To mechanistically explore the consequences of npNFH accumulation, we took advantage of *Sacs*$^{-/-}$ cerebellar cultures enriched in PCs, which recapitulate the main features observed *in vivo*. We discovered that mitochondrial (and also ER) trafficking to distal dendrites is altered in *Sacs*$^{-/-}$ primary PCs. The failure in transportation was not a consequence of altered mitochondrial metabolism or morphology, as we found that mitochondria manifest conserved ultrastructure, as well as unaltered ATP production and mitochondrial membrane potential, both *in vivo* and *ex vivo* in *Sacs*$^{-/-}$ PCs.

To identify the missing link between NF accumulation and defective mitochondrial (and ER) distribution, we immunoprecipitated endogenous sacsin in a simpler tool, i.e. SH-SY5Y cells differentiated into neurons. In these cells we previously demonstrated aberrant NF remodelling upon depletion of sacsin by genome editing. This approach allowed us to detect some physical sacsin interactors, all related to cytoskeleton. In addition to NFs, we pulled down plectin, a large cytolinker protein interacting both with NFs and mitochondria, and myosin Va, crucial for ER transport in dendrites. This suggests that abnormal NF accumulation in the absence of sacsin may oppose to mitochondrial and ER trafficking, thus favouring their docking in proximal dendrites. To validate plectin involvement in ARSACS pathogenesis, we revealed decreased plectin levels in *SACS*$^{-/-}$ SH-SY5Y cells and in a panel of ARSACS patient fibroblasts (analysis of plectin levels in cerebellum are now ongoing). These results support the idea that sacsin may act as a scaffold for cytoskeletal proteins, mediating a connection between cytoskeleton and organelles.

We thus hypothesized that defective mitochondrial and ER trafficking to PC dendrites could lead to pathologic Ca^{2+} deregulation in *Sacs*$^{-/-}$ PCs, leading to degeneration. In fact, both these organelles are crucial regulators of Ca^{2+} homeostasis. In particular, mitochondria not only provide ATP to active Ca^{2+} clearance systems at the plasma membrane and ER, but also exert themselves a fine shaping of Ca^{2+} signals in spines by accumulating Ca^{2+} into the matrix. In support of our hypothesis, two *in vivo* OMICS approaches revealed deregulation of many key players regulating Ca^{2+} homeostasis, which was further confirmed by increased phosphorylation of CamKIIβ and by Ca^{2+} imaging experiments in primary PCs.

These results provided us the rationale to test a pharmacological treatment with Ceftriaxone in the *Sacs*$^{-/-}$ mouse model. Ceftriaxone is a β-lactam antibiotic able to reduce glutamate concentration in inter-synaptic space and thus to attenuate Ca^{2+} influxes in post-synaptic PCs. Interestingly, we proved that Ceftriaxone administration, at both pre- and post-symptomatic stages, improves motor ability and delays PC degeneration in *Sacs*$^{-/-}$ mice. This treatment may represent a future therapeutic option for diagnosed pre-symptomatic ARSACS patients, but also for patients with overt symptoms, which are most cases.

Finally, our data revealed an early involvement of neuroinflammation in ARSACS disease progression, showing a remarkable astrocyte and microglia activation in *Sacs*$^{-/-}$ cerebellum as early as 1 month of age. Preliminary data suggest that Ceftriaxone treatment may target also this mechanism (probably via NF-kB signaling), offering neuroprotection in ARSACS by multiple mechanisms.

Overall, our data improve the knowledge of ARSACS pathogenesis and offer encouraging perspectives for ARSACS disease treatment.

I. Introduction

1. The cerebellum

For several years, the human brain was believed to contain about 100 billion neurons and they were not the prominent resident cell type in the brain, which was populated mainly by glial cells with a glia/neuron ratio of 10:1, concluding one trillion of glial cells were resident in the brain. Only in the last decades of the 1900s more precise estimates of total number of neurons (75-85 billion) and glial cells (40-130 billion) in the brain were published, but until the beginning of 21th century this notion was not accepted[1 2].

The initial misunderstanding estimation about the number of neurons was based on data obtained by analyses performed on cerebral cortex that comprises by volume about the majority (80–85%) of the adult human brain, and thus often considered to be equivalent to whole brain. In fact, several reports highlighted brain cerebral cortex represents 80-85% of total brain volume (1,200 g), while the cerebellum only 10% of volume (150 g) and the remaining components, brainstem, diencephalon and striatum reach 2–8% of the entire human brain volume (75–110 g)[2 3 4 5]. However recent studies taking into account the entire brain, comprising also cerebellum and other smaller regions, revealed drastic changes in the estimates of the total number of neurons. The cerebellum, indeed, is populated by a huge number of neurons, as well as a very low number of non-neuronal cells (glia)[6]. These counts showed among a total of 55-70 billion cells in the human cerebellum: 65 billion neurons, the majority of them represented by granule cells, with most of the remainder, about 3 billion, being glial cells, fixing glia/neuron ratio at 0,05[7 8].

1.1 Cerebellar gross anatomy and its neuroanatomic connections

The cerebellum, literally “the little brain”, represent only 10% of the total volume and weight of the brain but contains almost 80% of its neurons[4 7 8].

The anatomic description of cerebellum dates back to the 19th century when Purkinje, Golgi, and Cajal carried out their studies[9 10]. The cerebellum occupies the most posterior part of cranial fossa. It resides on the rostral roof of the fourth ventricle and it is placed in parallel to

the main motor and sensory systems, with which it is wired through a complex set of loops and connections. Moreover, it is in direct contact with the brainstem (occipital lobes of the brain), from which is separated by the extension of the dura matter called tentorium cerebelli, through which pass three symmetrical pairs of peduncles: the inferior cerebellar peduncle (also called the restiform body), the medium cerebellar peduncle (or brachium pontis), and the superior cerebellar peduncle (or brachium conjunctivum). All efferents and afferents of cerebellum pass through these peduncles to reach their targets (Fig. 1-2_Intro)[11 12 13].

Major cerebellar afferents and efferents

Peduncle	Tracts	Distribution	Laterality	Location of Cell Bodies
Cerebellar Afferents				
Inferior	Olivocerebellar tract	Cerebellar cortex and deep cerebellar nuclei	Contralateral	Inferior olivary nucleus
	Vestibulocerebellar tract	Flocculonodular lobe, caudal uvula, and fastigial nucleus	Ipsilateral	Vestibular nuclei and vestibular ganglion
	Posterior spinocerebellar tract	Lower extremity regions of the cerebellar cortex and nuclei	Ipsilateral	Clarke column
	Cuneocerebellar tract	Upper extremity and trunk regions of the cerebellar cortex and nuclei	Ipsilateral	Cuneate and external cuneate nuclei
	Rostral spinocerebellar tract	Upper extremity and trunk regions of the cerebellar cortex and nuclei	Ipsilateral	Intermediate zone and horn of the cervical enlargement
	Reticulocerebellar tract[1]	Cerebellar hemispheres and vermis, along with fastigial and interposed nuclei	Bilateral	Lateral reticular nucleus of the medulla oblongata
	Trigeminocerebellar tract	Related somatotopic regions of the cerebellar cortex and nuclei	Ipsilateral	Trigeminal nucleus
Middle	Pontocerebellar tract	Neocerebellar cortex and dentate nucleus	Contralateral	Pontine nuclei
Superior	Anterior spinocerebellar tract[a]	Lower extremity regions of the cerebellar cortex and nuclei	Ipsilateral	Clarke column
Cerebellar Efferents				
Inferior	Cerebellovestibular tract	Vestibular nucleus	Ipsilateral	Fastigial nucleus, vermis, and vestibulocerebellar cortex
Superior	Cerebellorubral fibers	Red nucleus	Contralateral	Dentate and interposed nuclei
	Cerebellothalamic fibers	Ventrolateral thalamic nucleus	Contralateral	Dentate and interposed nuclei
	Uncinate fasciculus	Vestibular, pontomedullary reticular, and thalamic nuclei	Contralateral	Fastigial nucleus
	Nucleo-olivary tract[b]	Inferior olive	Contralateral	Deep cerebellar nuclei

Figure 1_Intro. Cerebellar afferents and efferents[13].

The cerebellum consists of an outer layer of highly convoluted gray matter (cerebellar cortex), with many parallel folds called folia, surrounding a highly branched body of white matter known as *arbor vitae* (Latin for "tree of life"), where three pairs of deep cerebellar nuclei (DCN) embedded in the central cerebellar white matter (corpus medullare) reside. From medial to lateral, the deep nuclei are the fastigial, interposed (consisting of globose and emboliform nuclei), and the dentate nuclei (Fig. 2_Intro)[11 12 13].

The cerebellar structure comprises a series of highly regular and repetitive units, that share the same basic microcircuit. Different regions of the cerebellum receive projections from different parts of the brain and spinal cord, and project to different motor systems. In fact, anatomic connections/projections between cerebellum and cerebral cortex and spinal cord are highly topographically arranged, resulting in functional subregions of the cerebellum which can be broadly divided into sensorimotor, association/cognitive, and limbic regions. Nonetheless, the similarity of architecture and physiology in all regions of the cerebellum implies that different regions of the cerebellum perform similar computational operations on different inputs[11 13].

Anatomically, the cerebellum is divided into three lobes by two deep transverse fissures. The primary fissure on the dorsal surface separates the anterior and posterior lobes, which together form the body of the cerebellum, and the posterolateral fissure on the ventral surface separates the body of the cerebellum from the smaller flocculonodular lobe. Each lobe extends across the cerebellum from the midline to the most lateral tip. In the orthogonal, anterior-posterior direction two longitudinal furrows divide three regions: the midline vermis (Latin, "worm") and the cerebellar hemispheres, each of which is split into intermediate and lateral regions (Fig. 2_Intro)[11 13 14].

The cerebellum is also divisible into three areas that have characteristic roles in different kinds of movement: the vestibulocerebellum, spinocerebellum, and cerebrocerebellum (Fig. 2-3_Intro). The vestibulocerebellum consists of the flocculonodular lobe and is the most primitive part of the cerebellum, appearing first in fishes. It receives vestibular and visual inputs, projects directly to the vestibular nuclei in the brain stem bypassing the DCN, and participates in balance, other vestibular reflexes (median part), and eye movements and coordination (Fig. 3_Intro)[11 13 14].

The spinocerebellum comprises the vermis and intermediate parts of the hemispheres and appears later in phylogeny. It receives somatosensory and proprioceptive inputs from the spinal cord. The vermis receives visual, auditory, and vestibular input as well as somatic sensory input from the head and proximal parts of the body. It projects by way of the fastigial

nucleus to cortical and brain stem regions that give rise to the medial descending systems controlling proximal muscles of the body and limbs. The vermis governs posture and locomotion as well as eye movements. The adjacent intermediate parts of the hemispheres also receive somatosensory input from the limbs (distal portions). Neurons, here, project to the interposed nucleus, which provides inputs to lateral corticospinal and rubrospinal systems and controls the more distal muscles of the limbs and digits (Fig. 3_Intro)[11 13 14].

Finally, the cerebrocerebellum comprises the lateral parts of the hemispheres. These areas are phylogenetically most recent and are much larger in humans and apes than in other mammals. Almost all of the inputs to and outputs from this region involve connections with the cerebral cortex. The output is transmitted through the dentate nucleus, which projects to motor, premotor, and prefrontal cortices. The lateral hemispheres have many functions but seem to participate most extensively in planning and executing movement. They may also have a role in certain cognitive functions unconnected with motor planning, such as working memory (Fig. 3_Intro)[11 12 13].

The cerebellum is further subdivided into ten transverse lobules marked by roman numerals (lobules I–X). Each lobule encompasses a central portion in the vermis along with the adjacent two lateral segments in the hemispheres (Fig. 2_Intro)[13 14].

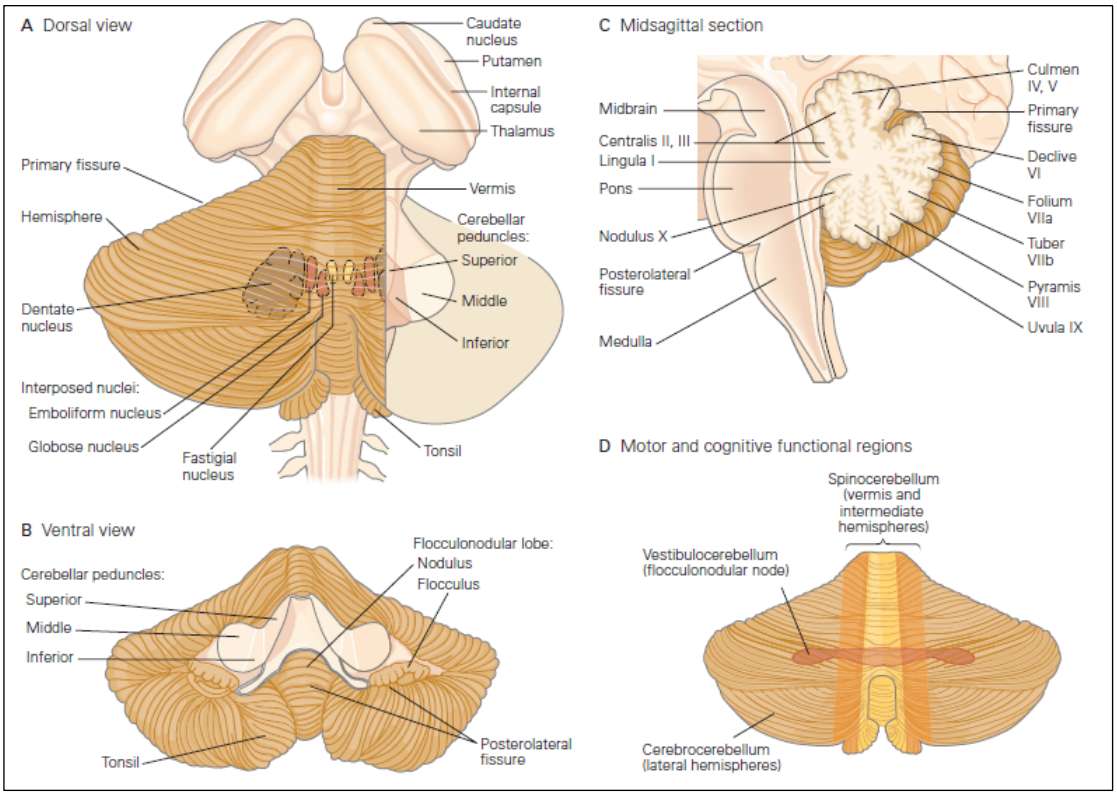

Figure 2_Intro. Gross features of the cerebellum: (A) dorsal and (B) ventral view, (C) midsagittal section and (D) functional regions[11].

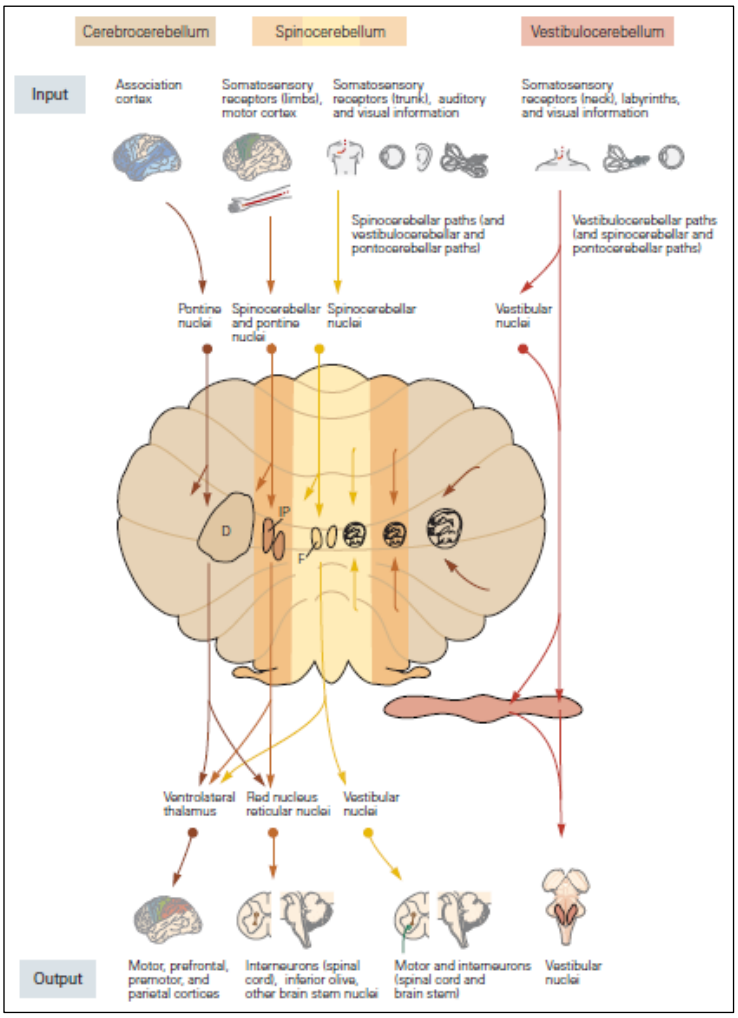

Figure 3_Intro. Three functional regions of cerebellum with different inputs and output targets[11].

1.2 The cerebellar cortex organization and microcircuits

The cerebellar cortex is organized into three layers having distinct kinds of neurons and perform different operations. The deepest or granular layer is the input layer. It contains a huge number of granule cells, estimated at 55-60 billion, which appear in histological sections as small, densely packed and darkly stained nuclei (Fig. 4_Intro). This layer also contains a few larger Golgi interneurons and, in some cerebellar regions, a smattering of other GABAergic neurons such as cells of Lugaro, unipolar brush cells, and chandelier cells (Fig. 5_Intro)[11 13 15]. This thick layer functions as the input layer for the cerebellar cortex because mossy fibers, one of the two principal afferent inputs to the cerebellum, terminate in this layer. The bulbous terminals of the mossy fibers excite granule cells and Golgi neurons in synaptic complexes called cerebellar glomeruli (Fig. 5_Intro)[11 13 16].

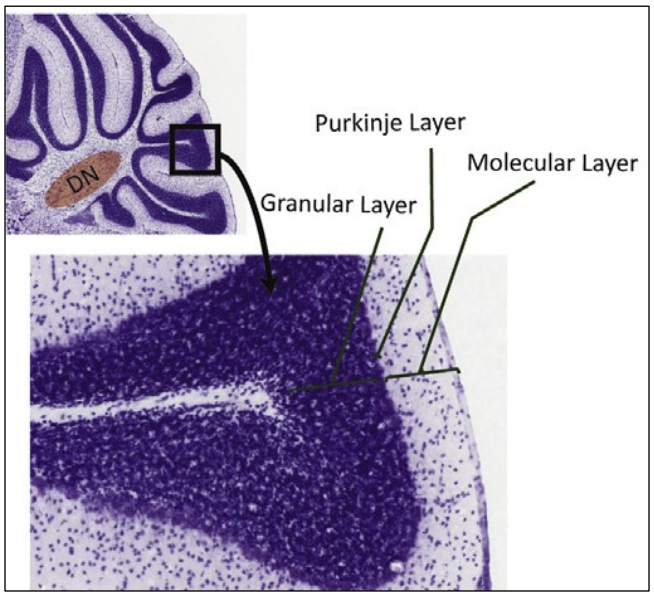

Figure 4_Intro. Sagittal section of mouse cerebellum showing layers of cerebellar cortex[13].

The middle, or Purkinje cell (PC) layer, is the output layer of the cerebellar cortex. This layer consists of a single sheet of PC bodies, which are 50 to 80 µm in diameter, interspersed with Bergmann glia supporting PC functions. The enormous branched dendritic tree of PC extends upward into the molecular layer where it receives inputs from the second major type of afferent fibers in the cerebellum, the so called climbing fibers, as well as from inhibitory and excitatory interneurons (Fig. 5_Intro). Rather, PC axons conduct the entire output of the cerebellar cortex, projecting to DCN in the underlying white matter or to the vestibular nuclei in the brain stem, where the GABA (γ-aminobutyric acid) neurotransmitter released by PC terminals has an inhibitory action[11 13 16].

The outermost, or molecular, layer is an important processing layer of the cerebellar cortex. It contains the cell bodies and dendrites of two types of inhibitory interneurons, the stellate and basket cells, as well as the extensive branched dendrites of PCs. It also contains axons of the granule cells, called parallel fibers, which run parallel to the long axis of the folia (Fig. 5_Intro). The spatially polarized dendrites of PCs cover extensive terrain in the anterior-posterior direction, but a very narrow territory in the medial-lateral direction. In this organization, since parallel fibers run in the medial-lateral direction and, thus, they are oriented perpendicular to PC dendritic trees, PCs are intercepted by hundreds of thousands of synaptic contacts with parallel fiber axons, that ascend into the molecular layer assuming a characteristic “T” conformation (Fig. 5_Intro)[11 13 16].

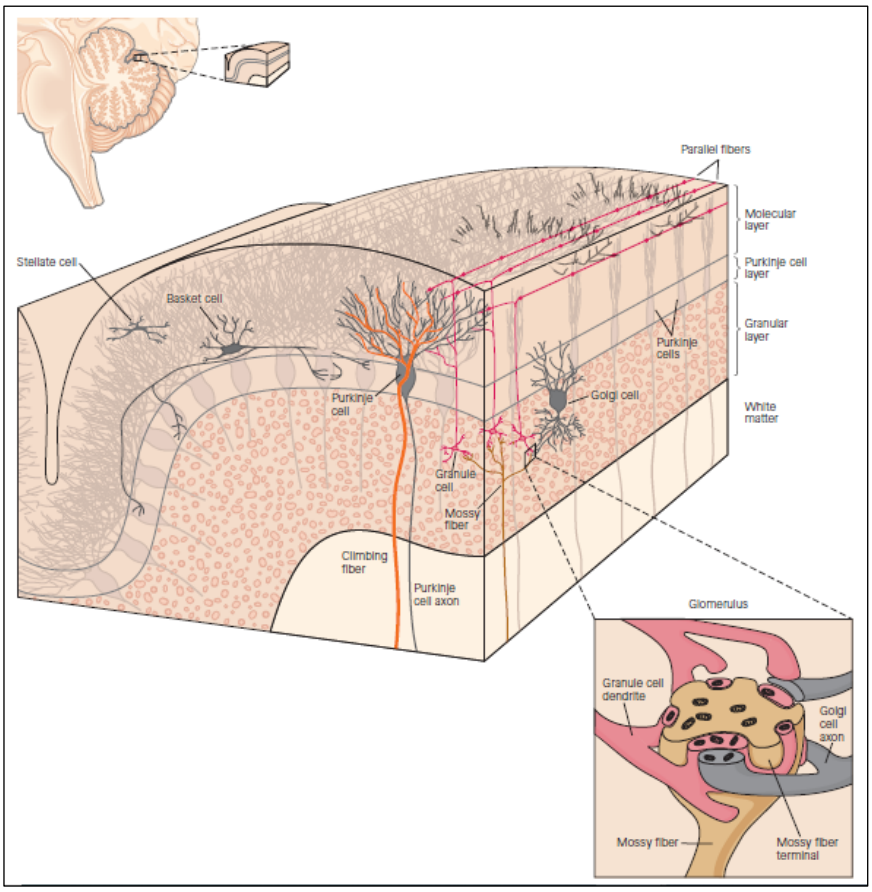

Figure 5_Intro. Cerebellar cortex show different cell type distributed in different layers[11].

As already mentioned, in the cerebellum there are two main types of afferent fibers, mossy fibers and climbing fibers, both forming excitatory synapses with cerebellar neurons but terminate in different layers of the cerebellar cortex producing different patterns of firing in PCs and, thus, probably mediating different functions.

Mossy fibers originate from cell bodies in the spinal cord and brain stem, and carry sensory information from the periphery as well as information from the cerebral cortex. They form excitatory synapses on the dendrites of the granule cells in the granular layer (Fig. 6_Intro). Each granule cell receives inputs from just a few mossy fibers, but the architecture of the granule cell axons distributes information widely from each mossy fiber to a large number of PCs. The mossy fiber input is highly convergent, in fact, each PC is contacted by axons from somewhere between 200 000 and 1 million granule cells[11 12 13].

Climbing fibers, on the other hand, originate in the inferior olivary nucleus and convey sensory information to the cerebellum from both the periphery and the cerebral cortex. The climbing fiber is so named because each cell enwraps the cell body and proximal dendrites of a PC making numerous synaptic contacts (Fig. 6_Intro). Each climbing fiber contacts up to 10 closely

placed PC, but each PC receives synaptic input from only a single climbing fiber. The terminals of the climbing fibers are arranged topographically in the cerebellar cortex: the axons from clusters of related olivary neurons terminate in thin parasagittal region that extend across several folia. In turn, PCs within one of these region project to a common group of deep nuclear neurons, so defining the so called longitudinal zones (Fig. 7_Intro)[13 16 17 18].

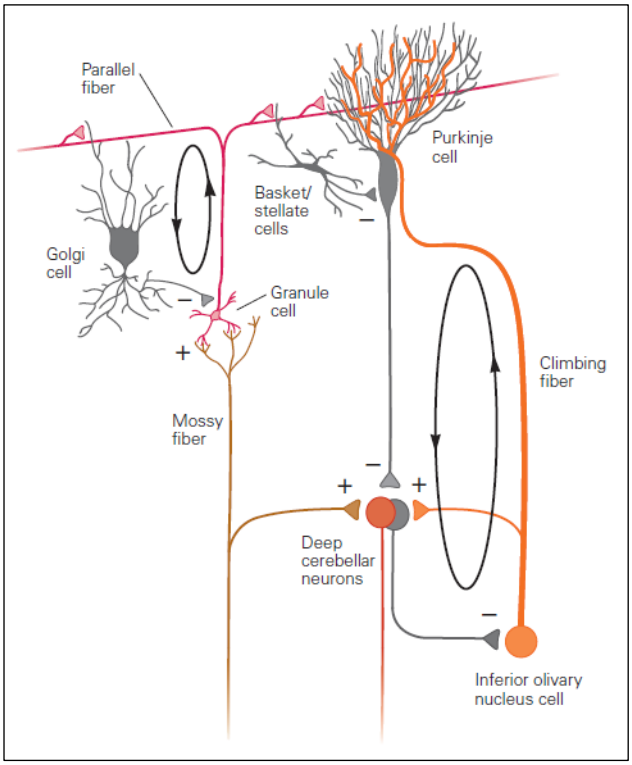

Figure 6_Intro. Synaptic organization of the cerebellar microcircuit[11].

Topographical unit	Description	Experimental basis
Longitudinal zone	A rostrocaudally extended array of Purkinje cells within the cerebellar cortex with specific olivocerebellar and cortico-nuclear connections and climbing fibre input relayed through a common set of olivocerebellar pathways	Anatomy and physiology
Module	A longitudinal zone of Purkinje cells together with its olivo-cortico-nuclear connections and associated recurrent pathways	Anatomy
Microzone	Subdivision of a longitudinal zone in which Purkinje cells have similar climbing fibre receptive fields	Physiology
Transverse zone	Region of cerebellar cortex identified by mediolateral gene expression boundaries	Gene expression patterns
Purkinje cell stripe/ band	Longitudinally oriented subregion of a transverse zone in which Purkinje cells have the same phenotype	Gene expression patterns
Patch	Region of cerebellar cortex with similar mossy fibre receptive fields in the granular layer	Physiology

Figure 7_Intro. Summary of different cerebellar topographical organisations[18].

The highly specific connectivity of the climbing fiber system contrasts markedly with the massive divergence of the mossy-parallel fibers circuit, and suggests that the climbing fiber system is specialized for precise control of the electrical activity of PCs. The climbing fiber system creates closed loops of circuity known as microzones, and each microzone has a strict somatotopic receptive field (Fig. 7-8_Intro). Moreover, molecular layer interneurons and Golgi

cells inputs and outputs are also limited to microzones they belong to. The combination of microzones along with their associated clusters within inferior olivary and DCN could be regarded as functional units (modules) of the cerebellum. Thus, cerebellum is regarded as a computational machine consisting of a large number of almost independent modules, which are similar in terms of internal structure, and as such, perform the same computation on any kind of input (motor or non-motor) that they receive[11 12 13 19].

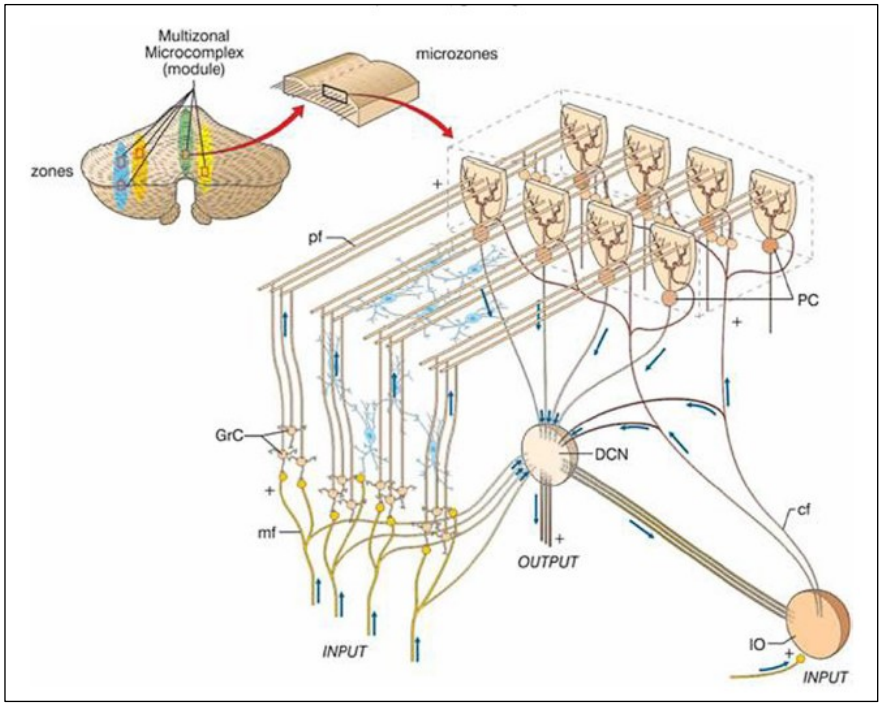

Figure 8_Intro. Schematic view of the architecture of the core cerebellar microcircuit within microzones[12].

Mossy and climbing fibers have different effects on the electrical activity of PCs. Climbing fibers have an unusually powerful influence. Each action potential in a climbing fiber generates a protracted, voltage-gated calcium (Ca^{2+}) conductance in the soma and dendrites of the post-synaptic PC. This results in prolonged depolarization that produces a complex spike: an initial large-amplitude action potential followed by a high-frequency burst of smaller-amplitude action potentials. Whether these smaller spikes are transmitted down the PC axon is not clear. In awake animals the climbing fibers spontaneously generate complex spikes at low rates, rarely more than one to three per second. When stimulated they fire single action potentials in temporal relation with specific sensory events. The climbing fiber system therefore seems specialized for event detection: the firing rate carries little or no information. Although climbing fibers fire only infrequently, synchronous firing in multiple climbing fibers enables them to signal important events. Synchrony seems to arise partly because neurons in the inferior olivary nucleus often are connected to one another electrotonically[11 12 13].

In contrast, parallel fibers produce only brief, small excitatory potentials in PCs. These potentials spread to the initial segment of the axon where they generate simple spikes that propagate down the axon. However, inputs from many parallel fibers are needed to have a substantial effect on the frequency of simple spikes, as each post-synaptic potential is tiny. In awake animals PCs emit a steady stream of simple spikes, with spontaneous firing rates as high as 100 per second even when an animal is sitting quietly. PCs fire at rates as high as several hundred spikes per second during active eye, arm, and face movements, presumably because of somatosensory, vestibular, and other sensory signals that converge on granule cells through the mossy fibers. Thus, the mossy fiber system encodes the magnitude and duration of peripheral stimuli or centrally generated behaviours by controlling the firing rate of simple spikes in PCs[11 12].

Finally, two different topographical units have been described based on the gene expression pattern. The first one presents the subdivision of cerebellar cortex into five (or six) transverse zones, both in the vermis and in the hemispheres. These transverse zones are: the anterior zone (AZ: ~lobules I–V in mouse), the central zone (CZ), further divided into the anterior CZa (~lobule VI) and the posterior CZp (~lobule VII), the posterior zone (PZ: ~lobules VIII to dorsal IX) and the nodular zone (NZ: ~ventral lobule IX and lobule X) (Fig. 7 and 9_Intro). Transverse zones overlap extensively and each of them comprise fewer than 10 000 PCs (in mouse)[18].

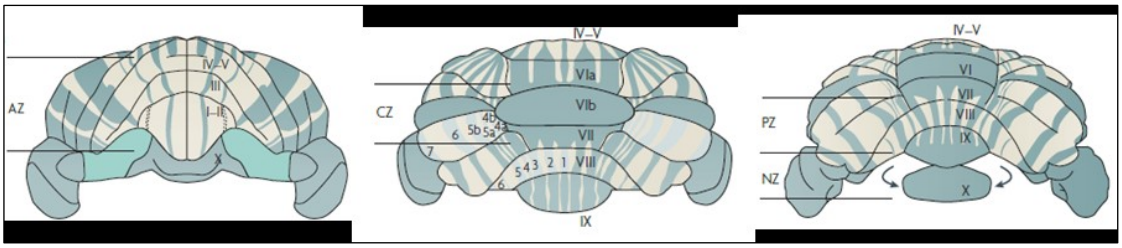

Figure 9_Intro. Cerebellar transverse zones and stripes[18].

Every transverse zone is segmented into a series of stripes oriented along the rostrocaudal axis and which are defined by the restricted expression of molecular markers (Fig. 7 and 9_Intro). The most comprehensively studied molecular marker is zebrin II (also known as aldolase C). Zebrin II is expressed by a subset of PCs (zebrin II+) that alternate with PCs that do not express this marker (zebrin II–), thus forming zebrin II+/– stripes. The zebrin II+/– stripes are symmetrically distributed across the midline, highly reproducible between individuals and conserved across species. Numerous other markers have been identified: sphingosine kinase 1a (SPHK1a), the CDK5 P39 activator, phospholipase Cβ3, excitatory amino-acid transporter 4 (EAAT4), metabotropic glutamate receptor 1a (mGluR1a), integrin β1 and the $GABA_{B2}$

receptor[18]. The stripe pattern of Purkinje cells differs between transverse zones. In fact, the AZ and PZ have alternating zebrin II+/– stripes, whereas the CZ and NZ are uniformly zebrin II+. Stripes are discontinuous across transverse zone boundaries, so it is wrong to assume, for example, that the first zebrin II+ stripe from the midline in the AZ is the same as the P1+ stripe in the NZ. In mice, a typical stripe therefore comprises only a few hundred PCs[15 16 18 20].

1.3 The function of the cerebellum

Most of the knowledge on the cerebellar function comes from the analysis of symptoms of cerebellar damage or lesion in humans and in experimental animal studies using pharmacological interventions, lesions and genetic manipulations. These investigations gave a clear impression that cerebellum participates in the control of movement as described originally by Joseph Babinski in 1899 and by Gordon Holmes in the 1920s[21].

In this scenario, cerebellar disorders are manifested in four symptoms:

1. The first and typical symptom is ataxia, the abnormal execution of multi-jointed voluntary movements, characterized by lack of coordination. Patients have problems initiating response movement with the affected limb and controlling the size of a movement (dysmetria), and the rate and regularity of repeated movements[11 21];
2. The second one is hypotonia, a diminished resistance to passive limb displacements. Hypotonia is also thought to be related to so-called “pendular reflexes”[11];
3. The third symptom is astasia-abasia, an inability to stand or walk. Astasia is loss of the ability to maintain a steady limb or body posture across multiple joints. While abasia is loss of the ability to maintain upright stance against gravity[11];
4. The fourth symptom of cerebellar disease is a form of tremor at the end of a movement, when patient attempts to stop the movement by using antagonist muscles[11].

A clear feature of cerebellar disorders is a loss of the automatic, unconscious nature of most movements, especially for motor acts made up of multiple sequential movements. Normally, movement is controlled seamlessly by cerebellar inputs and outputs. In presence of a malfunctioning cerebellum it seems that cerebral cortex needs to play a more active role in programming the details of motor actions[11].

The cerebellum is not only involved in control of movements but it has a role in planning movement. Clinical observations initially suggested that, like the rest of the cerebellum, the

lateral hemispheres (the cerebrocerebellum) are primarily concerned with motor function. However, recent clinical and experimental studies indicate that lateral hemispheres in humans have, also, perceptual and cognitive functions. In contrast to other regions of cerebellum, which receive sensory information more directly from the spinal cord, the lateral hemispheres receive input exclusively from the cerebral cortex. This cortical input is transmitted through pontine nuclei and middle cerebellar peduncle to contralateral dentate nucleus and lateral hemisphere. PCs in the lateral hemisphere project to the dentate nucleus. Most dentate axons exit the cerebellum through the superior cerebellar peduncle and terminate in two main sites: one terminus is an area of the contralateral ventrolateral thalamus that also receives input from the interposed nucleus. These thalamic cells project to premotor and primary motor cortex. The second principal terminus of dentate neurons is the contralateral red nucleus and these neurons project to the inferior olivary nucleus which, in turn, projects back to the contralateral cerebellum as climbing fibers, thus forming a recurrent loop.

When patients with cerebellar lesions attempt to make regular tapping movements with their hands or fingers, the rhythm is irregular, and the motions are variable in duration and force. Based on a theoretical model of how tapping movements are generated, it was inferred that medial cerebellar lesions interfere only with accurate execution of the response, whereas lateral cerebellar lesions interfere with the timing of serial events. Moreover, functional Magnetic Resonance Imaging (MRI) provides evidence that the lateral cerebellum has a role in other cognitive activities. Interestingly, the active area of the dentate nucleus is the area that receives input from the part of the cerebral cortex (area 46) involved in working memory. The dentate nucleus appears to be particularly important in processing sensory information for tasks that require complex spatial and temporal judgments, which are essential for complex motor actions and sequences of movements[11 22].

In summary, cerebellar function is not limited to motor coordination, accuracy and execution but it has a crucial role also in the motor planning, timing of serial movement execution, motor learning and also cognitive functions not strictly connected with motor control.

2. The ataxias

2.1 Cerebellar ataxias

Ataxias, literally “lack of order”, is a heterogeneous group of disorders affecting the cerebellum and sensory system. Cerebellar ataxias have different origin. It can be acquired (immune or with environmental involvement) or genetic. Genetic ataxias are a heterogeneous group of rare, mostly degenerative, diseases that share progressive cerebellar dysfunction and degeneration as main hallmarks.

Cerebellar ataxia is characterized by lack of coordination of muscle voluntary movements of the four limbs, manifesting with dysmetria, asynergy, dyschronometria and dysdiadochokinesia. It also causes asthenia and hypotonia, speech changes (dysarthria), and abnormalities in eye movement (nystagmus). Deficits in balance and walking reflect the proposed role of cerebellum in coordination, sensory integration, motor learning, and adaptation. Usually the primary (or in rare cases the secondary) symptom of cerebellar ataxia is movement incoordination and gait imbalance. These symptoms manifest in adulthood or adolescence, but in fewer cases already during childhood. Majority of ataxias have also a severe impact on daily life including difficulties with communication and mobility, in fact, for more severe or in the late stage of cerebellar ataxias may be required walking aids[23 24]. Patients lose motor coordination and independence, and their lifespan is often reduced. Supporting indicator of developing cerebellar ataxia are numerous falling, double or blurry vision, slurred speech, bad handwriting, and difficulties to perform hand tasks[25 26].

Their development is hampered by enormous genetic heterogeneity. By a genetic point of view genetic cerebellar ataxias can be subdivided into four classes based on inheritance mechanism:

1. Autosomal Dominant inheritance: these disorders are represented by Spinocerebellar ataxias (SCAs). As far today, were described at least 49 genetically distinct subtype of SCA. Each subtype is named SCA followed by a number that is progressive and represent the chronological order in which the disease locus or causative gene was identified. Genetically, the SCAs can be divided into two major groups: those caused by repeated expansions (both in exons and in introns) and those caused by non-repeat, conventional mutations (missense or nonsense mutations, insertions or deletions)[27 28 29 30];
2. Autosomal Recessive inheritance (ARCAs or named also with the acronym SCARs – Spinocerebellar Ataxias Recessive): to date, more than 100 genes were correlated with

ARCAs pathogenesis, but, in contrast to SCAs, the scientific community has not concluded on a single type of nomenclature[31 32 33];

3. X-linked inheritance: it a group of disorders affecting mainly males. Among cerebellar ataxias presenting mutations into sexual chromosome are counted FXTAS (Fragile X-associated tremor/ataxia syndrome - FMR1), ASAT (ABCB7), MRXSCH (Mental Retardation, X-linked, Syndromic, Christianson type - SLC9A6), Pelizeus-Merzbacher and ALD (Adrenoleukodystrophy);
4. Mitochondrial inheritance: this group of disease are often associated with seizures, myopathic features, ophtalmoplegia, retinopaty, diabitis.

Furthermore, the analysis of the genes involved/mutated in progressive cerebellar ataxias highlighted high connectivity on protein level and shared molecular processes. These processes include (Fig 10-11_Intro):

- ion homeostasis;
- endocytosis/transport;
- glutamate signalling;
- DNA processing and repair;
- proteasome/ubiquitin-mediated protein degradation;
- RNA processing/translation;
- RNA toxicity;
- autophagy;
- *m*-AAA complex-mediated mitochondrial proteostasis;
- energy transport;
- transcription;
- nuclear inclusion body formation[34].

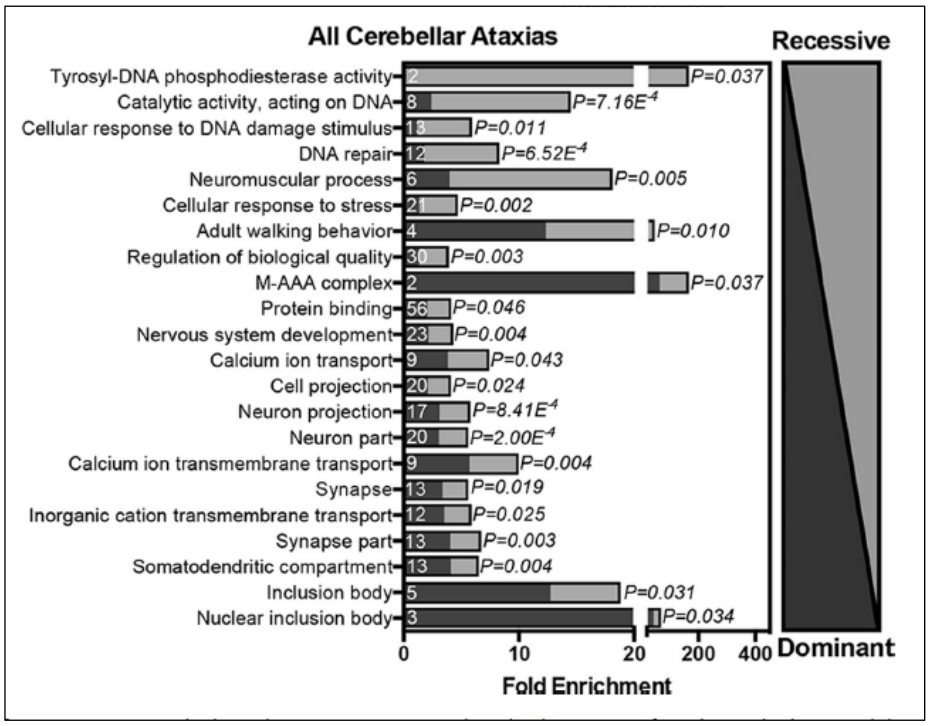

Figure 10_Intro. Cerebellar ataxia genes function in common biological processes[34].

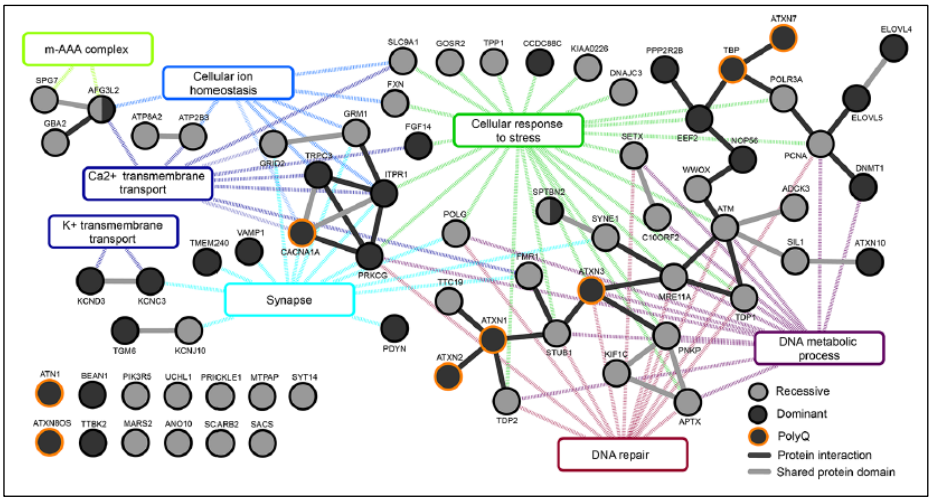

Figure 11_Intro. Interactome of proteins involved in ataxias[34].

How do these processes intersect and why does their disruption predominantly affect the cerebellum? To deeper explore these processes, different cell compartments were dissected. A crucial cellular district is the synapse, where signals are transmitted to generate accurate and coordinate movements after elaborating and processing of sensory inputs. Excitatory glutamatergic synapses into post-synaptic PC are crucial to produce autonomous firing properties, but the release of glutamate induce calcium (Ca^{2+}) entry into PCs via the activation of Ca^{2+} and Ca^{2+}-activated potassium channel. Massive Ca^{2+} influx need a precise and efficient control of ion homeostasis and so a proper Ca^{2+} buffering capacity. Altered firing rate and ion

homeostasis lead to neurodegeneration and for this reason mutations in genes coding these proteins are cause of ataxia pathogenesis (Fig. 12_Intro)[34 35 36 37 38].

Focusing on cell body, ion homeostasis and Ca^{2+} signaling play again an important role for proteostasis mechanisms at ER and Golgi membranes, intracellular signaling pathways, and the regulation of mitochondrial activity[39 40]. Moreover, due to their large dendritic trees and extensive firing properties, PCs have high metabolic demands that depend on energy (ATP) production by mitochondrial oxidative phosphorylation whch can result in excessive Reactive Oxygen Species (ROS) production. ROS can cause damage to lipids, proteins, and nucleic acids, which ultimately affect PC firing and induce PC degeneration. Many genes implicated in ataxias are, in fact, involved in cellular stress responses, counteracting stressors (e.g., ROS), and operate in the mitochondrial energy transport chain, mitochondrial and nuclear DNA repair, the *m*-AAA complex, unfolded protein response and regulation of apoptotic and autophagic processes (Fig. 12_Intro)[34 36].

Finally, also mutations in genes codifying proteins involved in nuclear functions can lead to cerebellar ataxias. It is well known that mature neurons in cerebellum cannot be replaced, and so, DNA repair processes are required to oppose the vulnerability of cerebellum. Possibly, DNA repair is a key homeostatic process in the cerebellum due to the high metabolic activity, oxidative load and intrinsic PC firing properties. In addition, cerebellar granule cells differentiating late (after birth) and by massive expansion, they generate replication stress-associated DNA damage, affecting granule cells and indirectly other cerebellar cell types including PCs to which they signal (Fig. 12_Intro)[34 41 42 43]. In the contest of genetic cerebellar ataxias, also transcription failures have to be cited. In fact, some of the most common dominant ataxias (SCA1, 2, 3, 6, 7, 17, and DRPLA) result from an expanded polyglutamine-encoding cytosine-adenine-guanine (CAG) repeat in ATXN1, ATXN2, ATXN3, CACNA1A, ATXN7, TBP and ATN1, respectively. Other repeat expansions are found in SCA8 (ATXN8/ATXN8OS), SCA10 (BEAN1), SCA36 (NOP56), FXTAS (FMR1) and Friedreich Ataxia (FA, FXN). In addition to disrupting the primary function of the mutated gene products, some repeat expansions have been shown to induce toxic gain-of-function mechanisms that evoke cellular stress responses to which the cerebellum may be particularly vulnerable. Accumulation of protein aggregates that can form nuclear inclusion bodies, dysregulated gene expression, overactivation of the chaperone and ubiquitin-proteasome system, disrupted RNA translation and processing, RNA toxicity, increased cellular ROS levels, reduction of the mitochondrial electrochemical gradient and DNA damage have all been reported in these genetic ataxias (Fig. 12_Intro)[43 44].

In summary, mutations in genes underlying ataxias frequently affect processes required for ion homeostasis and/or cellular stress response pathways. Notably, genes associated with recessive and dominant forms of ataxia act cooperatively in the affected processes, suggesting coherent biological mechanisms despite different mutational mechanisms and modes of inheritance. While the knowledge of the genetic causes of ataxias has increased significantly, effective therapies are unavailable. To this aim, more research is required to understand how dysfunction of these pathways can lead to preferential cerebellar degeneration. Based on the biological themes affected in ataxia, it would be interesting to design and test therapeutic interventions that specifically target or mitigate the harmful downstream effects of deregulated Ca^{2+} and ROS levels. Such therapeutic strategies could potentially benefit larger cohorts of ataxia patients with genetically heterogeneous, individually rare causes.

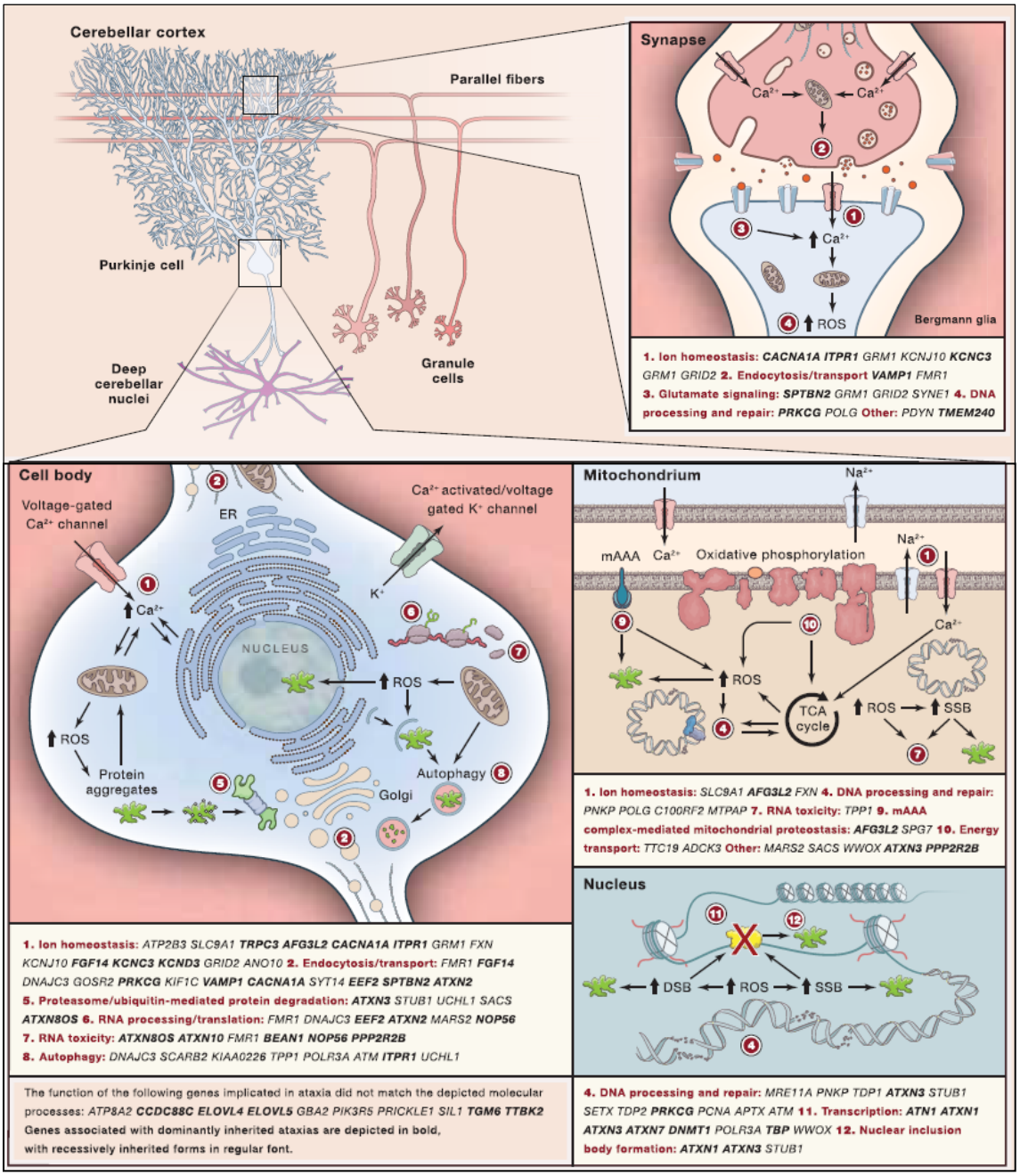

Figure 12_Intro. Biology of genetic ataxias[34].

2.2 Autosomal Recessive Ataxias (ARCAs)

Autosomal Recessive Ataxias (ARCAs) are a heterogeneous group of rare genetic diseases with an overall prevalence of 3–6/100 000. At present, recessive ataxias represent slightly more than 50% of all genetic ataxias[33] [45]. The progress in Next Generation Sequencing (NGS) techniques revolutionized the molecular diagnosis of ARCAs in the past 15 years and they enabled the identification of an expanding number of novel rare genes allowing to revise the

relative frequencies of ARCA genotypes. To date, more than 100 ARCA-associated genes have been identified[45] causing about 92 autosomal recessive diseases presenting ataxia as main feature[46]. Moreover, additional 89 autosomal recessive disorders show ataxia as part of the phenotypic spectrum (Fig. 13_Intro)[46 47]. Except for FA, which results from a non-coding repeat expansion, almost all other ARCA mutations identified so far constitute conventional mutations[45].

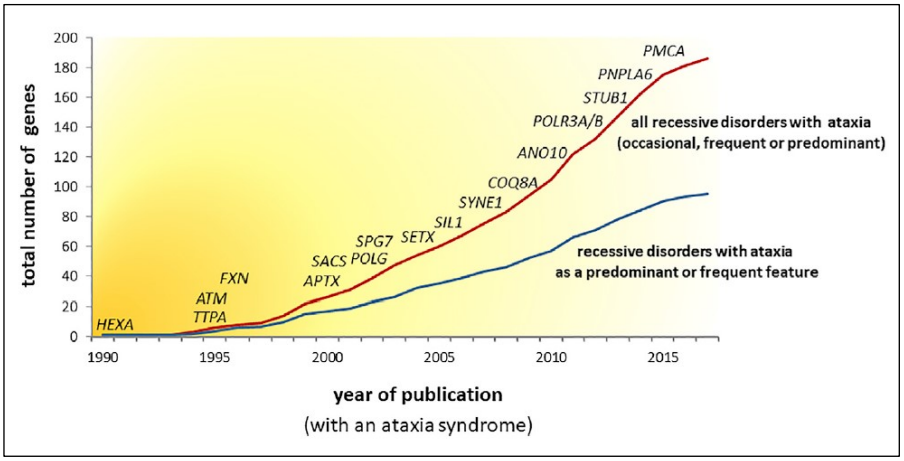

Figure 13_Intro. The number of known ARCA genes has reached almost 200, with numbers still continuously growing[46].

The majority of ARCAs share the common hallmark of progressive damage to the cerebellum and other nervous system elements, in fact, they have to be considered multisystemic disorders as neurodegeneration usually includes a broader motor and sensory neuropathy with several additional neurologic as well as non-neurologic systems affected[31 45 46].

ARCAs can be classified into different clusters based on molecular mechanisms and pathways altered by causal gene mutation:

1. Mitochondrial metabolism: several ARCAs either directly affect nuclear encoded mitochondrial proteins (e.g., FA, POLG, TWNK, COQ8A, SPG7, ATAD3A) or are indirectly linked to mitochondria metabolism (e.g., ARSACS). Mutations of mitochondrial proteins induce alterations of mitochondrial DNA maintenance, defective mitochondrial protein synthesis and quality control, oxidative damages, deficient coenzyme Q10 metabolism, altered mitochondrial dynamics and deficient energetic supply link to defective respiration[31 45 46 48];
2. DNA repair/genome stability: DNA repair pathways are impaired in several ARCAs, affecting different DNA repair mechanisms, including single- and double-strand break (DSB) repair and base excision repair (e.g., AT, AOA2, AOA1, AOA4). Mutations located in these genes increase susceptibility and predisposition for cancer and neurological

ataxic syndromes, suggesting cerebellum and in particular PCs have high vulnerability to DNA damage[31 46];

3. Complex lipid metabolism: ARCAs have been linked to disturbances in lipid biosynthesis and transport leading to accumulation of lipids inside cellular organelles. The main lipid classes affected are sterol lipids (e.g., NPC, CTX), glycerophospholipids (e.g., PNPLA6, PLA2G6), sphingolipids (e.g., MLD, Krabbe disease, Gaucher disease type3, GBA2, GM2 gangliosidosis, SPG26) and fatty acyls and prenol lipids (e.g., Refsum disease, DBP deficiency, peroxisome biogenesis disorder)[46 49].

2.3 The deregulation of Ca^{2+} homeostasis as a common signature for most ataxias

A fourth pathway typically found deregulated in ataxias, both SCAs and ARCAs, is Ca^{2+} homeostasis and downstream signalling cascade. Moreover, there are emerging data and evidences showing the pathogenesis of different ataxia-related gene mutations converge into a common cellular pathway highlighting the deregulation of Ca^{2+} homeostasis in cerebellar PCs that, causing cerebellar atrophy, leads to ataxia[50 51].

The fine spatial and temporal organisation of intracellular Ca^{2+} signals is fundamental in the Central Nervous System (CNS), perhaps more than in any other tissue. Ca^{2+} is a key molecule in signal transduction activating several biochemical cascades and participating in many physiological processes (from egg fertilization to death). Ca^{2+} signals control both short-term biological processes that occur in milliseconds (e.g., muscle contraction and neurotransmission) as well as long-term processes that require hour or several days (e.g., cell proliferation, differentiation, metabolism and also death)[52]. Moreover, the increase of cytosolic Ca^{2+} concentrations timely regulated in oscillations at a precise frequency determining the so called temporal Ca^{2+} signature[53 54]. The neuronal Ca^{2+} signaling machinery is, also, able to elicit an effect even from distance. In neurons, Ca^{2+} mediates essential signaling processes and plays an important role in synaptic plasticity. In fact, the regulation of Ca^{2+} concentrations in each compartment is a prerequisite for normal neuronal function and, due to their susceptibility, even slight perturbations in intracellular Ca^{2+} levels can drive to harmful effects (e.g., cellular dysfunctions and cell death).

Ca^{2+} signaling in PCs is important for normal cellular function as these neurons express a variety of Ca^{2+} channels, Ca^{2+}-sensitive kinases and phosphatases, Ca^{2+} sensors and Ca^{2+} buffers to tightly maintain Ca^{2+} homeostasis[51]. Moreover, glutamate, an excitatory neurotransmitter,

induces a transient increase in the cytosolic Ca^{2+} levels of PCs via activating ionotropic α-amino-3-hydroxyl-5-methyl-4-isoxazole-propionate (AMPA) receptors and metabotropic glutamate receptors (mGluR). Activation of AMPA receptors causes membrane depolarization, activation of voltage-gated Ca^{2+} channels (VGCC) and Ca^{2+} influx into the cytoplasm. On the other hand, activation of mGluR causes Ca^{2+} release from ER stores via activating inositol 1,4,5-triphosphate receptors (IP3R) to allow a transient increase in cytosolic Ca^{2+} levels. Initial Ca^{2+} signals is further amplified by Ca^{2+}-induced Ca^{2+} release mechanism, which involves activation of ryanodine receptors (RyanR), an intracellular Ca^{2+} release channels. When tightly controlled, a transient change in Ca^{2+} levels functions as an intracellular messenger important for gene transcription[55] and synaptic neurotransmission[56]. Aberrant Ca^{2+} levels can uncouple neuronal plasticity and activate toxic cascades leading to cell death. In case of unbalanced cytosolic Ca^{2+} concentration, excessive Ca^{2+} amount is taken up by Ca^{2+} buffer systems represented by PC binding proteins (i.e., calbindin, parvalbumin), plasma membrane Ca^{2+} transporters (e.g., Ca^{2+} ATPase, Na^{+}/Ca^{2+} exchanger) and organelle uptake via the sarcoplasmic-endoreticulum Ca^{2+} ATPase (SERCA) and mitochondrial uniporter (MCU)[54 57].

Several studies have implicated deranged Ca^{2+} signaling in neurodegenerative disorders culminating in the "Ca^{2+} hypothesis of neurodegeneration". This hypothesis states that as fundamental as Ca^{2+} levels are to cellular functions, and dysregulation of Ca^{2+} homeostasis is detrimental to neuronal survival[58]. Notably, disruption of intracellular Ca^{2+} signaling in PCs, very sensitive neurons, is believed to be a crucial mechanism in the pathogenesis of cerebellar ataxias. The importance of Ca^{2+} regulation in PCs is supported by the expression of great variety of Ca^{2+} channels, Ca^{2+}-dependent kinases, phosphatases and Ca^{2+}-binding proteins. And the other way around, mutations in Ca^{2+} channels, Ca^{2+}-dependent proteins and proteins involved in regulation of Ca^{2+} fluxes and handling (e.g., glutamate receptors) primarily affect PCs causing hereditary ataxias[50 59].

In this contest, at least 13 SCAs are caused due to pathogenic mutations in genes encoding Ca^{2+} signaling-related proteins (Table 1).

Ataxia name	Mutated gene	Function related to Ca^{2+} signal transduction	Impact on Ca^{2+}
SCA1	*ATXN1*	Transcriptional and splicing regulator of genes involved in Ca^{2+} regulation	Decreased expression of several Ca^{2+}-related proteins (e.g., mGLUR1a, IP3R1, SERCA2, TRPC3, and EAAT4) affecting Ca^{2+}

			homeostasis
SCA2	*ATXN2*	Mutant form specifically binds to IP3R1 and modulates its function	Increased mGLUR1a pathway sensitivity and Ca^{2+} release
SCA3	*ATXN3*	Mutant form interacts with IP3R1	Increased intracellular Ca^{2+} levels
SCA5	*SPTBN2/β-III spectrin*	Involved in the stabilization of the glutamate transporter EAAT4 in cellular membrane of PCs	Decreased EAAT4 expression causing defects in glutamate transport, faster mGLUR1-mediated slow EPSCs, mGLUR1 mislocalization and altered mGLUR1-IP3R1 signaling
SCA6	*CACNA1A*	The core component of voltage-dependent P/Q-type Ca^{2+} channels	Reduced Ca^{2+} currents in cerebellar PCs, impaired LTP and LTD, altered spontaneous PC activity
SCA13	*KCNC3*	Potassium voltage-gated channel subfamily C member 3 enriched in PCs	Broader PC action potential and increased amplitude of cytosolic Ca^{2+} signal in PCs
SCA14	*PKCγ*	Activated by IP3R1 regulating the function of TRPC3 and NMDAR1	Failed inactivation of TRPC3 channel and increased cytosolic Ca^{2+} levels
SCA15/SCA16 /SCA29	*ITPR1*	Activated by IP3 and functions as ligand-gated ion channel that releases Ca^{2+} from intracellular stores	Impaired LTD and synaptic transmission, deregulated intracellular Ca^{2+} concentration
SCA19/SCA22	*KCND3*	Potassium voltage-gated channel	Impaired neurotransmission, decreased expression of mGLUR1a
SCA27	*FGF14*	Regulator of P/Q-type Ca^{2+} channels based on its binding to C-terminus of voltage-gated Na^{+} channels	Reduced Ca^{2+} currents, diminished vesicular recycling and decreased EPSCs
SCA41	*TRPC3*	Non-selective Ca^{2+} permeant cation channel activated by DAG and PKCγ	Increased Ca^{2+} levels and impaired PC dendritic growth and synapse formation
SCA42	*CACNA1G*	Voltage-dependent T-type Ca^{2+} channel	Increased intracellular Ca^{2+} levels

SCA44	*GRM1*	Metabotropic glutamate receptor 1 activates PKCγ and IP3R1	Deregulated mGLUR1a activation and IP3 production influencing Ca^{2+} levels

In addition, also, at least 13 ARCAs are caused by pathogenic mutations in genes encoding for Ca^{2+}/ion channels or in genes regulating expression, function and signaling of Ca^{2+} pathways. Curiously, homozygous mutations of gene involved in dominant forms of ataxia, *SPTBN2*, *ITPR1* and *GRM1*, can cause severe form of ARCAs (Table 2).

Ataxia name	Mutated gene	Function related to Ca^{2+} signal transduction	Impact on Ca^{2+}
Gillespie Syndrome	*ITPR1*	Activated by IP3 and functions as a ligand-gated ion channel that releases Ca^{2+} from intracellular stores	Impaired LTD, synaptic transmission and intracellular Ca^{2+} concentrations
CAMRQ3	*CA8*	Regulator of IP3 binding to its receptor IP3R1	Increased IP3R1 activation and Ca^{2+} release from ER
SPARCA1	*SPTBN2*	Involved in the stabilization of the glutamate transporter EAAT4 in cellular membrane of PCs	Decreased EAAT4 expression causing defects in glutamate transport, faster mGLUR1-mediated slow EPSCs, mGLUR1 mislocalization and altered mGLUR1-IP3R1 signaling
SCAR13	*GRM1*	Metabotropic glutamate receptor 1 activates PKCγ and IP3R1	Reduced Ca^{2+} influx from IP3R1 and TRPC3 channels
Lichtenstein-Knorr Syndrome	*SLC9A1*	Na^{+}/H^{+} exchanger	Regulates pH, excitability and ions suck as Ca^{2+} concentration
SPAX9	*CHP1*	Calcineurin Like EF-Hand Protein 1 regulates vesicular trafficking, plasma membrane Na^{+}/H^{+} exchanger	Regulates pH, excitability and ions suck as Ca^{2+} concentration
SPG76	*CAPN1*	Ca^{2+}-sensitive cysteine proteases	Interacts with CDK5 and NR2B control to control NMDA-receptor degradation and

			synaptic plasticity
SCAR18	*GRID2*	Ionotropic glutamate receptor (GluRδ2) that works as part of signalling complex with mGLUR1. It also interacts with PKCγ and TRPC3	Increased mGLUR1 evoked-currents and increased Ca^{2+} levels
Cayman Ataxia	*ATCAY*	BNIP-H kinase binding protein	Regulates glutamate synthesis at synapse and binds to kinesin-1 and functions as adaptor for intracellular transport of specific cargos (mitochondria)
SLC17A5/ Siallin	*SLC17A5/Siallin*		Mediates aspartate and glutamate membrane potential-dependent uptake into synaptic vesicles
SCAR8	*SYNE1*	Involved in a linking network between nuclear lamina, organelles and actin-cytoskeleton	Disrupted glutamate receptor internalization and involved in rapid cycling of synaptic glutamate receptors
SCAR10	*ANO10*	Ca^{2+}-activated chloride channel	Dysregulated local Ca^{2+} signaling
SCAX1	*ATP2B3*	ATPase Ca^{2+} transporter of plasma membrane	Impaired Ca^{2+} ejection function leading to increased intracellular Ca^{2+} levels

Finally, in the context of alteration of Ca^{2+} homeostasis in ataxias a role for mitochondria has been demonstrated. In fact, mitochondrial function and Ca^{2+} signalling are intimately linked, in particular due to mitochondrial Ca^{2+} buffering capacity. Mitochondrial membrane potential $\Delta\Psi_{mito}$ represents the driving force for Ca^{2+} accumulation in the mitochondrial matrix through the MCU[52 54]. In addition, also ER is involved in Ca^{2+} homeostasis mechanisms cooperating with mitochondria. In fact, the ER, the major Ca^{2+} store of the cell, make close contacts with mitochondria, the so-called Mitochondrial Associated Membranes (MAMs). In the MAMs, as in proximity of plasma membrane, Ca^{2+}-signaling microdomains in which mitochondria are required for their Ca^{2+} buffering capacity are formed. In these regions, indeed, Ca^{2+} concentrations reach levels 100-times higher than in the rest of the cytosol. For example, during IP3-mediated Ca^{2+} release from the ER or Ca^{2+} influxes through Ca^{2+}-channels, energized

mitochondria are recruited to rapidly remove excessive Ca^{2+} internalized by transport systems of outer mitochondrial membrane (OMM) permeable to solutes smaller than 5 kDa and, thus, also Ca^{2+} thanks the abundant expression of voltage-dependent anion channels (VDAC). While the transport through ion-impermeable inner mitochondrial membrane (IMM) is mediated by the MCU[39 54 60]. The balance between Ca^{2+} uptake and release from these systems regulates several regulatory feedback activities based on Ca^{2+} levels in the cytosol. Thus, mitochondria, orchestrating Ca^{2+} concentrations, have an important role in modulating the activity and expression of Ca^{2+}-channels influencing their spatiotemporal properties[54].

To regulate Ca^{2+} levels by this mechanism, mitochondria position and distribution inside the cell is crucial. In neurons, mitochondria are transported and finely distributed where they are needed[61 62 63], such as in the synapse close to VGCCs and glutamate receptors to rapidly shape Ca^{2+}-transients strongly regulating neuronal activity. In the emerging picture where mitochondria are fundamental players in Ca^{2+} handling and homeostasis, their transport and positioning have been implicated in the pathogenesis of many brain disorders[64], and even more they have a critical role in PCs receiving an incredibly high number of glutamatergic synapses and handling huge metabolic demands[54]. This thesis is supported by the fact that mutations in mitochondrial proteins, affecting their properties, are often associated with PCs dysfunction and ataxia. For example, this is the case of loss-of-function mutations in AFG3L2 subunit of *m*-AAA complex, a mitochondrial protease system. AFG3L2 mutations are, indeed, responsible for two forms of ataxias, a dominant form (SCA28) and a recessive one (SPAX5)[65 66 67]. Both diseases present mitochondrial deficits associated with decreased respiration and dynamics, influencing mitochondrial trafficking and, thus, leading to elevated intracellular Ca^{2+} levels that trigger PC dark cell degeneration due to Ca^{2+} overload[68].

3. Autosomal Recessive Spastic Ataxia of Charlevoix-Saguenay

3.1 Autosomal Recessive Spastic Ataxia of Charlevoix-Saguenay is caused by mutations in the *SACS* gene

Autosomal Recessive Spastic Ataxia of Charlevoix-Saguenay (ARSACS - OMIM #270550) is a neurodegenerative disease characterized by early-onset cerebellar ataxia and caused by mutations in the *SACS* gene, which encodes the protein sacsin. The disease name is given by the region of Charlevoix-Saguenay-Lac-Saint-Jean (CSLS), in Québec (Canada), where the

frequency of healthy carriers is 1/22[69 70]. The disease was first described in 1979 by Bouchard et al.[71] in the Québécois patients. In 2000, Engert et al. identified for the first time two mutations in the *SACS* gene in Québec ARSACS families. One mutation is a single base deletion (g.8844delT) in homozygosis, which belongs to a major haplotype shared by 96% of ARSACS families by descending from an ancestral founder in the population that settled first in Québec. The second mutation is a nonsense substitution (g.7504C > T), which belongs to a minor ARSACS haplotype and that was found in six families in heterozygosis with the major deletion. Both mutations occur in the last gigantic exon and should produce a truncated protein[69]. Although these discoveries, ARSACS has been diagnosed worldwide, with the identification of more than 200 mutations, spread all over the *SACS* gene (Fig. 13_Intro).

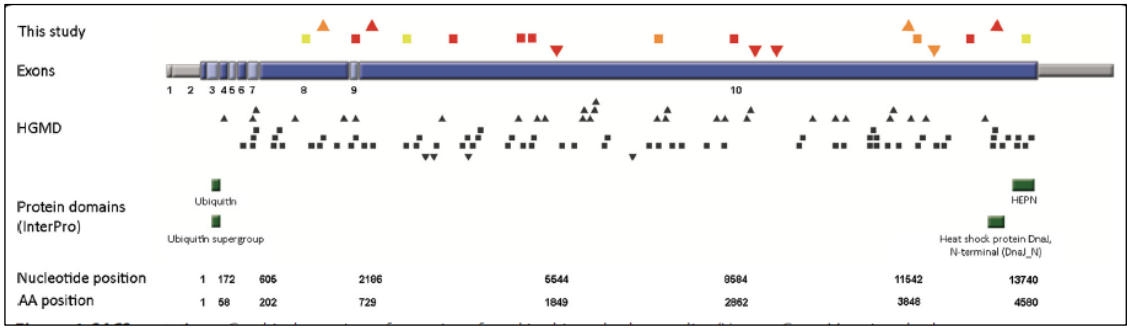

Figure 13_Intro. Graphical overview of *SACS* variants. Different mutation types are marked with different symbols: missense mutations = squares; insertions/duplications = triangles with downward orientation; deletions = triangles with upward orientation. Sequence variations identified in this study are coloured, with the colour indicating the pathogenicity class: red = pathogenic, orange = likely pathogenic, yellow = uncertain. Known protein domains of the sacsin protein are highlighted in green. AA = amino acid[72].

The disease is globally spread with no correlations between specific ethnicities and specific allele or disease frequency, and it is now considered the second most common recessive ataxia after Friedreich's ataxia (OMIM #229300). Most patients are homozygous for *SACS* mutations (45,2%), followed by compound heterozygous (32,9%) and any type of mutation has been reported[73], with missense substitutions being the most represented, but also macrodeletions, frameshifts changes and nonsense mutations have been observed[73].

The recessive pattern of clinical phenotype, and the fact that some mutations should lead to the production of a truncated protein, suggest that the molecular pathology mechanism is associated with loss-of-function of sacsin protein[70 72 74 75] . However, characterization of the outcomes of sacsin mutations at the protein level could be interesting to better understand genotype-phenotype correlation (manuscript in preparation in the lab).

3.2 ARSACS clinical manifestations

ARSACS is clinically characterized by progressive cerebellar ataxia, spasticity and sensory-motor axonal peripheral neuropathy. Most patients present with the above triad of symptoms, typically with early onset cerebellar ataxia secondarily followed by spasticity and later by neuropathy. Progressive degeneration of the cerebellar vermis has been documented in patients who underwent MRI and post-mortem analysis[70 71 72 73]. Other typical signs include dysarthria, distal amyotrophy (likely as consequence of neuropathy), limb weakness, sensory loss, pyramidal signs, and cerebellar eye manifestations (e.g., nystagmus). The clinical features obtained from 222 ARSACS patients reported by Xiromerisiou et al. suggest the mean for the age at onset is 3 years, ranging between 6 months and 40 years[73]. All three major clinical characteristics are present with a high frequency: the most common and earliest feature is cerebellar ataxia (78,9%), followed by the spasticity (78,1%) and then the polyneurophaty (73,7%). Additional atypical characteristics are intellectual disability, urinary dysfunction, epileptic disorders and hearing loss present with lower frequency[73]. In the classical French-Canadian phenotype[70], all patients presented all three major clinical manifestations, but the discovery of many clinical cases throughout the world has expanded the clinical spectrum, showing much more phenotype variability. Moreover, there are case reports of patients who do not develop spasticity in their lower limbs. On the other hand, dysarthria has been described as a common feature and it is likely a consequence of ataxia. In fact, the speech is slurred in childhood and becomes incomprehensible by adulthood[71].

Post-mortem brain analysis from ARSACS patients and MRI studies revealed a remarkable atrophy of superior and middle components of the cerebellar vermis, reported in 60,8% of the cases, associated with loss of PCs, starting very early in the disease course. Instead, the cerebellar hemispheres are less affected. Bilateral demyelination of both the corticospinal tract (that can account for spasticity and pyramidal signs common in ARSACS patients) and of the dorsal spinocerebellar tract were also observed. Moreover, Ocular Coherence Tomography (OCT) permitted to detect a peculiar increase of peripapillary Retinal Nerve Fiber Layer (RNFL) thickness in ARSACS patients, as demonstrated in literature by many papers and case reports[76–85]. This feature has been observed, to a lesser extent, also in carriers of ARSACS mutations[76 77]. While this characteristic is not present in other form of ataxia, both ARCAs and SCAs, that present RNFL thickness comparable to healthy controls[76]. In addition, to underline the uniqueness of this feature, RNFL thickness usually becomes thinner and thinner with aging.

ARSACS diagnosis includes MRI, fundoscopy, OCT, neurological evaluation and sensory and nerve conduction studies. However, since ARSACS patients present high clinical variability and many symptoms are shared by other recessive spinocerebellar ataxia, the ultimate diagnosis is made by genetic testing to identify mutations in *SACS* gene. Moreover, in many cases with uncertain variants it is still necessary to sequence other sets of ataxia-related genes in order to exclude alternative diagnosis[86]. To date, there are no curative therapies available for ARSACS patients, and the treatments on the market only alleviate the symptoms of the disease.

4. *SACS* gene expression and sacsin protein architecture and function

4.1 Characterization of *SACS* gene

The *SACS* locus is localized on chromosome 13q12.12 and was cloned for the first time by Engert et al. in 2000[69], who identified two mutations in the predicted coding sequence as leading to ARSACS. Initially, the gene was predicted to consist of a single giant exon, remarkably of 12 800 bps, which contained an open reading frame (ORF) of 11 500 bps. Then, other nine canonical exons were identified by retro-transcriptional PCR upstream the gigantic one, eight of which are coding, whereas one resides completely in the 5'UTR[74 87], for a total transcript of 15 600 bps. The last gigantic exon is now known to be 12 868 bp long, which is the longest exon ever identified in the vertebrate genome. The final predicted ORF encodes for a protein of 4579 amino acids and has a molecular weight of 520 kDa. There are not paralogue genes to SACS in the human genome. However, sacsin is highly conserved in mammals. Mouse genome is predicted to express a homologue protein with length and weight identical to human sacsin.

4.2 Expression of *SACS* gene in mammalian tissues

Investigation of *SACS* expression and localization in mammalian tissues was initially carried out by Northern blot analysis, which revealed highest sacsin mRNA expression in human dermal fibroblasts and in different tissues, including brain, heart, and skeletal muscles. A low expression was seen in pancreas and no expression was detected in lung, liver, and kidney[69]. Specific analysis of CNS tissues in human, rat, and monkeys by mRNA *in situ* hybridization confirmed general high expression in all the brain with the most intense areas being the

cerebral cortex, the hippocampus, and the granule cell layer of the cerebellum[69]. Parfitt et al. experimentally characterized sacsin protein for the first time[87]. Analysis by WB on mouse and rat tissue extracts shows that sacsin is specifically expressed in brain and particularly in cerebral cortex and cerebellum, whereas protein levels are low in heart and testis and absent in spinal cord, lung, liver, spleen and kidney (Fig. 14_Intro)[87]. However, WB analysis performed in the lab shows that sacsin is expressed also in spinal cord (data not shown) and this hypothesis is further corroborated by experimental data on primary DRG neurons and motor neurons obtained by Gentil and collaborators (see paragraph 5.1, page 57)[88].

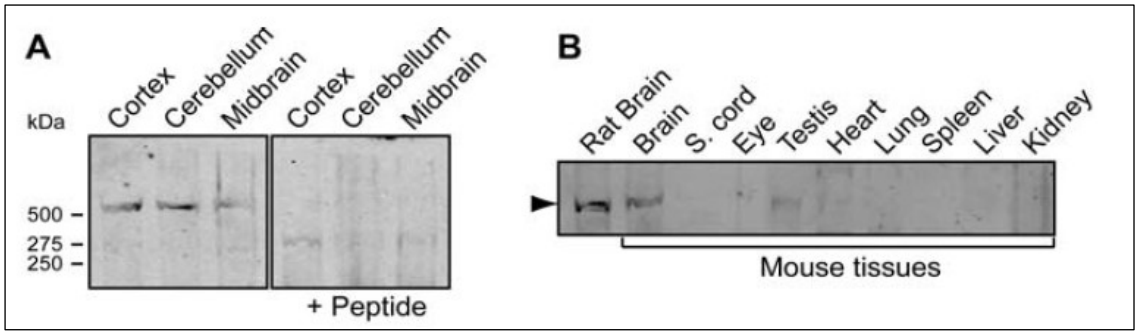

Figure 14_Intro. Sacsin expression in central nervous system by WB. WB analysis of different mouse and rat tissue extracts with polyclonal antiserum directed toward sacsin C-terminal region (residues 4489-4503). The band was not detected when the antiserum was pre-incubated with the immunizing peptide[87].

Further analysis of CNS, in sagittal brain section from 300 days-old controls and *Sacs*$^{-/-}$ mice tissues by immunohistochemistry using antibody against sacsin, confirmed that sacsin is a neuronal protein widely expressed in most areas of the brain (Fig. 15_Intro)[89]. In particular, the most extensive labeling was observed in cell bodies, dendrites and axons of cerebellar PCs, certain neurons of the DCN and several neurons in the pons and the medulla (Fig. 15_Intro). In some areas, such the thalamus, the hippocampus and the isocortex area, sacsin expression seems more restricted to neuronal processes (Fig. 15_Intro). On the contrary, in some areas such the olfactory bulb, superior olivary complex neurons and visual and motor cerebral cortex areas, sacsin seems prevalently expressed in cells bodies (Fig. 15_Intro)[89].

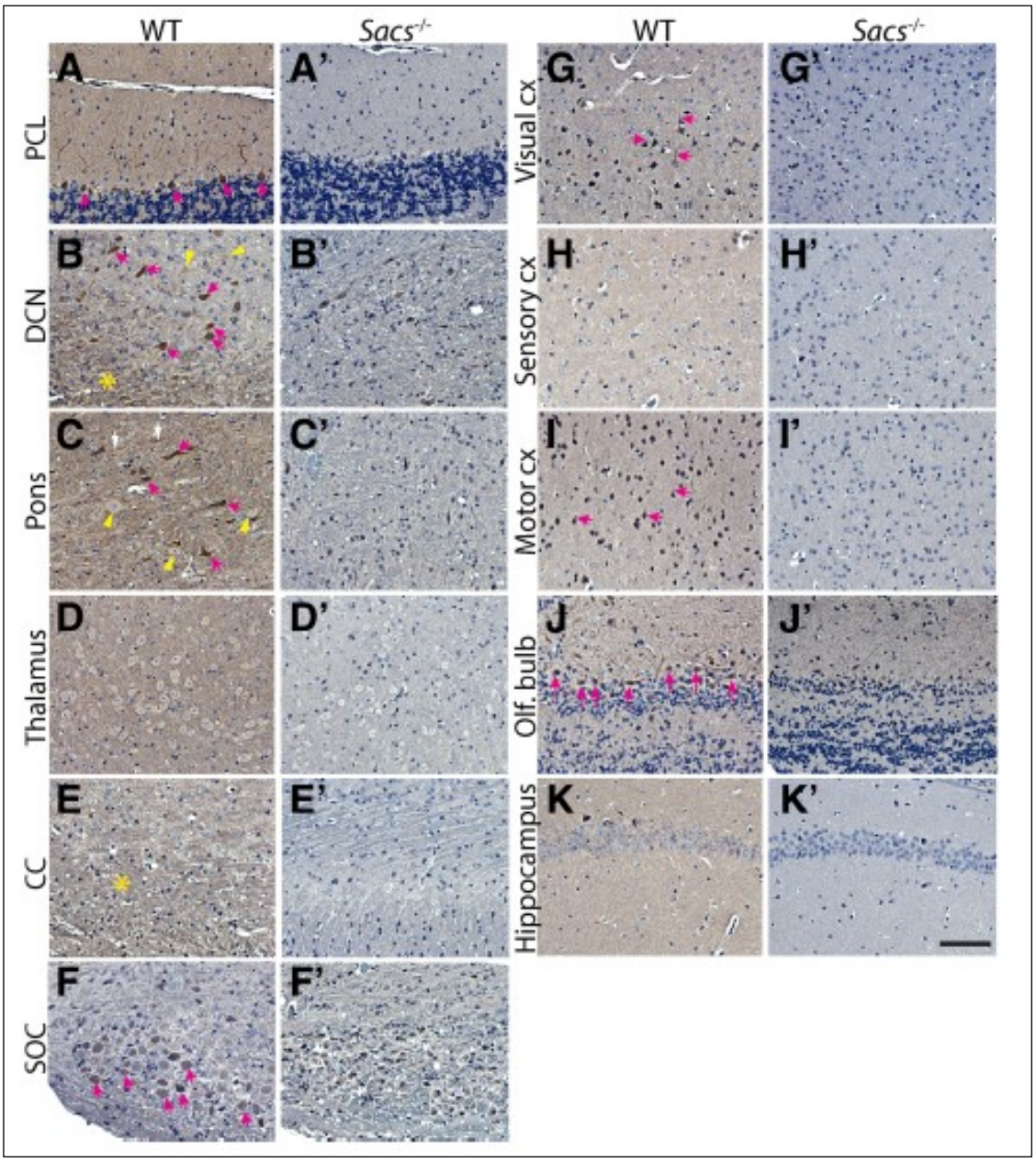

Figure 15_Intro. Sacsin expression in CNS neurons. Immunohistochemistry using antibody against sacsin on sagittal brain sections from 300 day-old control mice demonstrate the widespread sacsin expression in several CNS populations (PCL: Purkinje Cell layer. DCN: Dorsal Cochlear Nucleus. CC: Corpus Callosum. SOC: Superior Olivary Complex)[89].

4.3 Subcellular localization of sacsin protein

After 18 years since its discovery, sacsin subcellular localization is still unknown. Few works assessed experimentally sacsin localization[90] [87] and results were irreproducible in our lab. Bioinformatics analysis reveals that sacsin does not possess any characterized protein sorting signal. Immunofluorescence analysis, using antibodies directed toward both N-terminal and C-

terminal sacsin portion, gave the same staining pattern characterised by a diffused cytosolic distribution with some punctate spots in the nucleus (Fig. 16_Intro, left)[87]. Moreover, they reported partial co-localization to mitochondria by double labelling of sacsin and mitochondrial markers in different cell types (Fig. 16_Intro, right)[90].

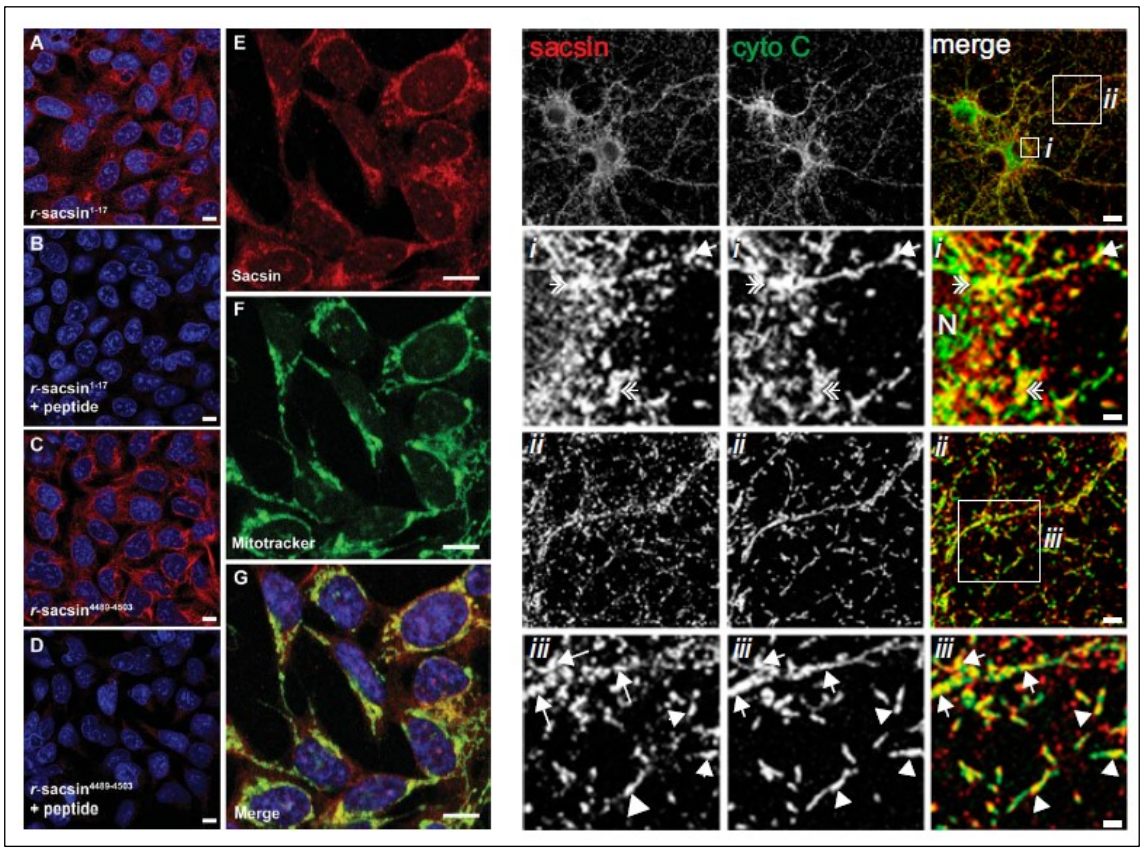

Figure 16_Intro. Sacsin subcellular localization in immunofluorescence. Left: immunofluorescence of sacsin protein, with antibodies directed toward N-terminal (A) and C-terminal (C) portion of sacsin (green), and mitochondria (red) in SH-SY5Y cells[87]. Right: immunofluorescence of COS-7 and HeLa cells marked with antibodies directed against sacsin (red) and cytochrome C (green)[90].

The hypothesis of mitochondrial partial localization is interesting, since ARSACS pathogenesis might be linked to impairment of mitochondrial dynamics (as discussed in 3.4 paragraph). Moreover, due to sacsin huge dimensions and lack of mitochondrial matrix targeting peptides in its sequence, it is highly unlikely that sacsin is translocated inside mitochondria. Also, sacsin physical interaction with the OMM remains a controversial point. Interaction between endogenous Dynamin-related protein 1 (DRP1) and an exogenous protein encoding a FLAG-tagged sacsin N-terminal fragment was reported by co-IP[90]. DRP1 is a GTPase dynamin and is a key mediator of mitochondrial fission[90 91]. However, also this result was not reconfirmed in our lab in endogenous conditions by co-immunoprecipating endogenous sacsin with available antibodies.

4.4 Sacsin protein domains and structure

Sacsin is a complex multimodular protein, with a total length of 4579 amino acids. Such huge dimension has hampered biochemical studies of the protein, due to the difficulty of cloning and expressing it in a heterologous system. The only available information on sacsin functions have been obtained by bioinformatics analyses of the sequence and by the expression of small sub regions of the protein *in vitro.* Anyway, bioinformatic analysis reveals the presence, from the N-terminal to the C- terminal, of:

- Ubiquitin-Like domain (UbL) putatively able to bind the proteasome[87];
- three novel supra-domains defined as sacsin Internal RePeaTs (SIRPT) 1, 2 and 3[74 92], each containing an H_ATPase_c domain homologous to Hsp90 chaperone family[69 92];
- Xeroderma Pigmentosum complementation group C (XPC) binding domain (XPCB) related to Rad23 and speculated to bind the ubiquitin ligase Ube3A[93];
- J domain, homologous to Hsp40 co-chaperone family able to bind Hsp70[69 87];
- Higher Eukaryotes and Prokaryotes Nucleotide-binding domain (HEPN) able to bind GTP and analogues substrates[94].

General view of sacsin architecture is displayed in Fig. 17_Intro.

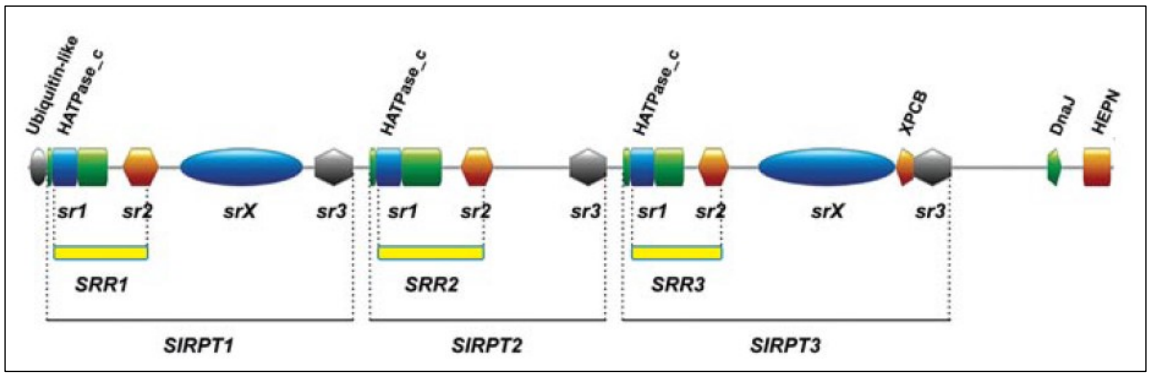

Figure 17_Intro. Schematic view of sacsin architecture[74].

These results indicate sacsin possesses different domains involved in proteostasis, which suggest it may have a role as a molecular chaperone or as a co-chaperon. However, the validity of these results is limited due to the fact they were all obtained by generating and cloning a single domain of sacsin protein and therefore we do not know how the single domains work and integrate in the context of the entire protein. Therefore, sacsin role inside the cell is still an open issue.

4.5 Functional studies of ARSACS pathophysiology in cellular models

Bioinformatics studies of sacsin domains present in literature allowed us to suppose that this protein is involved in protein quality control. Results from our and other labs in cell models of sacsin depletion revealed that this protein is involved in cytoskeletal remodeling and mitochondrial shape. But how these two mechanisms are interlinked was not clarified yet.

Intermediate filament remodeling

As a collaborative effort with other groups, our lab demonstrated that the absence of sacsin causes a dramatic vimentin remodeling. Confocal imaging revealed that vimentin filaments were bundled in perinuclear accumulations in ARSACS patient fibroblasts, whereas vimentin was evenly distributed throughout the cytoplasm in control cells (Fig. 18_Intro)[95]. This result was further confirmed in HEK293 *SACS*$^{-/-}$ cell line: these cells exhibited perinuclear collapse of the vimentin network as observed in ARSACS patient fibroblasts. Interestingly, these perinuclear bundles of vimentin were rescued by transfection of a plasmid for expression of full-length sacsin-GFP (Fig. 19_Intro)[95]. Abnormalities in actin microfilament or microtubule organization were not observed, however, co-labeling with anti-tubulin revealed that the vimentin accumulations formed in close proximity to the MTOC[95]. Vimentin is the major intermediate filament (IF) protein expressed in fibroblasts. The assembly of IFs is a complex and ordered process: IFs proteins form coiled-coil dimers through association of their rod domains, and these dimers then further dimerize to form nonpolar tetramers through antiparallel association. Eight tetramers then associate laterally into non-ionic detergent-insoluble precursors which then anneal end-to-end into an immature filament of 18nm. Radial compaction of the immature filament into a 10-nm mature filament is the final step of IF assembly[88]. IF turnover can occur by severing and reannealing of the existing filament and by exchange of individual subunits. However, the regulating processes of the assembly and maintenance of IF network are not well understood up to now[88].

IF remodeling is conserved also in neurons, as both ARSACS mouse models and autoptic brain samples from patients revealed abnormally dense bundles of NFs (details in paragraph 5.1).

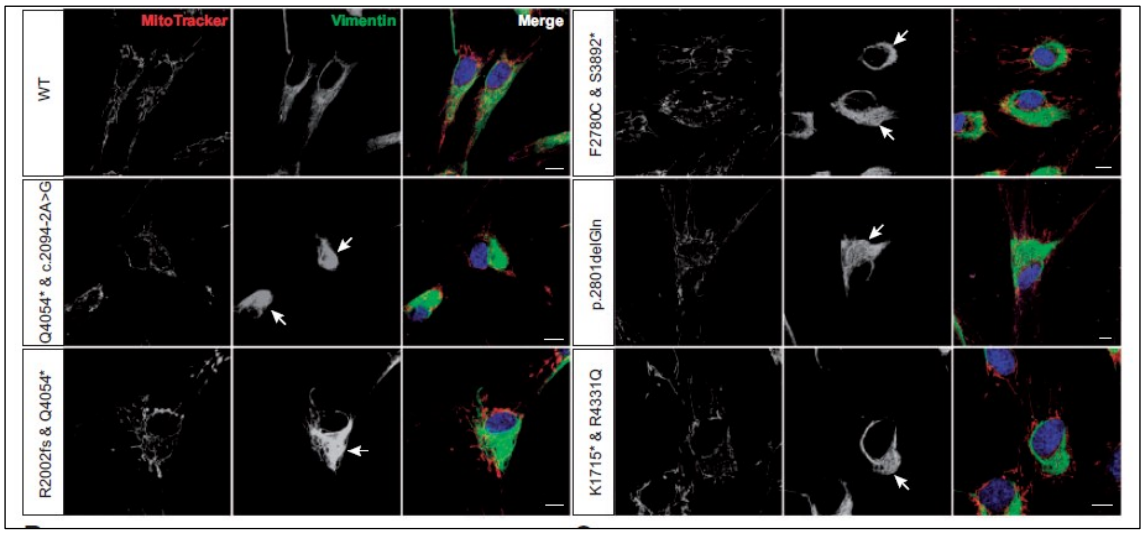

Figure 18_Intro. Abnormal accumulations of vimentin IF in ARSACS patient HDFs. Representative confocal images of five ARSACS patient HDFs and a wild-type control HDF line that were stained for mitochondria (MitoTracker) and immunolabelled for vimentin. Cells were also stained with DAPI to detect nuclei. Arrows indicate areas of abnormal perinuclear vimentin accumulation. Scale bar = 10 µm[95].

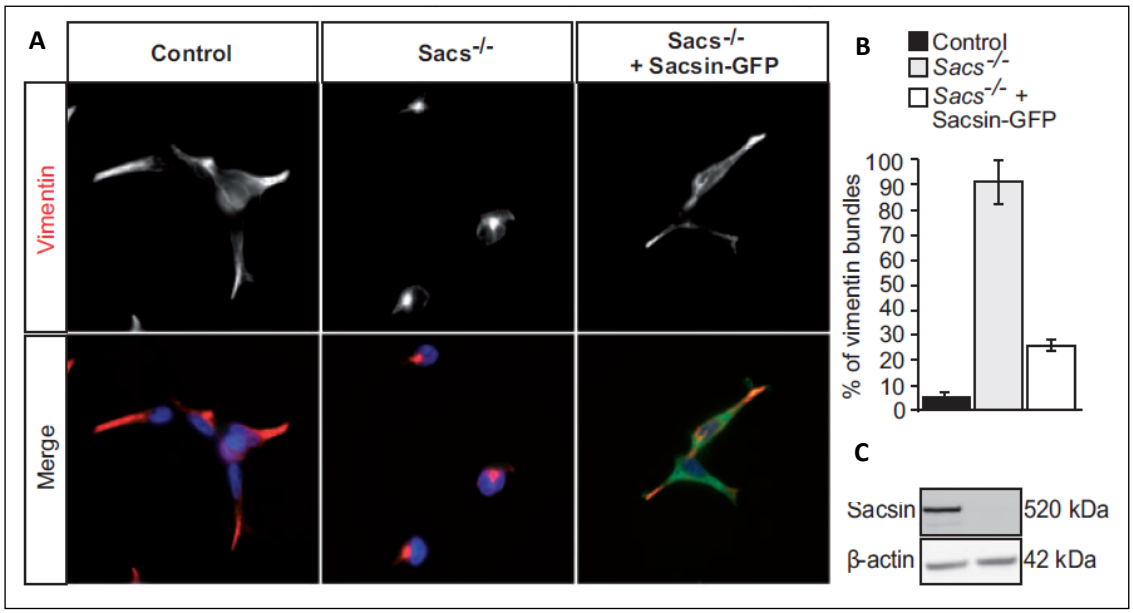

Figure 19_Intro. Abnormal accumulations of vimentin is rescued by sacsin full-length expression. (A) Representative confocal images of CRISPR generated *SACS*$^{-/-}$ HEK293 cells and *SACS*$^{-/-}$ HEK293 transfected with a plasmid for expression of full-length sacsin-GFP. Cells were processed for immunofluorescent detection of vimentin and counterstained with DAPI; (B) The percentage of cells with a collapsed vimentin network was then quantified for each condition; (C) Sacsin immunoblot of total lysates from control and *SACS*$^{-/-}$ HEK293 cells[95].

Altered mitochondrial dynamics, bioenergetics and transport

Another interesting evidence emerging from studies in sacsin-depleted cellular models is the link between sacsin to basic processes of mitochondrial biology, such as mitochondrial dynamics, functionality and transport in neurons. Sacsin involvement in mitochondrial

dynamics was established by investigating mitochondrial morphology both in siRNA-mediated *SACS* knockdown in SH-SY5Y cells and in patient fibroblasts. In these models, the mitochondrial network appears more fused than in the wild-type conditions. In patient fibroblasts bulbed mitochondria are present, which are a typical sign of extreme mitochondrial hyperfusion (Fig. 20_Intro)[90]. In addition, a recent work from our lab and other labs showed displacement of mitochondria to areas peripheral to the abnormal accumulations of vimentin in ARSACS patient fibroblasts[95].

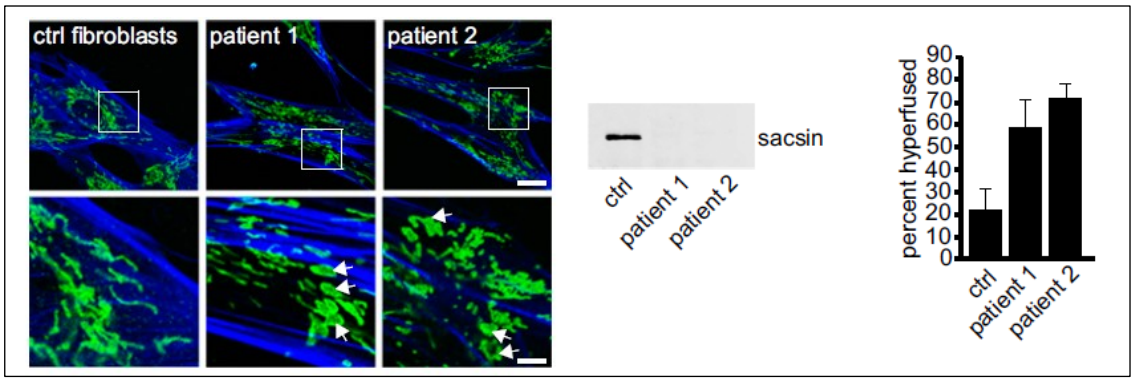

Figure 20_Intro. Mitochondrial bulbed structures in ARSACS patient fibroblasts. Immunofluorescence using antibody against TOM20 (green), a mitochondrial marker, and against phalloidin (blue), which marks actin filaments. Arrows indicate bulbed-like mitochondria, which are mitochondria extremely fused. On the right sacsin amount of each patient cell line and quantitative analysis of hyperfused mitochondria (%)[90].

At steady state, both siRNA-mediated *SACS* knockdown SH-SY5Y cells and ARSACS patient fibroblasts show reduced membrane potential, seen as lower TMRM (Tetramethylrhodamine methyl ester) intensity signal, indicating a general altered functionality of mitochondria[90]. Moreover, SH-SY5Y cells stained with the red fluorescent dye Mitotracker, which marks specifically mitochondria, were treated with the uncoupling agent CCCP. Since Mitotracker accumulation in mitochondria is sensitive to alterations in membrane potential, treatment with CCCP, that dissipates the potential, cancels the Mitotracker fluorescent signal, whereas CCCP washout is expected to recover fluorescent signal. In SH-SY5Y *SACS*-knockdown cells the recovery of signal is much slower than in the control condition[90]. Bradshaw et al. further demonstrated impairment of mitochondrial bioenergetics in ARSACS patient fibroblasts and SH-SY5Y *SACS*-knockdown cells. In both models, they found by microarray analysis, a reduction of expression of genes encoding the oxidative phosphorylation (OXPHOS) complexes and an increase in the expression of genes related to oxidative stress, suggesting an accumulation of oxidative damage in absence of sacsin, a clear consequence of mitochondrial impairment[96]. Moreover, in ARSACS patient cells and SH-SY5Y *SACS*-knockdown cells, oxygen consumption rate was reduced, compared to control, both in basal conditions and upon inhibition of

complex IV with oligomycin, upon the uncoupling agent FCCP and inhibition of complex I and III with rotenone and antimycin A (Fig. 21_Intro)[96].

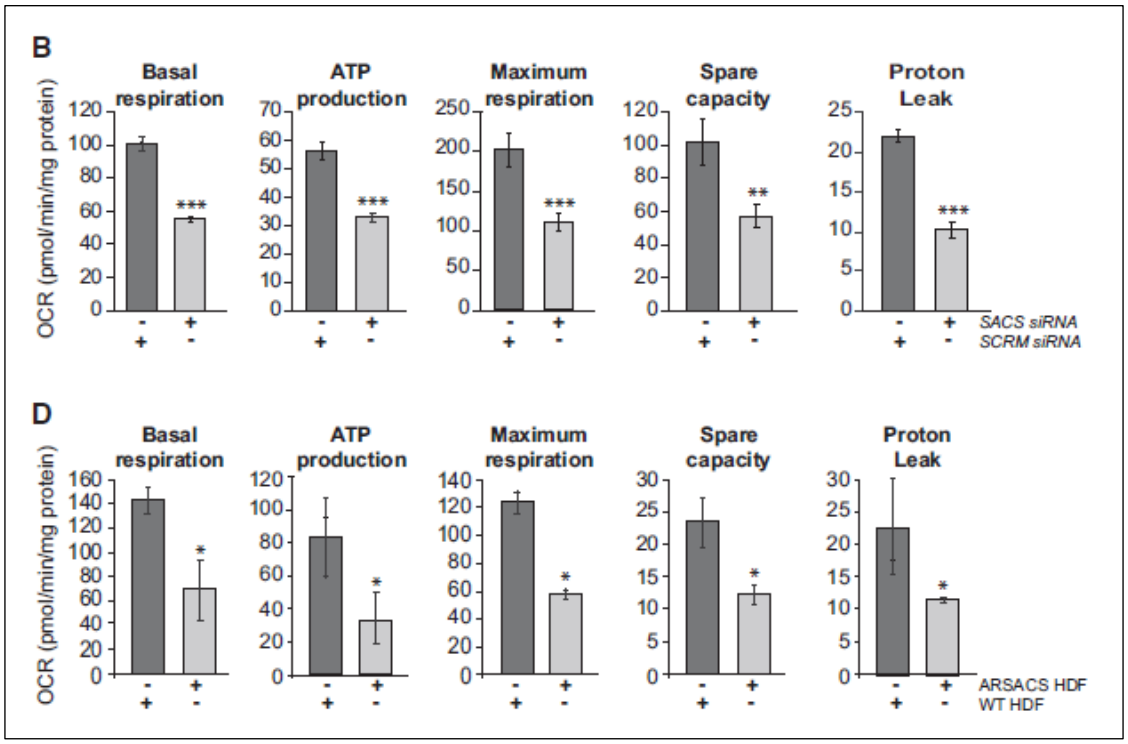

Figure 21_Intro. Bioenergetics function of mitochondria is impaired in *SACS* knockdown and ARSACS patient cells. (B-D) Comparison of basal respiration, ATP production, proton leak, maximum respiration and spare capacity in cells transfected with siRNAs targeting *SACS* and control siRNAs (B) and in ARSACS patient and control fibroblasts (D)[96].

Another aspect of mitochondrial biology affected in the absence of sacsin is mitochondrial transport and localization within neurons. siRNA-mediated *Sacs*-knockdown in cultured murine hippocampal neurons showed indeed a reduced number of mitochondria localized to distal dendrites and an abnormal accumulation, as well as aggregation of mitochondria in the soma and proximal regions of dendrites (Fig. 22_Intro)[90]. In these neurons, dendrite morphology was altered (observing a reduction in number and thinner diameter) with respect to controls (Fig. 22_Intro)[90]. Although hippocampal neurons seem not to be involved in ARSACS, hence not being the best model to study mitochondrial dynamics, this result indicates a mitochondrial defective transport [97].

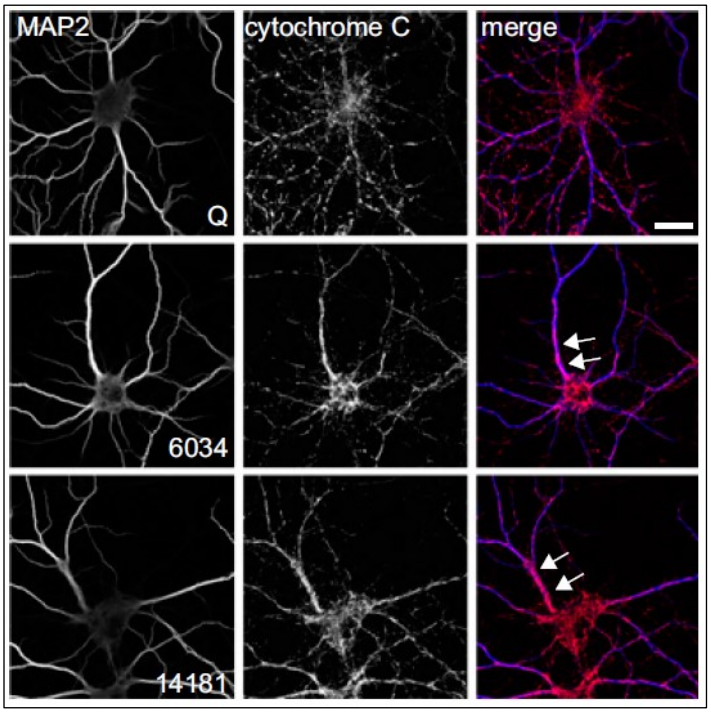

Figure 22_Intro. Sacsin loss of function alters the distribution of mitochondria in neurons. Cultured hippocampal neurons transfected with *Sacs* (6034 and 14181) and scrambled siRNA immunodecorated with antibodies directed against Cytochrome C (in red). Arrows indicate accumulated mitochondria in proximal dendrites[90].

In conclusion, ARSACS cellular model showed two main pathological phenotypes: IF accumulation and altered mitochondrial dynamics, bioenergetics and trafficking. However, which of these phenotypes is the earliest one in ARSACS pathological cascade, and their relevance in PCs is still not clear.

5. Mouse models of ARSACS pathophysiology

5.1 *Sacs*$^{-/-}$ mouse model

Both bioinformatics and *in vitro* approaches illustrated so far have intrinsic limitations as they cannot assess or predict the function of sacsin protein in the context of a complex living organism. Moreover, cellular models used *in vitro* were not the primary cell types involved in ARSACS pathogenesis. To study sacsin function in a physiological context, *Sacs*$^{-/-}$ mice have been generated by gene targeting in ESCs cells and their characterization was assessed in two different works[90] [98]. Because they recapitulate main ARSACS symptoms, these murine lines represent good models of ARSACS pathogenesis. In detail, *Sacs*$^{-/-}$ mice show early onset ataxia and motor deficit starting from 40 days of age and definitely overt at 3 months of age, when beam walking and rotarod test underlined balance defects and general motor incoordination,

respectively. These deficits progressively get worse (Fig. 23_Intro)[98]. Moreover, at similar stage (4 months of age) *Sacs*$^{-/-}$ mice develop associated muscular wasting and weakness as showed by inverted grid test (Fig. 23_Intro), as described in ARSACS patients[98].

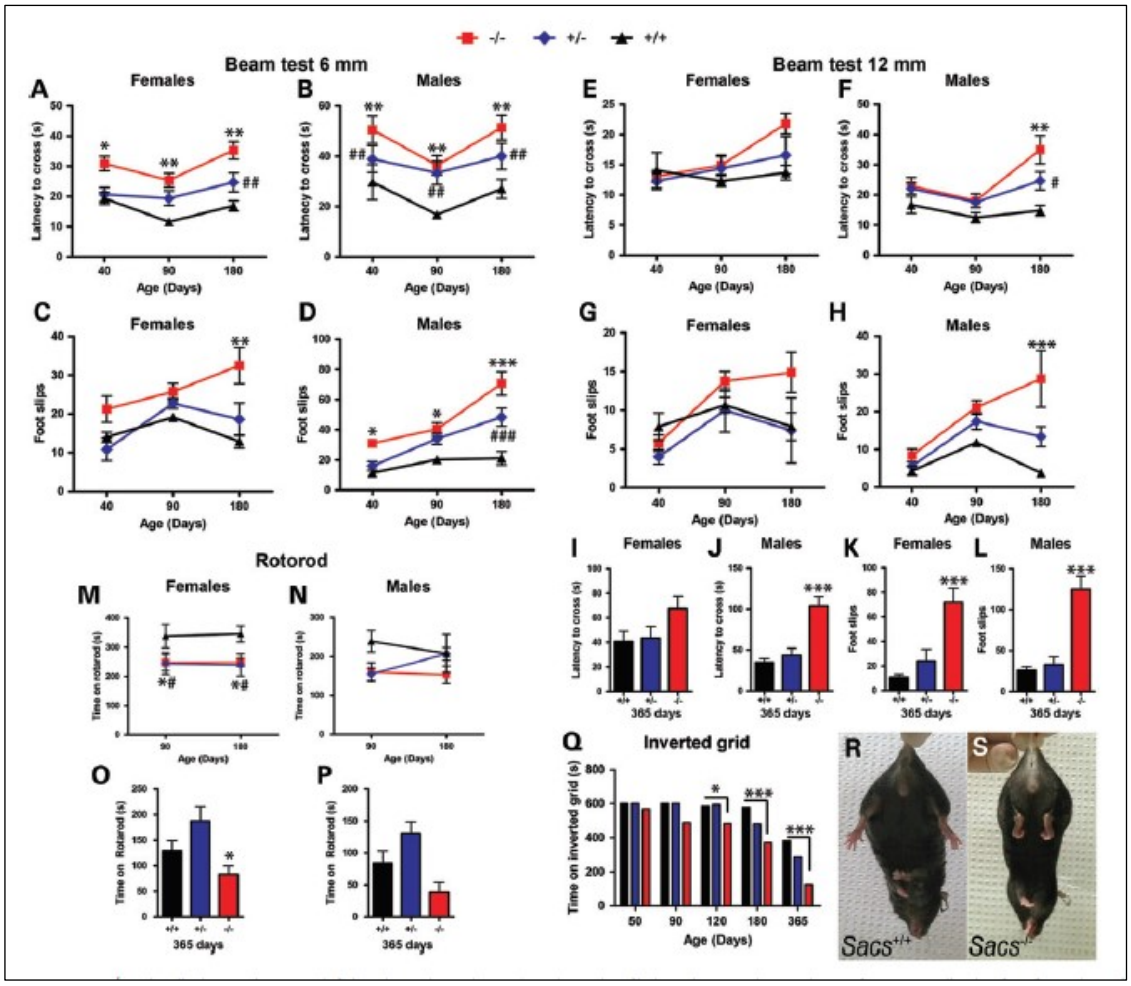

Figure 23_Intro. *Sacs*$^{-/-}$ mice display ataxia, motor deficit and muscle weakness. (A-P)Results of balance beam and rotarod tests of motor coordination at 40, 90 and 180 days of age; (Q) Inverted grid test of mice at 50–365 days; (R-S) Representative hindlimb clasping reflex exhibited from 1-year-old *Sacs*$^{-/-}$ (S) and wild-type (R) mice[98].

As further evidence of cerebellar ataxia, *Sacs*$^{-/-}$ mouse model manifests PC loss quite early by 3 months of animal life, and this PC degeneration is prominent in the anterior lobules of cerebellum, similar to ARSACS patients (Fig. 24_Intro)[98]. However, unlike patients, PC loss in *Sacs*$^{-/-}$ mice is not limited to vermis, but spreads to cerebellar hemispheres. Moreover, PC axons show progressive swelling starting from 1 month of age, suggesting that there is an axonal degeneration that precedes the loss of the cell body (Fig. 24_Intro)[98]. Although silver staining of corticospinal tract shows signs of neurodegeneration suggesting spasticity, histological examination does not reveal, differently from ARSACS patients, morphological alteration or reduction of axon number in mice up to 2 years of age[98]. On the contrary,

peripheral neuropathy is observed in *Sacs*$^{-/-}$ mice as reduction (of about 25% in respect to control) of spinal motor neurons total number at 2 years of age and reduction of myelinated axons larger than 7-10 µm in diameter with concomitant increased percentage of myelinated axons of smaller dimension (3-4 µm)[98]. However, spasticity and neuropathy were found only at late stages of disease progression underlining that the *Sacs*$^{-/-}$ mouse model manifests mainly an ataxic phenotype.

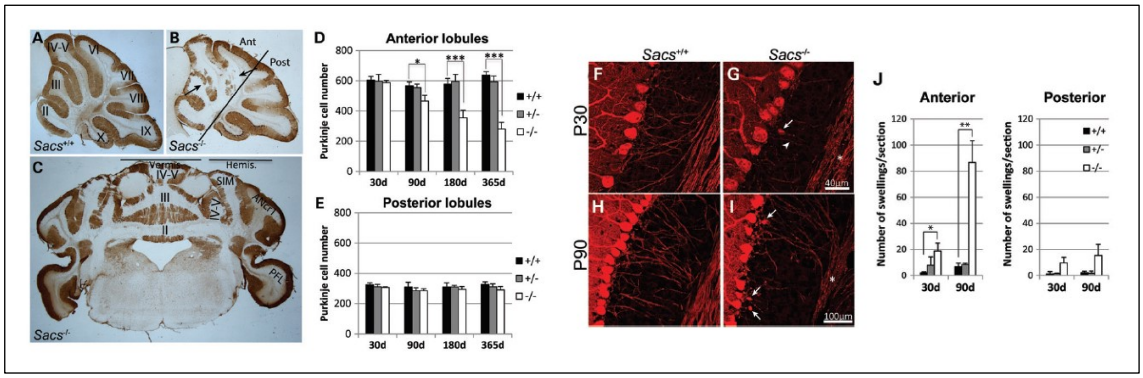

Figure 24_Intro. Progressive PC loss and axonal swellings in *Sacs*$^{-/-}$ mouse. (A-E) Anti-calbindin immunohistochemistry on mid-sagittal brain sections from 365-day-old *Sacs*$^{+/+}$ (A) and *Sacs*$^{-/-}$ (B) mice, and PC count in the cerebellar anterior (D) and posterior (E) lobules. (G-J) Anti-calbindin labeling of cerebellar parasagittal brain sections of 30-day-old *Sacs*$^{-/-}$ mice to investigate dystrophic axons (asterisk and arrowhead in G) in *Sacs*$^{+/+}$ mice compared with controls (F-I). And relative quantifications (J)[98].

NFs, the IF expressed by neurons, consist of three subunits, light (NFL), medium (NFM) heavy (NFH) chain molecular weight, that undergo cytoskeletal phosphorylation and dephosphorylation cycles[99]. Immunohistochemical examination of P14 *Sacs*$^{-/-}$ mice compared with wild-type controls revealed accumulation of NFH, marked with pan-NFH antibody (that recognizes both phosphorylated and non-phosphorylated NFH subunit), in proximal dendrites in many areas of central nervous system, especially in thalamus, PCs and DCN in cerebellum, and superior olivary nucleus (Fig. 25_Intro)[98]. The deregulation in NF distribution was found to be the first sign of cytopathological alteration, both in *Sacs*$^{-/-}$ mice and in ARSACS patient neurons[98]. This evidence was further confirmed by immunolabeling with antibody against NFH in 4-week old dissociated spinal cord culture: bundling of NFs was detected in the soma of *Sacs*$^{-/-}$ motor and sensory neurons[95]. A similar accumulation of NFH in proximal dendrites was also observed in corticospinal neurons of layer 5 and in PCs from an ARSACS patient (Fig. 25_Intro)[98]. Immunofluorescence of PC layer in tissue sections derived from *Sacs*$^{-/-}$ mice with antibodies specific for npNFH (SMI32) showed increased signal in soma and dendrites in respect to wild-type mice, whereas staining with antibodies specific for pNFH (SMI31) failed to show significant differences[98]. Similar results, increased npNFH to total NFH ratio in *Sacs*$^{-/-}$ mice relative to controls and unchanged levels of pNFH, was confirmed also by Western Blot (WB)

on cerebellar extracts, with pan-NFH and npNFH immunodecoration[98]. In wild-type motor neurons the NF network are distributed neatly along the entire soma, while in *Sacs*$^{-/-}$ mouse model motor neurons, NFs fuse into linear bundles and in dorsal root ganglia (DRG) sensory neurons they form juxtanuclear balls similar to vimentin bundles in fibroblasts previously described[95].

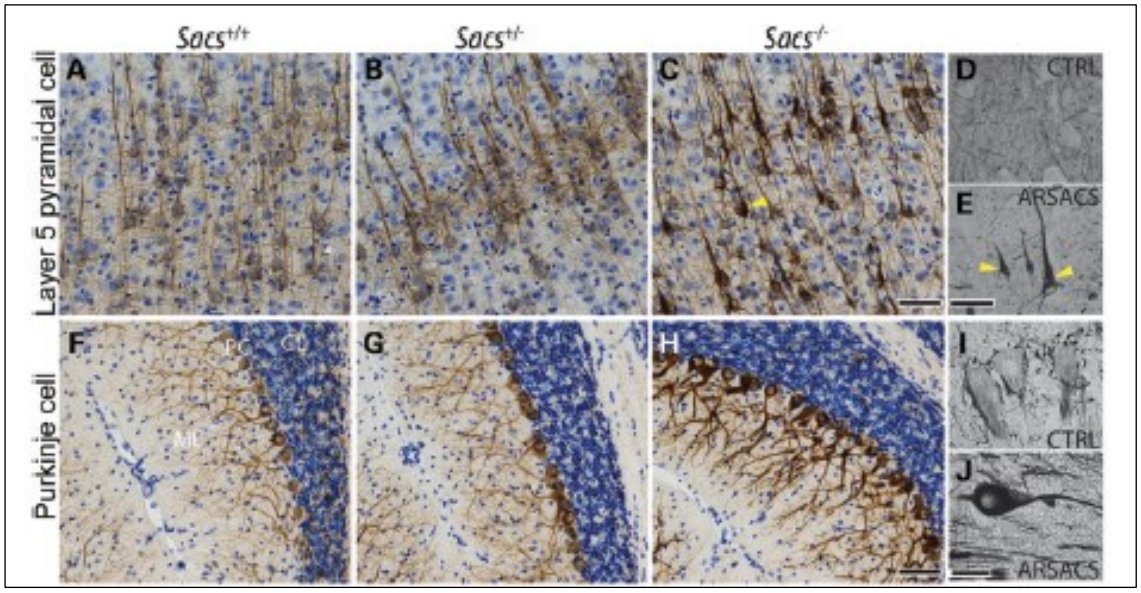

Figure 25_Intro. NF accumulations in *Sacs*$^{-/-}$ and ARSACS neurons. (A-J) NFH immunohistochemistry on sagittal brain sections of 180-day-old mice (A-C, F-H) and on brain sections from a human control autopsy case (D and I) and one ARSACS case (E and J)[98].

In a recent work, Gentil et al. further demonstrated on *Sacs*$^{-/-}$ mouse model the role of sacsin in regulating NF dynamics[88]. After reconfirming the presence of NF bundles in cultured spinal motor neurons and DRG neurons derived from *Sacs*$^{-/-}$ mice, they detected all the components of NFs bundles by immunohistochemistry: NFL, NFM, NFH, peripherin and a-internexin (Fig. 26_Intro)[88]. Transmission electron microscopy (TEM) showed NFs bundles extending from around the nucleus and coursing through dendritic processes and organelles (Fig. 26_Intro), including mitochondria, largely excluded to the periphery[88], in line with what observed for ARSACS patient fibroblasts[95]. Strikingly, the microinjection of plasmids encoding full-length sacsin GFP-tagged in 6-wk-old *Sacs*$^{-/-}$ spinal cord DRG culture resolves NF bundles after 2 days (Fig. 26_Intro)[88]. Moreover, EGFP sacsin was found to embrace NFs bundles, indicating a strong association (Fig. 26_Intro)[88]. In addition, by FRAP experiments on NFH-GFP in motor neurons, turnover of NF bundles resulted impaired, but not absent, compared to physiologically distributed NF turnover. On the contrary, turnover of normally distributed NF in *Sacs*$^{+/+}$ and *Sacs*$^{-/-}$ mouse cells was comparable, implying a secondary, rather than primary, defect, perhaps due to impaired access of necessary factors into the packed NF[88].

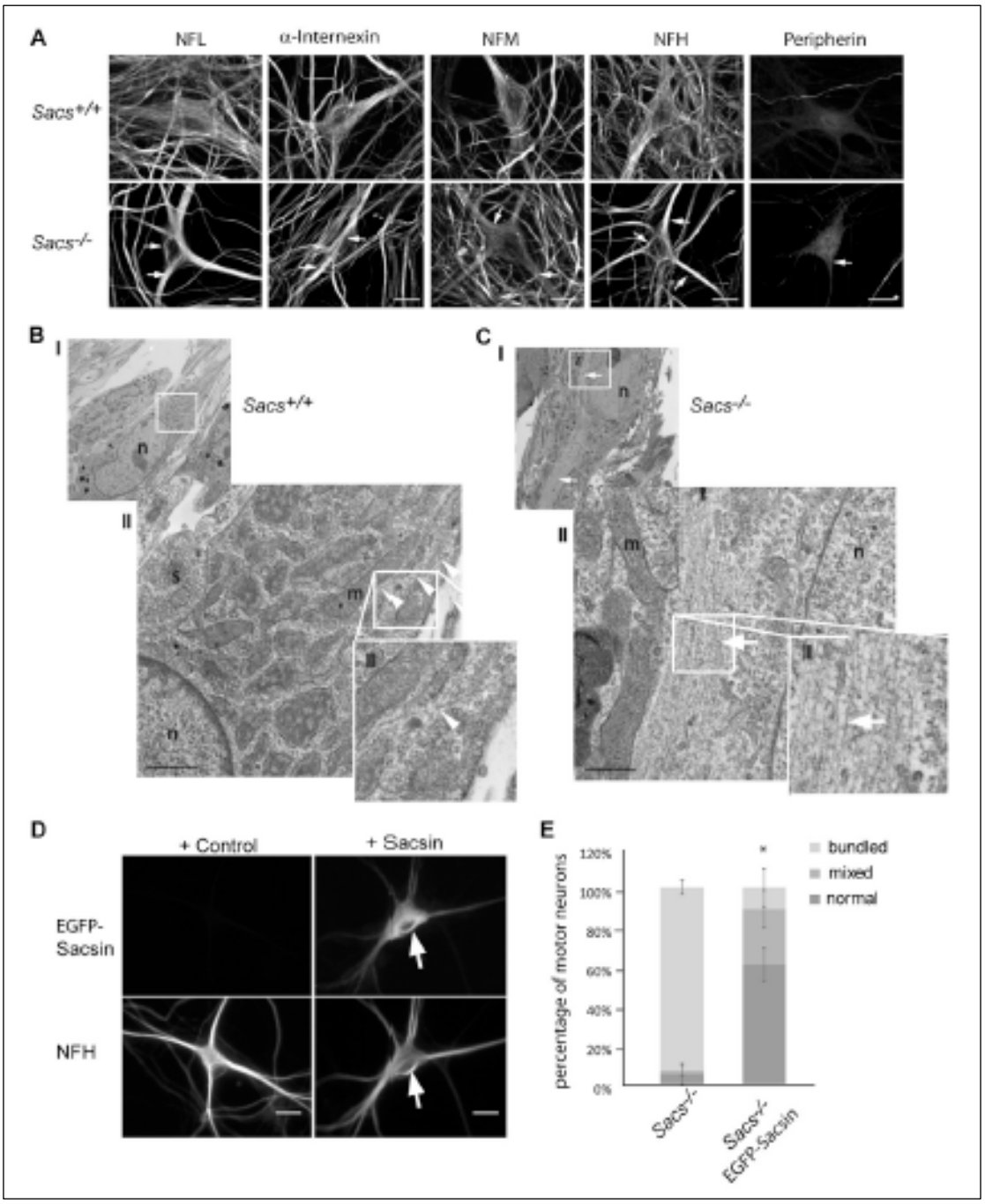

Figure 26_Intro. Loss of sacsin induces bundling of NF containing multiple NF proteins. (A) Representative images of motor neurons in 3-wk-old dissociated spinal cord DRG cultures; (B-C) Representative electron microscopy images of motor neurons in 6-wk-old dissociated spinal cord DRG cultures (*Sacs*$^{+/+}$ and *Sacs*$^{-/-}$); (D) Resolution of NF bundles in neurons ectopically expressing full-length sacsin; (E) Quantitation of the effect of EGFP-sacsin on the presence of NF bundles in *Sacs*$^{-/-}$ motor neurons as the percentage of neurons exhibiting a normal NF network, NF bundles, or mixed[88].

Finally, Ady et al. tested electrophysiological parameters of *Sacs*$^{-/-}$ PCs. In this contest, they proved the alteration of glutamatergic synaptic transmission after the onset of motor phenotype. In fact, the measure of excitatory post-synaptic currents (mEPSC) showed

enhanced amplitude and reduced frequency (Fig. 27_Intro, upper part)[100] suggesting altered glutamatergic inputs to *Sacs*$^{-/-}$ PCs. Moreover, since PC death occurs predominantly in anterior lobules, they examined PC spiking output recording fired action potentials in anterior lobule III in P40 *Sacs*$^{-/-}$ mice and wild-type controls. They observed firing rates of *Sacs*$^{-/-}$ PCs were lower, covering a narrower range of frequencies, but without significant difference in the regularity of firing (Fig. 27_Intro, lower part)[100]. They also verified the changes in firing were observed also at earlier stages (P20) in anterior lobules that later exhibit PC death, but not in posterior lobules that are unaffected[100]. Moreover, they demonstrated that at high current injection amplitudes *Sacs*$^{-/-}$ PCs fire at significantly reduced frequencies compared to wild-type PCs[100]. However, no significant difference were observed in the maximum instantaneous firing frequency[100]. These results suggest that reduced PC firing frequency in *Sacs*$^{-/-}$ mice may be linked to their inability to sustain high-frequency firing. To confirm functional GABAergic pre-synaptic terminals, they found comparable number of puncta that stain for a pre-synaptic GABA terminal marker (VGAT) that co-localizes with calbindin-positive puncta, suggesting normal synaptic output in the DCN[100].

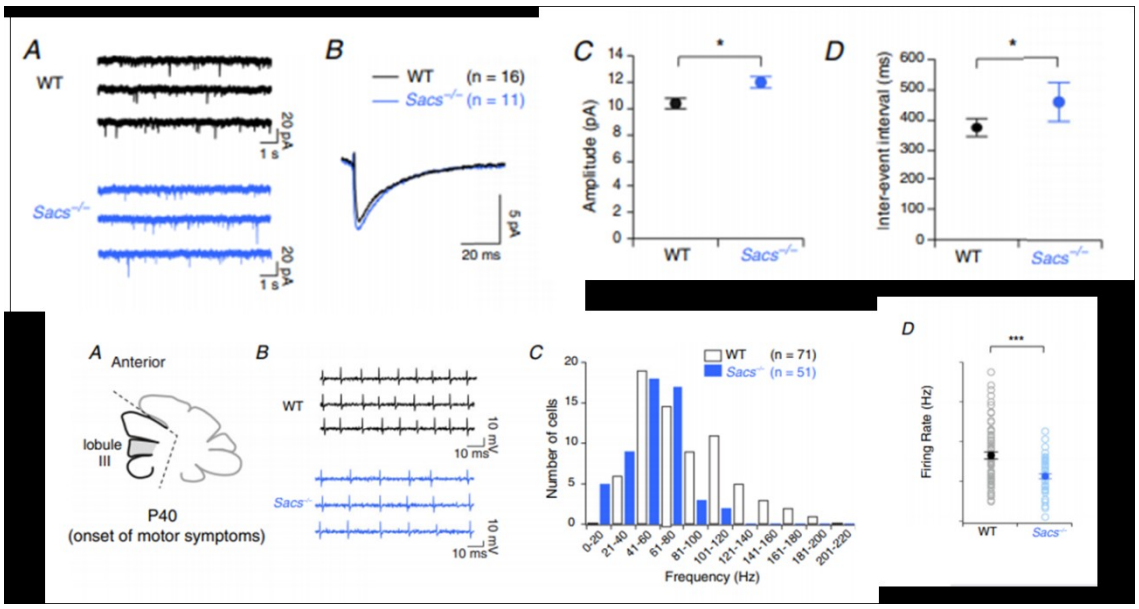

Figure 27_Intro. *Sacs*$^{-/-}$ PCs show altered glutamatergic input and reduced firing rate. Upper part: (A) Sample traces of AMPA-mediated miniature current recordings from representative wild-type (top, black) and *Sacs*$^{-/-}$ PCs (bottom, blue); (B) Average traces of AMPA-mediated mEPSCs from wild-type and *Sacs*$^{-/-}$ Purkinje cells; (C-D) Average measurements of mEPSC amplitude (C) and inter-event interval (D in wild-type and *Sacs*$^{-/-}$ PCs. Lower part: (B)Sample spike trains from representative wild-type (top, black) and *Sacs*$^{-/-}$ (bottom, blue) PCs from anterior lobule III; (C-D) Frequency histogram of PC firing (C) and firing rate (D) observed in *Sacs*$^{-/-}$ mice[100].

5.2 *Sacs*$^{R272C/R272C}$ KI mouse model

In ARSACS, have been described several types of mutations that spread over the entire *SACS* gene length. However, in ARSACS mutations spectrum, the most common type of mutations are missense mutations[73]. Furthermore, SIRPT (Sacsin Internal RePeaTs) repeated regions make up more than 80% of the total sacsin protein, so having a SIRPT mutated mouse model would help to better understand the sacsin function. For these reasons, a novel *Sacs*^{R272C} (c.816C > T) knock-in (KI) mouse model have been generated by Brais group using traditional gene targeting techniques[89]. This mutation lies at the end of the homologous HATPase_C domain in the first sr1 and it was described in homozygote state in two cases in Canada[101]. Molecular analysis shows a striking reduction of sacsin protein in *Sacs*^{R272C} mice compared to controls and heterozygous mice, while no difference in *Sacs* mRNA was observed between *Sacs*^{R272C} mice, heterozygous mice and controls (Fig. 28_Intro)[89].

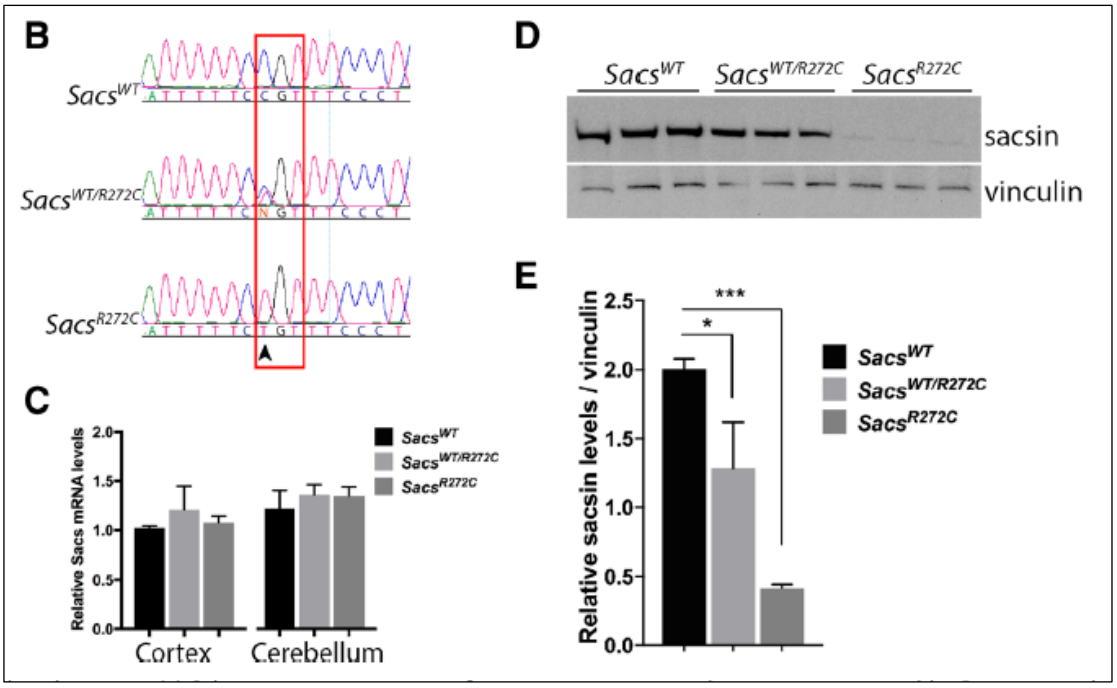

Figure 28_Intro. *Sacs*^{R272C} KI mice. (B) Sanger sequencing of mouse tail genomic DNA; (C) qRT-PCR of RNA purified from cortex and cerebella showing no significant difference between *Sacs* RNA levels of R272C, heterozygous and control mice; (D-E) WB analysis reveals significant reduction in mutant sacsin protein levels in cerebella of *Sacs*^{R272C} and heterozygous mice (D) and protein level quantification (E)[89].

Sacs^{R272C} mice display an early balance deficit (mostly males) and muscle weakness comparable though possibly a little milder to the one observed in the *Sacs*$^{-/-}$ mice, while no general motor coordination impairments have been assessed[89]. Nissl-stained sections from 45 days-old *Sacs*^{R272C} mice demonstrate normal cerebellar structure and lobulation compared to age-matched controls, but a significant PC loss in the anterior lobules was detected starting at 90

days of age, as observed in *Sacs*$^{-/-}$ mice, progressing through one year of age[89]. Unlike *Sacs*$^{-/-}$ mice, PC loss also in the posterior lobules was found in one-year-old *Sacs*^{R272C} mice[89]. Moreover, P90 *Sacs*^{R272C} mice PCs present also a ~ 25% reduction in their firing frequency, similar to the reduction found at earlier ages in *Sacs*$^{-/-}$ mice[89].

To explore if *Sacs*^{R272C} mice present the same characteristic IF bundling as *Sacs*$^{-/-}$ animals, immunolabeling using a pan-NFH antibody was performed on sagittal brain section from 300 days-old mice[89]. *Sacs*^{R272C} mice, in line with *Sacs*$^{-/-}$ mice, display distinct NFH somatodendritic labeling in several CNS neuronal populations (e.g., cerebellar PC, neurons in layer II-III and V of the isocortex, CA1, CA2 and CA3 pyramidal neurons of the hippocampal formation and neurons in the thalamus).

Moreover, NFH immunofluorescence show strong labeling in PC dendrites as well as in cell bodies compared to very light immunolabeling in controls and heterozygous animals[89]. NFH labeling in *Sacs*^{R272C} mice identifies mislocalization of NFH in PC bodies and dendrites compared to controls where no NFH is detected in these cellular compartments. WB analysis revealed an increase in both, NFH protein levels, as well as, most significantly, in the npNFH, which has also been previously reported in the *Sacs*$^{-/-}$ mice[89].

In conclusion, *Sacs*$^{-/-}$ and *Sacs*^{R272C} mouse models well recapitulate the main alterations of ARSACS. They present the same phenotype, showing ataxia due to cerebellar degeneration, with loss of PCs, neuropathy and consequent muscle wasting, although spasticity seems to be less severe than in patients[98] [89]. Moreover, both *Sacs*$^{-/-}$ and *Sacs*^{R272C} PCs present NFH and npNFH accumulation in the somatodendritic region of neurons. This accumulation is in line with vimentin bundling observed in study on ARSACS cellular model[95]. For this reason, it provides suitable tools to further investigate ARSACS cytopathology and therapeutic treatments.

II. Aim of the work

ARSACS is a childhood onset neurodegenerative disease mainly characterized by cerebellar ataxia later associated with lower limb spasticity and peripheral neuropathy.

ARSACS is caused by mutations in *SACS* gene, one of the biggest genes in the human genome and, so far, more than 200 loss-of-function mutations have been identified worldwide. *SACS* gene encodes for sacsin, a huge multimodular protein highly expressed in CNS and in particular in cerebellum, with the highest levels in PCs. Loss of PCs is indeed the prominent neuropathological feature of both ARSACS patients and ARSACS mouse models.

Although several studies have been performed, most of them in cellular models, sacsin function is still unknown and ARSACS molecular pathogenetic cascade remains largely unclarified.

To date, the cooperative work of several groups showed that the absence of sacsin has two main consequences: (i) the alteration of mitochondrial dynamics and bioenergetics, and (ii) the remodeling of intermediate filament cytoskeleton. However, how these phenotypes are mechanistically interlinked and how they cause PC degeneration remains unclear. The major limitation of the published studies is that they were performed in cell models (patient fibroblasts, *SACS*$^{-/-}$ HEK293 cells or undifferentiated *SACS*$^{-/-}$ SH-SY5Y cells) or in primary neurons not primarily affected in the disease (DRGs). Up to now, a detailed study of ARSACS pathogenesis, which uncovers the relevance of the above-mentioned phenotypes specifically in PCs, is missing. The incomplete knowledge of ARSACS pathogenesis entails the lack of specific medication. In fact, no treatments are available for ARSACS patients so far.

My PhD thesis work aimed at dissecting and targeting ARSACS pathogenesis, with a special focus on PC degeneration, which is the prominent and earliest feature of the disease. To this end, my studies were primarily conducted *ex vivo* in primary cerebellar cultures enriched in PCs and *in vivo* in cerebellum, taking advantage of the *Sacs*$^{-/-}$ mouse model generated by our collaborators in Canada.

In the first part of the work, I investigated in depth NF accumulation in PCs. I performed a time course analysis *in vivo* and *ex vivo* to understand how early this phenotype arises, and also imaging and EM analyses to better understand its cerebellar and subcellular localization.

Then, I dissected the consequences of aberrant NF accumulation on organelle trafficking in *Sacs*$^{-/-}$ PCs and consequently on Ca^{2+} homeostasis. In this context, by exploiting two *in vitro/ex vivo* models recapitulating ARSACS features (*SACS*$^{-/-}$ SH-SY5Y cells differentiated into neurons and primary PCs) integrated with different OMICS approaches (proteomics and transcriptomics *in vivo*), I managed to improve the dissection of ARSACS pathogenetic cascade. Also, I unravelled new interesting deregulated pathways caused by the absence of sacsin and discovered additional key players involved in ARSACS pathogenesis.

These mechanistic studies provided us a strong rationale to test a pharmacological treatment in the *Sacs*$^{-/-}$ mouse. We employed a repurposed drug, Ceftriaxone, which targets Ca^{2+} homeostasis, a feature common to several ataxias. The drug treatment resulted successful at both pre- and post-symptomatic stages, opening new perspectives for ARSACS treatment. Furthermore, the detailed comprehension of the mechanism by which Ceftriaxone exerts its efficacy allowed us to uncover a new possible feature of ARSACS pathogenesis, which could be also targeted for therapy.

III. Material & Methods

Declaration

This thesis has been composed by myself and has not been used in any previous application for a degree. Throughout the text I use both "I" and We" interchangeably. All the results presented here were obtained by myself, except for the data in Fig. 10_Results (immunoprecipitation of sacsin in SH-SY5Y cells).

Animals and drug administration

In this study, we used the Sacs$^{-/-}$ mouse model[98]. *Sacs*$^{-/-}$ and wild-type littermates (which were the experimental subjects) were obtained by breeding *Sacs*$^{+/-}$ male and female mice. Experiments involving animals were performed in accordance with experimental protocols approved by the IACUC of San Raffaele Scientific Institute.

For the pre-symptomatic treatment, Ceftriaxone (Fidia Farmaceutici) was administered monthly to 1-month-old mice (2 months before the onset of motor impairment in *Sacs*$^{-/-}$ mice[98]) by daily intraperitoneal (i.p.) injection at dose of 200 mg/kg body weight for 5 consecutive days[66] till 5-month-old. Instead, for the post-symptomatic treatment, Ceftriaxone was administered monthly to mice at 5 months of age by daily i.p. injection at dose of 200 mg/kg body weight for 5 consecutive days till the stage of 7 months of age.

Behavioural tests

Beam-walking (BW) test to assess motor balance was performed for 3 consecutive days (in each day the mice performed 3 trials on the beam, 7mm x 90cm suspended 40cm above bedding), after two days of training. The number of hindfoot missteps and the time required to cross the beam (latency) was evaluated, as previously described[68]. The mean of all the trials was scored.

Rotarod test was set up to investigate motor coordination at late stages. After 2 days of intensive training (3 session per day at the beginning with fixed speed at 4 rpm and then with

acceleration from 4 to 40 rpm), mice were tested for resistance to run on rotating rod (4-40 rpm in 5' interval of time). Latency time until the mouse falls from the rod was recorded and the mean of 3 day trials was scored[102].

Finally, Novel Object Recognition Test (NORT) was used to explore cognition. Mice were first habituated to the arena (plexiglass 53x38x21) in the absence of objects for 15' (day1, in the morning). On the same day, in the afternoon, two similar objects were presented to each mouse for 10' (A' and A"), after which the mice were returned to their home cage. 24h later, the same animals were tested for 10' in the arena with a familiar object (A') and a new object (B, different for shape, colour and texture). The index of discrimination was calculated as percentage of new object B preference: (time exploring each object) / (time exploring both objects) x 100[103].

Histological analyses

For histological analyses, mice were sacrificed in the presence of anaesthesia (2,2,2-Tribromoethanol, Sigma-Aldrich). Transcardially perfusion was performed and then the cerebellum was isolated. For histology tissues were fixed in 4% paraformaldehyde-2,5M glutaraldehyde in 0,12M cacodylate buffer solution. 1µm semithin sections of cerebellum were cut and stained with toluidine blue. Images of anterior lobules of cerebellum were acquired on Olympus BX51 microscope equipped with a 20X objective lens (Leica Microsystems). While for immunohistochemistry (IHC) assays, after tissue isolation, cerebella were fixed in 4% paraformaldehyde (2h, 4°C), then dehydrated in 30% sucrose solution (over/night, 4°C) and finally included in optimal cutting temperature solution. Cryostat sagittal slices were cut at the thickness of 20µm.

Electron Microscopy analysis

Electron Microscopy (EM) were done in collaboration with the Unit of Neuropathology of San Raffaele Institute. Cerebella were incubated in glutaraldehyde fixative to perform standard EM experiments. Several cells were evaluated in a single sample for a total 3 *Sacs*$^{-/-}$ versus 3 wild-type tissues.

SDS-PAGE and WB analysis

For WBs, briefly, tissues were homogenized in 100 mM Tris-HCl (pH 7.4), 1 mM EDTA (pH 8), 1% Triton X-100 and 150 mM NaCl supplemented with Protease Inhibitor Cocktail (PIC, Sigma-Aldrich) and Phosphatase Inhibitor Cocktail (Merck) using a Dounce homogenizer and incubated for 30' on ice. Cell debris were discarded by centrifugation at 18000 g for 10' at 4°C. Commercially available antibodies were used for the detection of NFL, CaMKIIβ and pCaMKIIβ (Santa Cruz Biotechnology Inc.), NFM and pNFH (Biolegend), npNFH (Calbiochem, Merck KGaA), sacsin and plectin (Abcam), IP3R1 (Novus Biologicals), and calnexin (Sigma-Aldrich, Merck KGaA). Secondary antibodies included Horseradish Peroxidase (HRP)-conjugated anti-mouse and anti-rabbit IgG (Amersham Bioscience).

Co-immunoprecipitation

SH-SY5Y cells were collected and freshly lysed in lysis buffer (5 mM EDTA pH 8.0, Triton X-100 0,1% in PBS1X and PIC (Sigma-Aldrich, Merck KGaA)) with a Dounce homogenizer. Total homogenate was centrifuged 8000 g for 10' at 4°C to discard cell debris and supernatant was collected. 1 mg of total protein lysate was incubated 2h with magnetic Dynabeads Protein A (ThermoFisher Scientific) to depauperate the lysate from aspecific interactions with the beads; new Dynabeads Protein A were linked to the antibody (6 ug per mg of lysate) for 30' at room temperature and after 3 washes in lysis buffer, Dynabeads-antibody complex was incubated with the precleared lysate over/night at 4°C on a wheel. After 5 washes in lysis buffer, the antigen was eluted from the Dynabeads-antibody complex in Urea 8 M Tris-HCl pH 8 on rotation for 30'. Immunoprecipitated eluates were sent to Mass Spectrometry facility for LC-MS/MS and/or loaded on SDS-PAGE for WB analysis.

Proteomics analysis: Mass Spectrometry

Mouse cerebella (6 months of age) or neuron differentiated-SH-SY5Y cells were lysed in 8 M Urea, 100 mM Tris-HCl pH 8 and PIC in a Dounce homogenizer, then centrifuged 4000g for 20' at 4°C to eliminate unbroken tissue or cell debris, and then quantified by Bradford analysis.

Samples were processed by powerful technology of Label Free Quantitation (LFQ)[104] in collaboration with the proteomics facility Cogentech (IFOM, Milan). To determine the significance of the differential proteins was used the cut-off determined by LogFoldChange > 0,39 and p value < 0,05. The significant deregulated proteins obtained in this way were

submitted to GProfiler Enrichment analysis (https://biit.cs.ut.ee/gprofiler/gost)[105] in order to identify the Gene Ontology (GO) categories involved in phenotypic changes due to sacsin depletion.

Transcriptomics analysis: RNA sequencing

Standard RNA sequencing analysis was performed on total RNA extracted from cerebellum with RNeasy kit (Qiagen) as described in the datatsheet. Libraries were prepared using True-Seq® stranded mRNA® for mRNA Sequencing (Illumina, San Diego, CA), according to the manufacturer's instructions. Sequencing was performed on a NextSeq 500 machine (Illumina, San Diego, CA) obtaining 30 million single-end reads per sample on average. Only genes with a Counts per million (CPM) value higher than 1 in at least three samples were retained. Gene expression read counts were exported and analysed in R environment (v. 3.6.2) to identify differentially expressed genes (DEGs). The DEG analysis was performed with the package DESeq2 available in Bioconductor comparing different experimental groups. To determine the significance of the differential genes was used the cut-off determined by FDR filter (Adjusted p_value < 0,1), more trustable filter as based on the p_adj value, which is corrected to avoid false positives (caused by the presence of outliers). It is also able to detect smaller differences (lower log_2FC), shared by all the samples of a group. The significant deregulated genes obtained in this way were submitted to GProfiler Enrichment analysis[105] in order to identify the GO categories involved in phenotypic changes due to a variable (genotype or treatment).

Transcriptomic data were also validated by quantitative Real-Time PCR (qRT-PCR). cDNA was generated using SuperScript IV Reverse Transcriptase kit (Invitrogen) and processed by qRT-PCR using the SYBR green chemistry (Light cycler 480, SYBR green I master, Roche) to evaluate gene expression levels. Specific PCR-primer sequences were the following:

Gene	Sequence
Nefh FW	AAGCACCAAGGAGTCACTGG
Nefh REV	ACTCGGACCAAAGCCAATCC
Lcn2 FW	AGCTACAATGTCACCTCCATCC
Lcn2 REV	TGGCGAACTGGTTGTAGTCC
Pycard FW	CACAGAAGTGGACGGAGTGC
Pycard REV	AGGTCCATCACCAAGTAGGG
Tyrobp FW	GTGACACTTTCCCAAGATGC
Tyrobp REV	CTGGTCTCTGACCCTGAAGC
Hprt1 FW	ACATTGTGGCCCTCTGTGTG
Hprt1 REV	TTATGTCCCCCGTTGACTGA

Primary PC cultures

To obtain primary PC cultures, a modified version of previously described protocol developed in the lab[106] was used. Cerebella from newborn mice were incubated in HBSS 1X (Invitrogen) containing 0,5 U/ml papain (Sigma-Aldrich, Merck KGaA), 1,25 mM cystein-HCl, 0.025 mM EDTA, and 1 mg/ml DNase I (EMD Millipore) for 30' at 37°C. Tissues were then dissociated by mechanical trituration. The reaction was blocked with 10% horse serum (Invitrogen), and samples were centrifuged at 200 g for 10'. The cellular pellet was washed twice in HBSS 1X and re-suspended in cultured medium containing Neurobasal Plus (Invitrogen), B27 Plus supplement (Invitrogen), 200 mg/ml D-glucose, 2 mM GlutaMax (Invitrogen), 100 U/ml PenStrep (Invitrogen), 1% horse serum (Invitrogen), 3 mM KCl, and 50 ng/ml neuronal growth factor (NGF) 2.5S (Envigo). Cells were plated at a density of $1,5 \times 10^5/cm^2$ on coverslips (13 mm or 24 mm in diameter) coated with 0,1 µg/µl Poly-L-Lysine (Sigma-Aldrich, Merck KGaA).

Immunofluorescence assays

For immunofluorescence experiments, fixed cells were blocked and permeabilized with 10% goat serum and 0,5% Triton X-100 in PBS 1X solution (1h, RT), and then incubated in 5% goat serum and 0,2% Triton X-100 in PBS 1X solution with primary antibodies (over/night, 4°C): rabbit anti-calbindin 28 kDa (300; Swant), mouse anti-calbindin (Synaptic System), mouse anti-OxPhos complex IV subunit I (Invitrogen), rabbit calreticulin (Sigma-Aldrich, Merck KGaA),

mouse anti-non-phosphorylated NFH (SMI32, Calbiochem, Merck KGaA), anti-rabbit GFAP (Dako), anti-rabbit Iba1 (Wako). Secondary Antibodies conjugated with Alexa 488 and Alexa 596 (Invitrogen) were added in 5% goat serum and 0,2% Triton X-100 in PBS 1X solution (2h, RT) and finally DAPI staining was performed (5', RT).

Morphometric analyses of primary PCs

Stacks of consecutive confocal images of immunofluorescence performed on primary PCs were taken at 0,1 µm intervals using the UltraVIEW Confocal Microscope (PerkinElmer). Analyses of soma and dendrite area and mitochondria volume were performed using Volocity 3D Image Analysis Software (version 5.5.1, PerkinElmer). For mitochondrial and ER volume evaluation, a region of interest (ROI) was drawn to cover the profile of each PC (or dendrites only). A threshold for red signal (mitochondria) and green signal (PCs) was set to exclude the background. We considered mitochondria belonging to PCs those with red signal exclusively intersecting the green signal.

Ca^{2+} imaging

Basal levels of cytosolic [Ca^{2+}] measurements were performed as previously described[107]. Fura-2 acetoxymethyl ester (Calbiochem, Merck KGaA) loading was performed at 37°C (4 µM, 40') in Krebs' Ringer's HEPES buffer (containing 5 mM KCl, 125 mM NaCl, 2 mM $CaCl_2$, 1,2 mM $MgSO_4$, 1,2 mM KH_2PO_4, 6 mM glucose and 20 mM HEPES pH 7.4). In this way when the K^+ concentration was increased in the solution, the concentration of Na^+ was adjusted to maintain isotonicity. Excitation wavelengths of 340 and 380 nm were used with an emission wavelength of 510 nm. The 340 and 380 nm wavelengths for fura-2 excitation were provided by a Polychrome IV (Till Photonics, Martinsried, Germany) through the epifluorescence pathway. The 340/380 fura-2 ratio was calculated as mean values within ROIs drawn in the neuronal soma. While cytosolic [Ca^{2+}] fold change measurements were performed with Calbryte 520 (AAT Bioquest) following datasheet protocol. Cell loading was performed at 37°C (5 µM, 30') in HBSS 1X buffer. Calbryte 520 images were acquired on a widefield Zeiss Axio-Observer.Z1 microscope equipped with a 20X objective lens (Carl Zeiss Microscopy). Excitation wavelengths of 492 nm were used, with an emission wavelength of 514 nm. The evoked Ca^{2+}-response (fold change, $\Delta F/F_0$) was calculated as mean values within ROIs drawn in neuronal

soma (Fiji-ImageJ software, https://imagej.net/Fiji). 30mM KCl was administered to promote plasma membrane depolarization and Ca^{2+} entry.

Measurement of $\Delta\Psi_{mito}$

$\Delta\Psi_{mito}$ was measured using the potentiometric dye TMRM (Invitrogen). Primary PCs at 14 DIV were incubated with 50 nM TMRM, 2 mM CsH (Vinci-Biochem), and 2 mg/ml Hoechst 33342 (Invitrogen) in phenol red–free HBSS 1X for 30' at 37°C. Imaging of TMRM fluorescence was performed using an Axio Observer.Z1 inverted microscope (Zeiss). Data represent the average of 4 images acquired every 15". FCCP (1 µM) was added at the end of acquisition. Images were analysed using Fiji-ImageJ software.

In vivo ATP assay

To measure mitochondrial ATP production in cerebellum, we isolated fresh mitochondria by differential centrifugation as previously described[108]. Immediately after isolation (to avoid freeze and thaw cycles that could damage cristae), we incubated mitochondria at 37° C for 30' in a respiratory buffer (0,25 M sucrose, 20 mm MOPS, 1 mm EDTA, 5 mM inorganic phosphate, 0,1% BSA fatty acid free and 1 mM ADP, pH 7.4). By providing pyruvate/malate (5 and 1 mM, respectively) as substrates, we stimulated ATP synthesis dependent on complexes I, II, III, IV and V. ATP production was then measured by luminometric assay as previously reported[108].

Statistical analyses

For statistical evaluation of phenotypes (imaging, WB) in *Sacs*$^{-/-}$ cells or mice compared with wild-type controls, we performed unpaired t-test, 2-tails (applying Welch's correction). Regarding pharmacological treatment with Ceftriaxone, for statistical comparisons we applied Two-way ANOVA and Tukey's multicomparison test (GraphPad Prism software, https://www.graphpad.com/scientific-software/prism/).

IV. Results

1. NFH accumulation is an early event in ARSACS pathogenesis and causes defective mitochondrial distribution in *Sacs*$^{-/-}$ PCs

1.1 npNFH accumulation occurs perinatally in the Sacs$^{-/-}$ mouse

IF cytoskeleton derangement is the most conserved cellular phenotype observed in different sacsin-depleted models, both ARSACS patient fibroblasts[95] [88] and primary neurons[95]. Moreover, an accumulation of NFs, the IFs of neurons[89] [98], has been observed in the CNS of ARSACS patients and mouse models.

NFs are a class of cytoskeletal proteins composed by three major subunits in mature neurons: light (NFL), medium (NFM) and heavy (NFH) molecular-weight subunits[109] [110] [111]. All NF subunits are phosphorylated at their amino-terminal head domain, whereas only the high-molecular-mass subunits (NFH and NFM) are extensively phosphorylated along their carboxy-terminal tail domains[111] [112]. The phosphorylation of head domain occurs in the cell body and phosphate turnover on this domain is relatively dynamic when NFs enter the axon. While more extensive phosphorylation of NFM and NFH tail domains is delayed until newly formed NFs have translocated into axons with slower turnover[111]. It is well known that the phosphorylation state of NFs affects subunit assembly and disassembly ability and, thus, their transport[111] [113]. A deeper investigation by immunohistochemistry in the ARSACS mouse models revealed a striking and specific NFH accumulation in different brain regions, including PCs in cerebellum[98]. WB analysis confirmed a prominent accumulation of npNFH, while pNFH was unchanged in every brain area [89] [98].

Based on this data, we decided to better investigate NF alteration in ARSACS, dissecting its onset and specific localization in the cerebellum of *Sacs*$^{-/-}$ mice. We first performed WB analysis on total cerebellar lysates derived from *Sacs*$^{-/-}$ mice and relative wild-type controls at 5 months of age, when *Sacs*$^{-/-}$ mice show clear PC loss and overt motor deficit. At this stage, the npNFH amount was drastically increased in *Sacs*$^{-/-}$ cerebella in comparison to wild-type samples (Fig. 1A_Results), while, as expected, other NF subunit levels (pNFH, NFM and NFL) were unchanged between the two genotypes (Fig. 1B_Results). Quantitative Real-Time PCR

(qRT-PCR) underlined no difference in *Nefh* gene expression (normalized on *Hprt1*) in *Sacs*$^{-/-}$ cerebella compared to wild-type controls (Fig. 1C_Results), excluding a transcriptional upregulation of *Nefh* subunit.

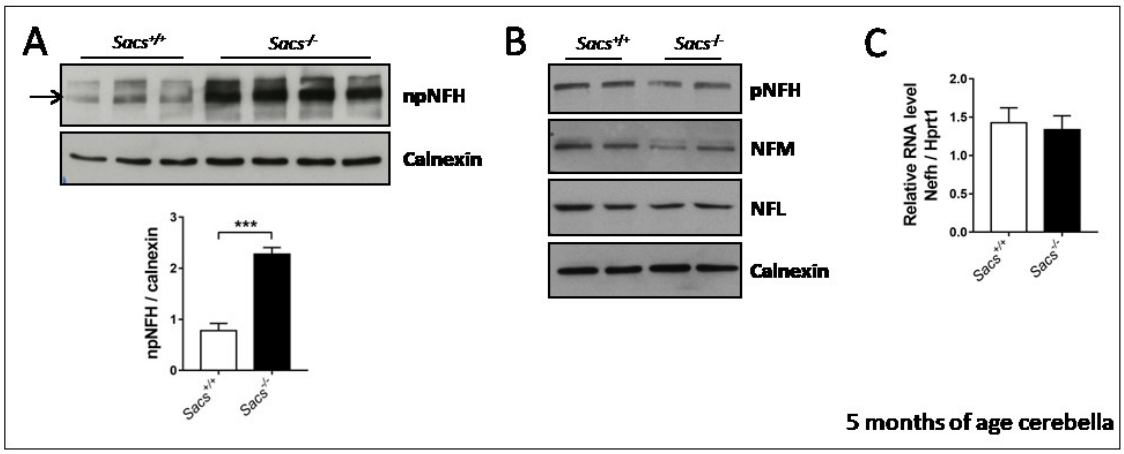

Figure 1_Results. npNFH accumulation in *Sacs*$^{-/-}$ cerebellum caused by post-transcriptional regulation. (A) WB analysis showing levels of npNFH (lower band as indicated by the arrow) in *Sacs*$^{-/-}$ and wild-type control cerebella at 5 months of age with relative quantitation (normalized on calnexin). Bars represent mean±SEM; n=4; Welch's t-test: ***p<0,001; (B) WB analysis showing different NF subunit levels in *Sacs*$^{-/-}$ and wild-type control cerebella at 5 months of age; (C) qRT-PCR showing levels of *Nefh* mRNA (relative to *Hprt1* mRNA) in *Sacs*$^{-/-}$ and wild-type control cerebella at 5 months of age. Bars represent mean±SEM; n=5; Welch's t-test: ns.

At the same age, we performed npNFH immunostaining in cerebellar cryostat slices obtained by *Sacs*$^{-/-}$ and wild-type 5 months-old mice. Curiously, abnormal npNFH accumulation in *Sacs*$^{-/-}$ proximal dendrites was appreciated mainly in PCs residing in the anterior lobule, while the staining in posterior lobules was comparable with wild-type PCs (Fig. 2A_Results). This evidence supports the hypothesis that npNFH accumulation is closely correlated to specific neuronal degeneration suggesting that PCs located in the anterior lobules are more sensitive to the absence of sacsin. To improve resolution, we also performed electron microscopy (EM) on longitudinal sections of PC neurites, likely axons where NFs are easily detectable. In 5 months-old *Sacs*$^{-/-}$ samples we discriminated abnormal densely packed 10-nm structures compatible with NFs, confirming cytoskeletal alteration. These structures were not found in wild-type PCs (Fig. 2B_Results).

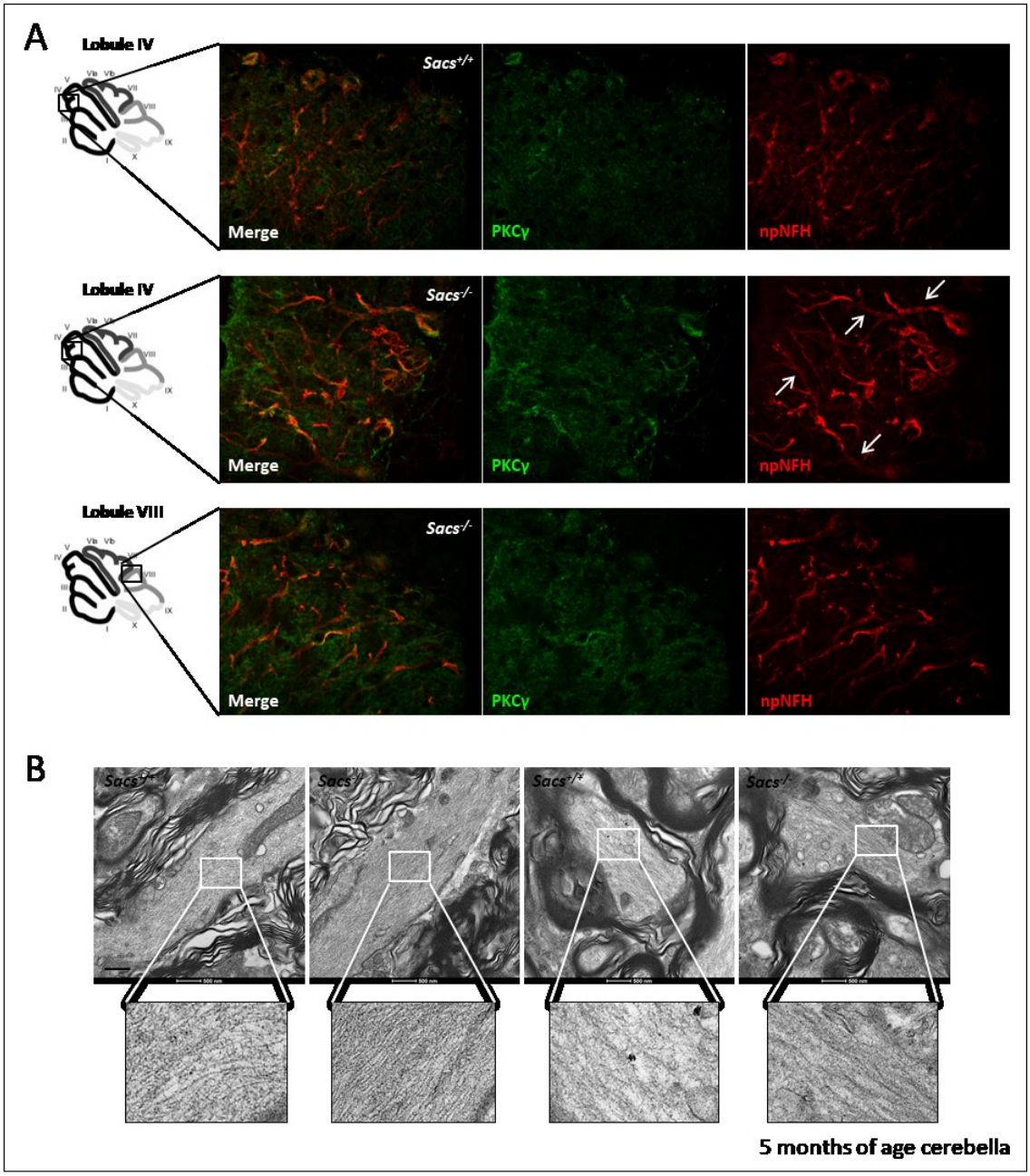

Figure 2_Results. *In vivo* NF redistribution and accumulation in neurites of *Sacs*$^{-/-}$ PCs located in anterior lobules of cerebellum. (A) Representative images of immunofluorescence analysis showing npNFH redistribution (indicated by arrows) in anterior lobule *Sacs*$^{-/-}$ PCs (marked by PKCγ) at 5 months of age compared with wild-type controls; (B) Representative EM images (150.000X magnification) of PC neurites and synapses showing packed structures in *Sacs*$^{-/-}$ PCs in comparison with wild-type control at 5 months of age. Scale bar=500nm.

To dissect the precise onset of NF accumulation in the *Sacs*$^{-/-}$ mouse, we checked this phenotype at 1 month of age (pre-symptomatic stage). At this stage, we found again a significant increase of npNFH levels by WB analysis in *Sacs*$^{-/-}$ whole cerebellar lysates compared to age-match controls (Fig. 3A_Results). This molecular feature was already present at P15, representing to our knowledge the earliest pathological phenotype in *Sacs*$^{-/-}$ mice (Fig. 3B_Results).

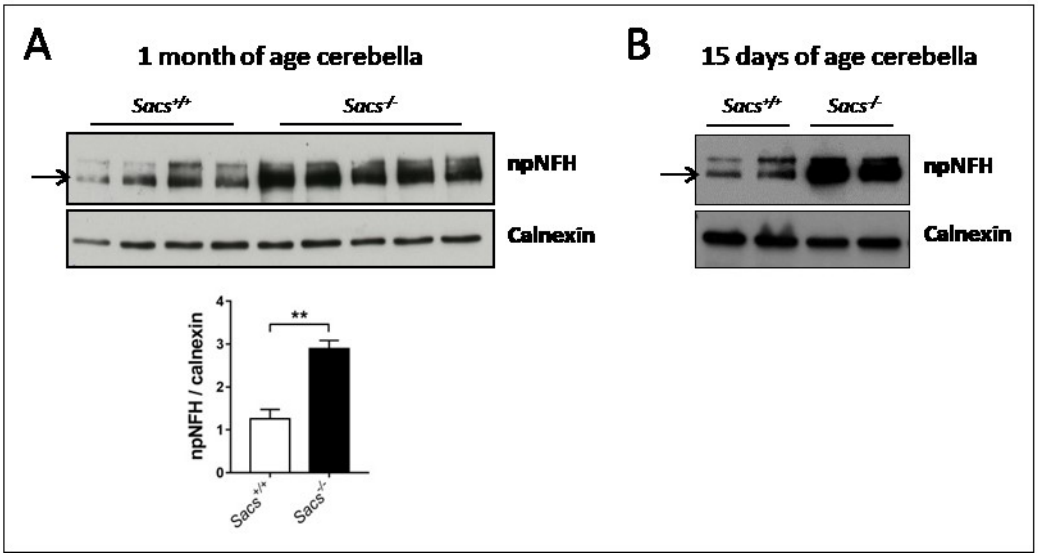

Figure 3_Results. Early npNFH accumulation in *Sacs*$^{-/-}$ cerebellum. (A) WB analysis showing levels of npNFH (lower band as indicated by the arrow) in *Sacs*$^{-/-}$ and wild-type control cerebella at 1 months of age with relative quantitation (normalized on calnexin). Bars represent mean±SEM; n=5; Welch's t-test: **p<0,01; (B) WB analysis showing levels of npNFH (lower band as indicated by the arrow) in *Sacs*$^{-/-}$ and wild-type control cerebella at 15 days of age.

1.2 SH-SY5Y cells differentiated into neurons and primary *Sacs*$^{-/-}$ PCs recapitulate npNFH accumulation in their neurites

To dissect mechanistically the cascade of events triggered by sacsin depletion by imaging and molecular biology experiments, we decided to employ *in vitro* and *ex vivo* models recapitulating features observed *in vivo* in the *Sacs*$^{-/-}$ mouse. For this purpose, we took advantage of (i) SH-SY5Y cells, a neuron-like cell type, whose *SACS*$^{-/-}$ clones were previously generated in the lab by CRISPR-Cas9 technology, and (ii) primary cerebellar cultures enriched in PCs adopting a purification protocol optimized in the lab[66].

We demonstrated a striking IF accumulation in *SACS*$^{-/-}$ SH-SY5Y cells, both undifferentiated and differentiated into neurons. In fact, both vimentin and NFH staining in undifferentiated *SACS*$^{-/-}$ SH-SY5Y clones displayed a striking cytoskeletal remodeling that was not detected in wild-type control cells (Fig. 4A). NFH accumulation was appreciated also in SH-SY5Y clones after 10 days of differentiation treatment with retinoic acid and BDNF[114], in both soma and neurites. In these differentiated cells, vimentin is expressed at very low level, as expected in mature neurons[115] (Fig. 4B).

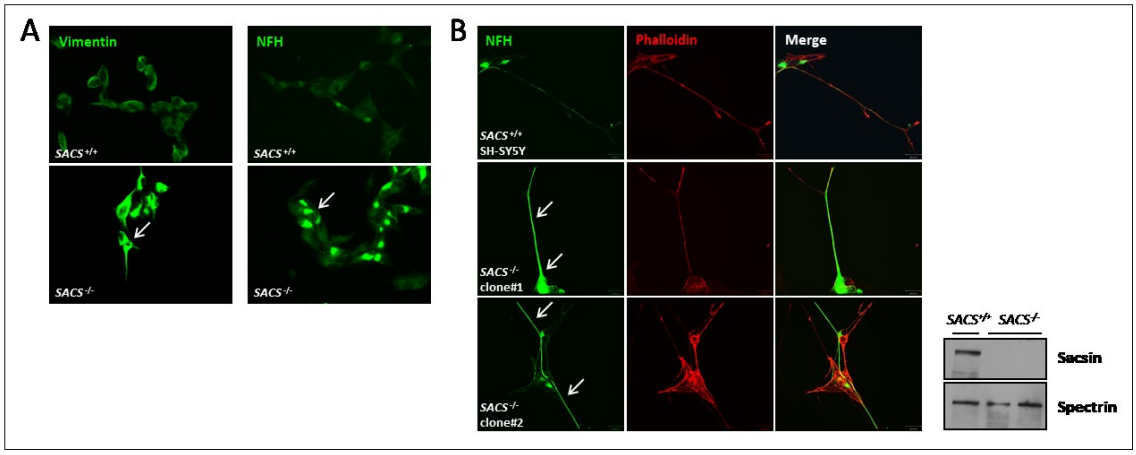

Figure 4_Results. *SACS*$^{-/-}$ SH-SY5Y cells undifferentiated and differentiated into neurons show IF remodeling. (A) Representative images of immunofluorescence analysis showing vimentin and NFH redistribution in undifferentiated *SACS*$^{-/-}$ SH-SY5Y cells compared with *SACS*$^{+/+}$ controls; (B) Representative images of immunofluorescence analysis showing NFH accumulation in neuron-like differentiated *SACS*$^{-/-}$ SH-SY5Y cells compared with *SACS*$^{+/+}$ controls; WB to check sacsin levels in different clones. Arrows indicate IF accumulation.

In parallel, we investigated NFH accumulation in primary cerebellar cultures. In our experimental settings, primary cerebellar cultures are highly heterogeneous in terms of cell types, with PCs representing only the 10% of total cells, while the remaining 90% of cells are crucial for PC survival. In detail, 60% of cells in the cultures are glial cells, critical elements for PC support and synapse formation, 20% are other cerebellar neurons, such as granules cells, basket cells and Golgi cells, and 10% are fibroblasts. We derived primary cerebellar cultures from P0 pups and kept them in culture up to 20-22 days *in vitro* (DIV), considering that they reach maturation around DIV15.

At DIV1 the number and morphology of PCs in *Sacs*$^{-/-}$ cultures were comparable to controls (Fig. 5A and B_Results), while at DIV10 PC density was drastically reduced in *Sacs*$^{-/-}$ cultures respect to wild-type controls (Fig. 5C_Results). Similar to what observed in the ARSACS mouse[98], the degeneration process seemed to be a peculiar feature of PCs, as nuclei resulted comparable in number between the two genotypes demonstrating unchanged quantity of other neurons and glial cells (Fig. 5D_Results).

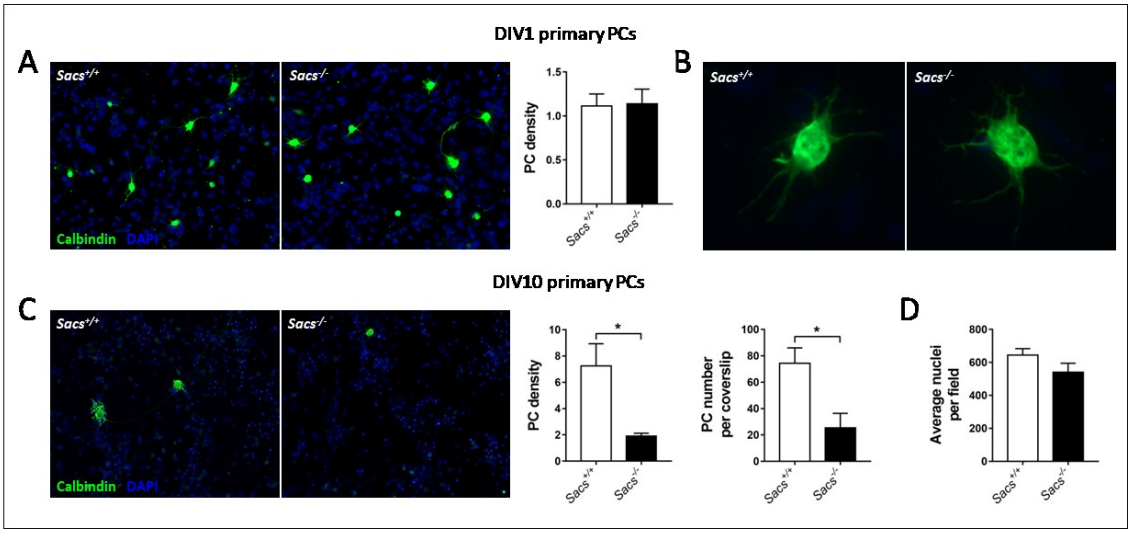

Figure 5_Results. Primary cerebellar cultures show specific PC death recapitulating the degeneration observed in *Sacs*$^{-/-}$ mouse cerebellum. (A) Immunofluorescence analysis (in green PCs stained with calbindin, 20X) of a representative field of DIV1 *Sacs*$^{-/-}$ and wild-type cerebellar cultures with relative quantitation of PC density. Bars represent mean±SEM; n=7; Welch's t-test: ns; (B) Representative images of DIV1 *Sacs*$^{-/-}$ and wild-type PCs at higher magnification to appreciate their morphology; (C) Immunofluorescence analysis (in green PCs stained with calbindin, 20X) of a representative field of DIV10 *Sacs*$^{-/-}$ and wild-type cerebellar cultures with relative quantitation of PC density and total number of PCs per coverslip. Bars represent mean±SEM; n=8; Welch's t-test: *p<0,05; (D) Quantitation of number of nuclei per field. Bars represent mean±SEM; n=8 (average of 5 field each); Welch's t-test: ns.

As at DIV15 PCs appeared nicely arborized and spiny, we decided to fix DIV15 as the timepoint for the analyses, also to avoid suffering due to prolonged maintenance in culture. At this stage, we first tested if NF derangement was a feature preserved also in *Sacs*$^{-/-}$ primary PCs. We performed immunofluorescence in DIV15 cultures using anti-npNFH and anti-calbindin antibody (to mark PCs). Confocal images showed a striking npNFH accumulation in *Sacs*$^{-/-}$ proximal PC dendrites (Fig. 6A_Results).

These data indicate that both differentiated SH-SY5Y cells and especially primary PCs represent valid tools to investigate the pathophysiology of ARSACS.

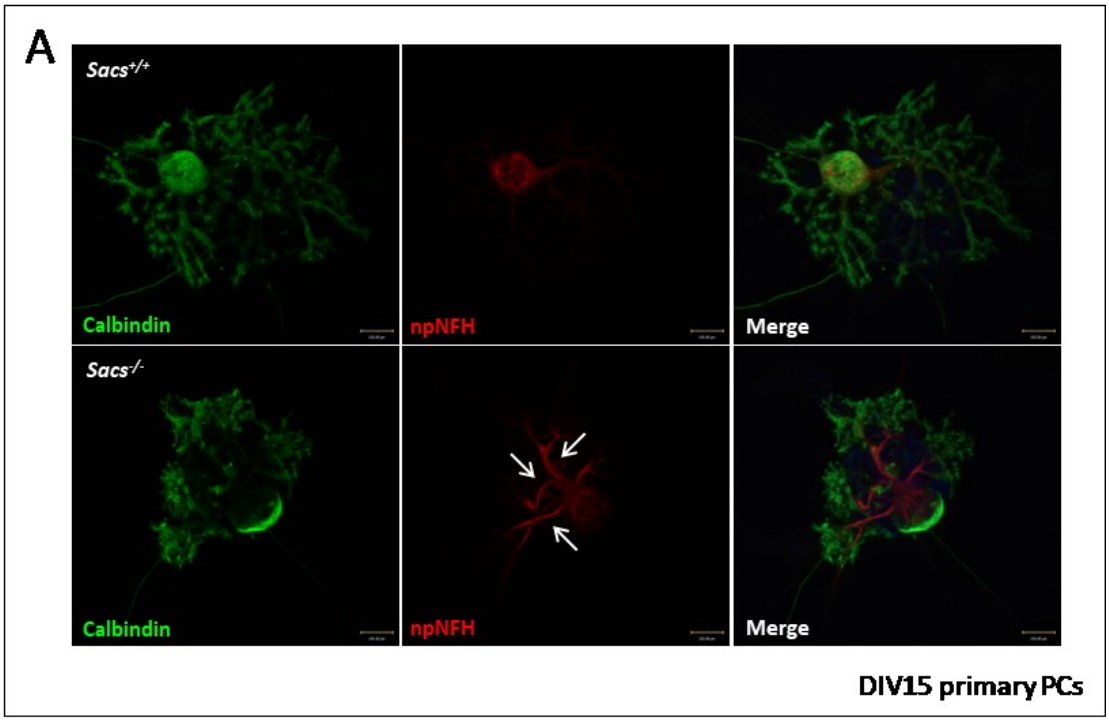

Figure 6_Results. *Sacs*$^{-/-}$ primary PCs recapitulate npNFH accumulation in proximal dendrites. (A) Representative confocal images (63X) of DIV15 *Sacs*$^{-/-}$ and wild-type PCs stained in green with calbindin, while in red npNFH signal. Arrows highlight npNFH accumulation. Scale bar=13µm.

1.3 *Sacs*$^{-/-}$ primary PCs show defective distribution of mitochondria

We next decided to explore in depth the consequences of npNFH accumulation in proximal dendrites on organelle trafficking to the periphery. We focused primarily on mitochondrial trafficking, which is essential in each kind of neurons, but especially in PCs[64 66]. Long-range transport of mitochondria occurs on microtubules, while actin filaments and NFs mediate short-range movement, docking and transient immobilization[116 117]. NFH subunit was also demonstrated to be the key player in the interaction with mitochondria, where NFH phosphorylation state and mitochondrial membrane potential assume critical roles[116]. Furthermore, mitochondrial trafficking could be affected also by mitochondrial network morphology[118 119], which was previously found altered in ARSACS fibroblasts and *SACS*$^{-/-}$ SH-SY5Y cells[96].

We thus explored mitochondrial distribution in primary *Sacs*$^{-/-}$ PCs at DIV15. Double staining marking mitochondria with anti-CoxIV and PCs with anti-calbindin antibodies revealed that mitochondria were not properly distributed in distal dendrites of *Sacs*$^{-/-}$ PCs (Fig. 7A_Results). The 3D reconstruction of several confocal stack images and volumetric analysis confirmed that

the volume of dendritic mitochondria (normalized on dendritic volume) found in PC neurites was significantly reduced in *Sacs*$^{-/-}$ neurons compared to wild-type controls (Fig. 7B_Results), while total PC mitochondrial volume (normalized on total PC volume) was unaltered (Fig. 7C_Results). These results suggest that mitochondria are not properly transported to nerve terminals in the absence of sacsin. We also evaluated the metabolic status of mitochondria testing mitochondrial membrane potential ($\Delta\Psi_{mito}$) by live-imaging measurement of the potentiometric dye TMRM in DIV15 *Sacs*$^{-/-}$ PCs and relative wild-type controls. Preliminary data showed no change in $\Delta\Psi_{mito}$ (Fig. 7D_Results). These results suggest that, although inefficiently trafficked, mitochondria are metabolically unaltered in *Sacs*$^{-/-}$ PCs.

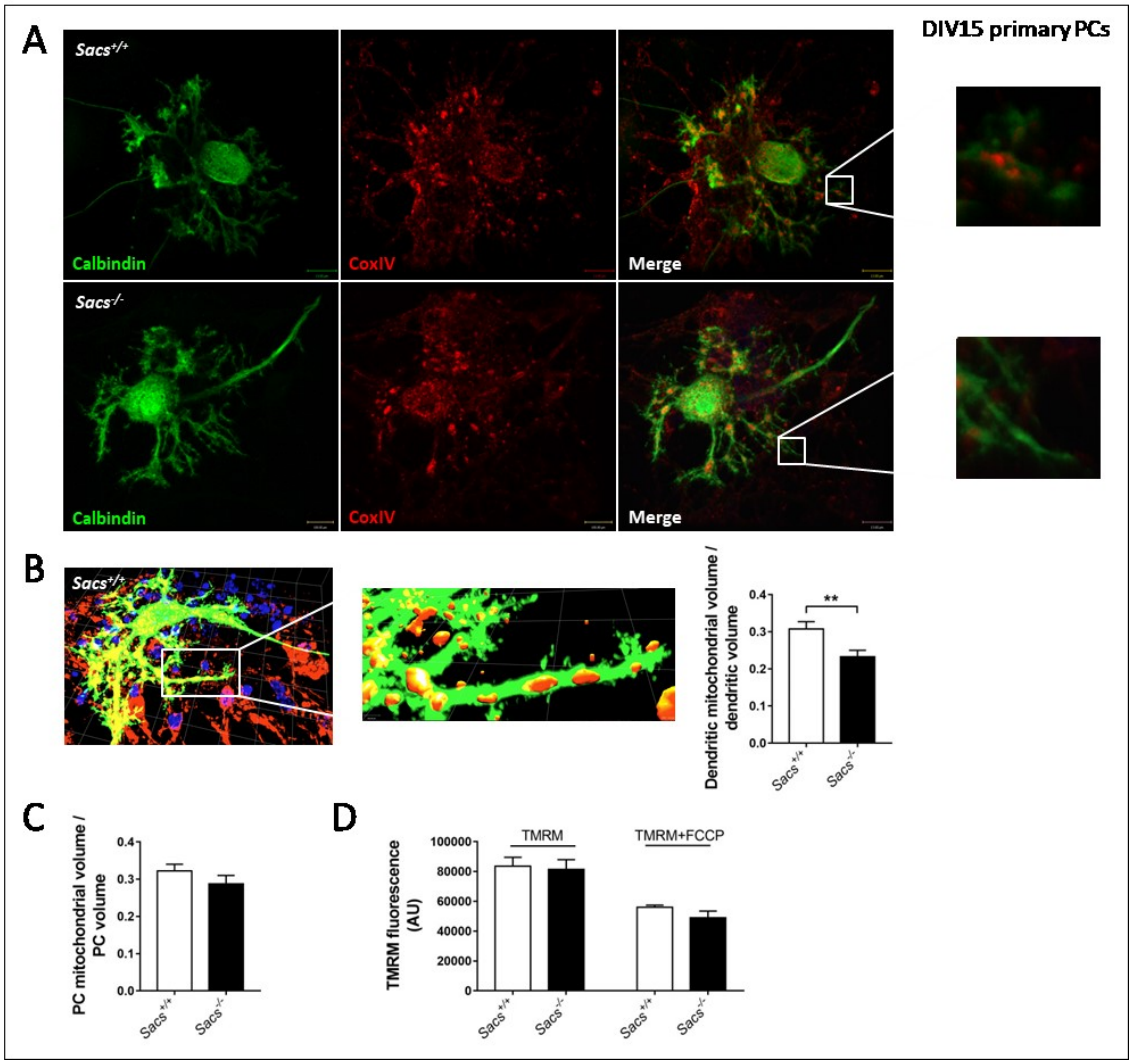

Figure 7_Results. Defective mitochondrial distribution in *Sacs*$^{-/-}$ primary PCs. (A) Representative confocal images (63X) of DIV15 *Sacs*$^{-/-}$ and wild-type PCs stained in green with calbindin, while in red mitochondrial marker CoxIV. Scale bar=13µm; (B) Representation of volumetric 3D reconstruction of confocal stacks and quantitation of dendritic mitochondrial volume (normalized on dendrite volume). Bars represent mean±SEM; n= at least 12; Welch's t-test: **p<0,01; (C) Volumetric analysis of total mitochondrial volume (normalized on total PC volume) in DIV15 *Sacs*$^{-/-}$ and wild-type PCs. Bars represent mean±SEM; n= at least 12; Welch's t-test: ns; (D) Preliminary analysis of $\Delta\Psi_{mito}$ in

primary PCs by live-imaging measurement of TMRM fluorescence intensity in soma. Bars represent mean±SEM; n=3; Welch's t-test: ns.

Interestingly, preliminary data indicate that defective cellular trafficking impacts not only on mitochondria, but also on ER (Fig. 8A_Results). Indeed, staining ER with anti-calreticulin and PCs with anti-calbindin antibodies in DIV15 *Sacs*$^{-/-}$ PCs followed by 3D reconstruction and volumetric analysis (Fig. 8B_Results) revealed reduced amount of ER in dendrites, if matched with wild-type controls.

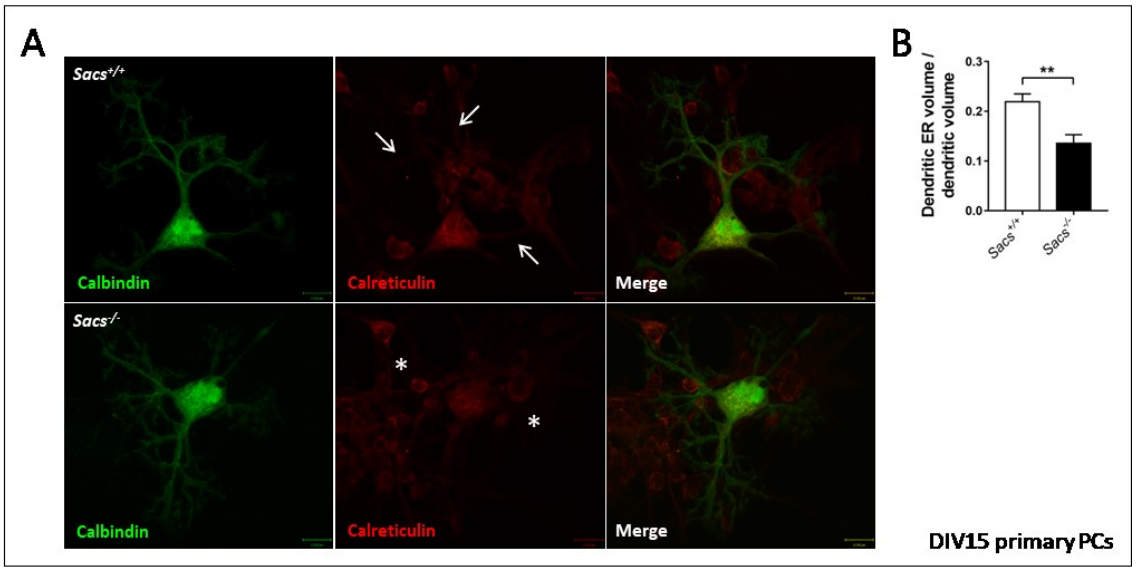

Figure 8_Results. *Sacs*$^{-/-}$ primary PCs show reduced ER trafficking in dendrites. (A) Representative confocal images (63X) of DIV15 *Sacs*$^{-/-}$ and wild-type PCs stained in green with calbindin, while in red ER marker calreticulin. Arrows indicate ER, while asterisks highlight dendritic ER depletion. Scale bar=13µm; (B) Quantitative volumetric analysis of ER volume in dendrites. Bars represent mean±SEM; n= at least 16; Welch's t-test: **p<0,01.

Altogether, this experimental evidence shows that aberrant NF organisation in proximal dendrites causes a global defective organelle distribution in *Sacs*$^{-/-}$ PCs.

1.4 Mitochondrial structure and functionality are not altered in *Sacs*$^{-/-}$ cerebella

After testing in primary PCs mitochondrial trafficking, which is a highly complicated task *in vivo* due to the complex cyto-architecture of the cerebellar cortex, we decided to further investigate mitochondrial integrity and functionality *in vivo,* also considering the TMRM data in primary PCs. We performed EM analysis of PC soma and synaptic terminals *in vivo* to visualize mitochondrial ultrastructure. High resolution images underlined intact inner and outer membranes, with well-defined cristae organisation both in wild-type and in *Sacs*$^{-/-}$ cerebella at 5 months of age (Fig. 9A_Results).

We also tested mitochondrial ATP production in freshly isolated mitochondria from cerebellum of *Sacs*$^{-/-}$ mice and relative wild-type controls at 5 months of age. In contrast with data showing altered mitochondrial respiration in ARSACS fibroblasts and *SACS*$^{-/-}$ SH-SY5Y cells[96], in mouse cerebellum we found no differences in mitochondrial ATP levels produced by *Sacs*$^{-/-}$ compared to wild-type, both at the basal level and upon stimulation with pyruvate (Fig. 9B_Results). This result indicates that mitochondrial electron transport chain is not altered in *Sacs*$^{-/-}$ PCs and, together with conserved ultrastructure, it suggests that mitochondria are healthy at 5 months, a stage in which motor defects are already manifested in ARSACS mouse model.

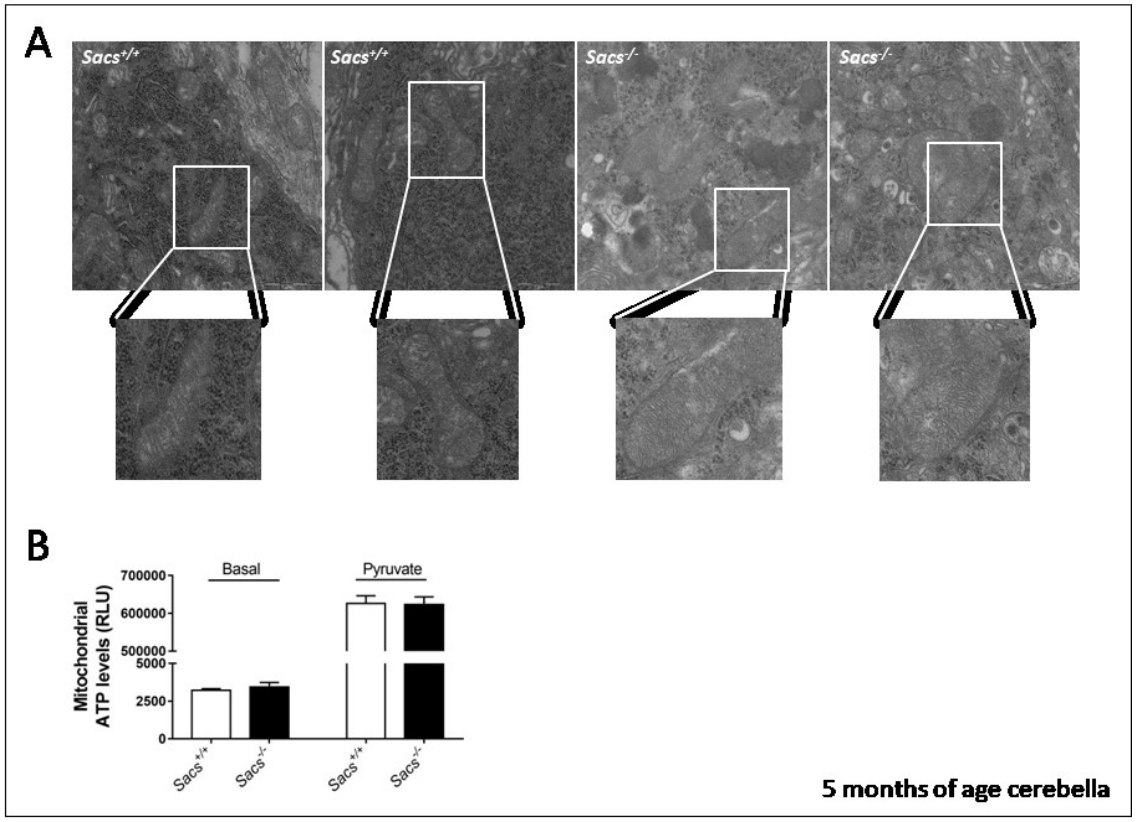

Figure 9_Results. *Sacs*$^{-/-}$ PCs show unaltered mitochondrial ultrastructure and normal ATP production. (A) Representative EM images (150.000X magnification) of PC showing intact IMM and OMM in *Sacs*$^{-/-}$ PCs comparable with wild-type control at 5 months of age. Scale bar=500nm; (B) ATP production analysis in freshly isolated mitochondria at basal level and upon pyruvate addition. Bars represent mean±SEM; n=5; Welch's t-test: ns.

Summarizing, the results obtained so far suggest us that in *Sacs*$^{-/-}$ PCs npNFH accumulation is an early event that appears just after birth and it is a peculiar features of anterior lobules PCs, the cerebellar region where later we appreciate PC loss. Moreover, the formation of this abnormal NF bundles in proximal dendrites impacts on mitochondrial and ER distribution throughout distal neuronal processes. Although mitochondria are healthy and functional, they are reduced in number at the synaptic terminals in *Sacs*$^{-/-}$ cerebellum.

1.5 Sacsin physically interacts with plectin, a cytoskeletal linker involved also in mitochondrial transport

To find a mechanistic link between sacsin, NFs and mitochondria, we decided to immunoprecipitate endogenous sacsin in order to identify its interactors. Since both cerebellum and primary PC cultures are a heterogeneous population with several non-neuronal contaminants, we selected SH-SY5Y cell differentiated into neurons, a homogeneous cell line that expresses considerable levels of sacsin. Moreover, *SACS*$^{-/-}$ SH-SY5Y cells recapitulate NF accumulation (as demonstrated in previous paragraphs, Results 1.2).

Immunoprecipitation of sacsin is a highly complex task because of its huge dimension (> 500 kDa). In the lab, my colleague Fabiana Longo was able to immunoprecipitate sacsin in wild-type SH-SY5Y cells differentiated into neurons, using *SACS*$^{-/-}$ SH-SY5Y cells as negative control (Fig. 10A_Results). Label Free Quantitation (LFQ)-Mass Spectrometry (MS) of eluates, identified 67 specific sacsin interactors (absent in *SACS*$^{-/-}$ SH-SY5Y cells). STRING association enrichment underlined that sacsin physical interactors cluster in specific categories related to supramolecular fiber, actin filament and cytoskeleton organization (Fig. 10B_Results) supporting the hypothesis that sacsin may act as a scaffold for cytoskeletal proteins. Moreover, NFL and NFM subunits were found directly interacting with sacsin, instead NFH was not pulled down probably due to its high molecular weight. On the contrary, no mitochondrial proteins were identified, suggesting that sacsin does not directly interact with mitochondria. Interestingly, with sacsin we co-immunoprecipitated plectin, a giant (500 kDa) multifunctional cytolinker protein interacting with both IF and mitochondria[120]. Of note, in literature plectin was found connecting mitochondria to all types of IF[121] and in neurons also microtubules to NFs affecting organelle trafficking[122]. Another interesting interactor was myosin Va, which in literature is reported to be crucial for both mitochondrial and ER transport in dendrites[123] (Fig. 10C_Results)

Since plectin can interact both with IF and mitochondria, two main players altered when sacsin is mutated or absent[95] [88] [96], we decided to focus our attention on this putative sacsin interactor. In this direction, a confirmation of plectin involvement in ARSACS pathogenesis was obtained by the analysis of plectin levels in two different clones of *SACS*$^{-/-}$ SH-SY5Y cells. Plectin amount, indeed, was drastically decreased in both *SACS*$^{-/-}$ SH-SY5Y clones compared with wild-type controls (Fig. 10D_Results). A comparable result was also found by analyzing plectin levels in a panel of ARSACS patient fibroblasts presenting different *SACS* mutations. Plectin amount was significantly reduced in all ARSACS patient fibroblasts respect to 3 different control lines

(Fig. 10E_Results). Although cerebellum proteomics data (see following paragraph, Results 2.1) did not highlight a significant alteration of plectin levels comparing *Sacs*$^{-/-}$ and wild-type tissues, we are now investigating further its amount or potential mislocalization by WB analysis and imaging analyses. Altogether these results revealed that plectin could be involved in ARSACS pathogenesis, as it physically interacts with sacsin and its level are affected by the absence of sacsin.

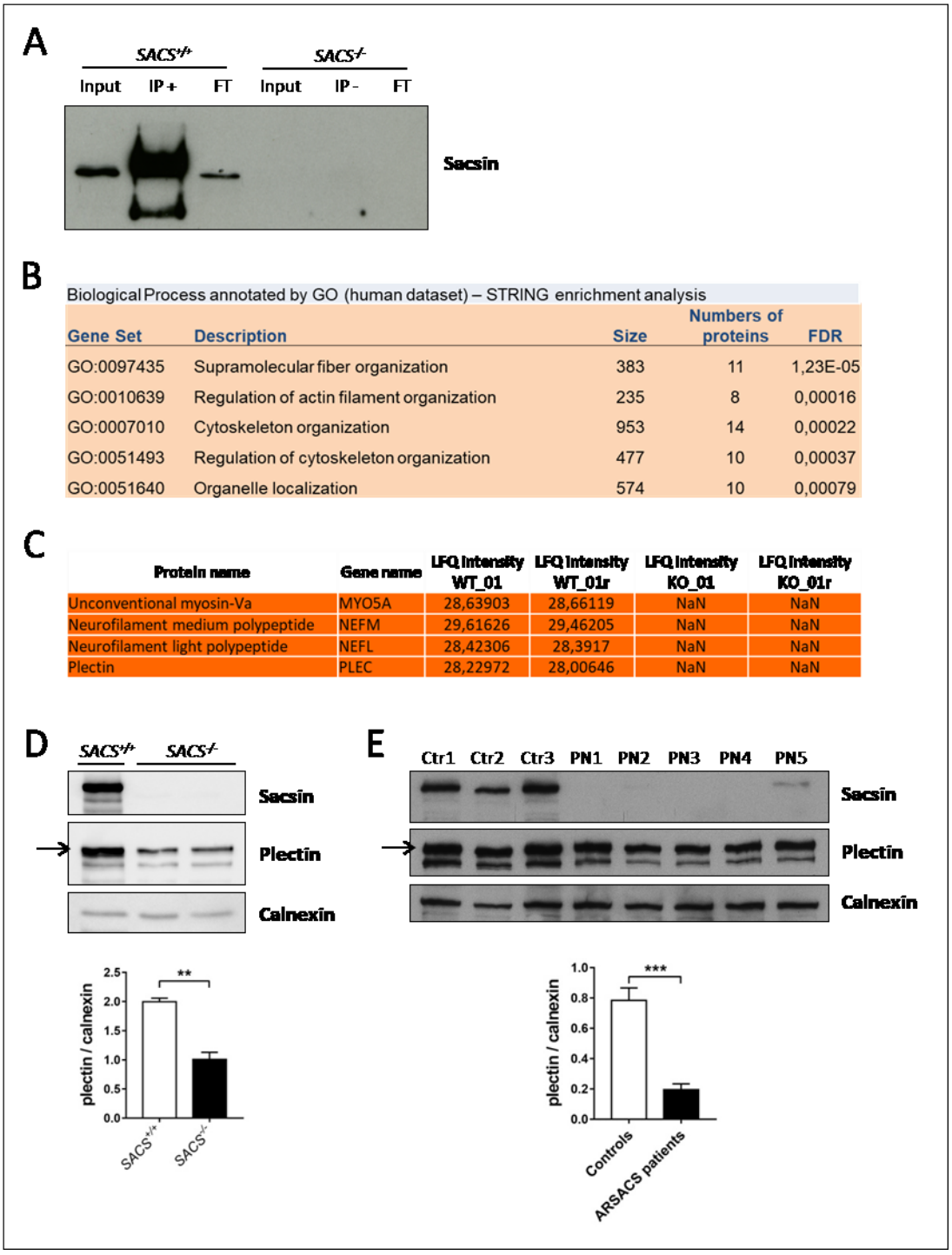

Gene Set	Description	Size	Numbers of proteins	FDR
GO:0097435	Supramolecular fiber organization	383	11	1,23E-05
GO:0010639	Regulation of actin filament organization	235	8	0,00016
GO:0007010	Cytoskeleton organization	953	14	0,00022
GO:0051493	Regulation of cytoskeleton organization	477	10	0,00037
GO:0051640	Organelle localization	574	10	0,00079

Protein name	Gene name	LFQ Intensity WT_01	LFQ Intensity WT_01r	LFQ Intensity KO_01	LFQ Intensity KO_01r
Unconventional myosin-Va	MYO5A	28,63903	28,66119	NaN	NaN
Neurofilament medium polypeptide	NEFM	29,61626	29,46205	NaN	NaN
Neurofilament light polypeptide	NEFL	28,42306	28,3917	NaN	NaN
Plectin	PLEC	28,22972	28,00646	NaN	NaN

Figure 10_Results. Sacsin physically interacts with plectin, whose levels are downregulated in sacin-depleted cells. (A) Sacsin immunoprecipitation in *SACS*$^{-/-}$ SH-SY5Y cells. FT= Flow through; (B) Gene Ontology STRING enrichment output of sacsin co-immunoprecipated proteins; (C) LFQ intensity of selected sacsin cytoskeletal interactors; (D) WB analysis showing levels of plectin in *SACS*$^{-/-}$ and *SACS*$^{+/+}$ SH-SY5Y cells with relative quantitation (normalized on calnexin). Bars represent mean±SEM; n=4; Welch's t-test: **p<0,01; (E) WB analysis showing levels of plectin in a panel of ARSACS fibroblast and three different control cell lines with relative quantitation (normalized on calnexin). Bars represent mean±SEM; n= 3 controls vs 5 patient lines; Welch's t-test: ***p<0,001.

2. Alteration of mitochondrial trafficking due to cytoskeleton remodeling leads to the deregulation of Ca^{2+} homeostasis in PC distal dendrites

2.1 Integrated OMICS approaches disclose deregulation of Ca^{2+} homeostasis in *Sacs*$^{-/-}$ cerebella

We hypothesized that the remodeling of NFs affecting mitochondrial (and ER) trafficking could have a huge impact on Ca^{2+} homeostasis with severe downstream effects in *Sacs*$^{-/-}$ mice. In fact, in neurons Ca^{2+} signaling regulates a large number of neuronal function such as growth and differentiation, neuronal excitability controlling brain rhythms and information processing and, also, synaptic plasticity that monitors learning and memory[124 125]. For these reasons, deranged cellular Ca^{2+} concentration could contribute to pathophysiological conditions such as necrosis, apoptosis, autophagy deficits, and degeneration[58 125]. A fine regulation of free cytosolic Ca^{2+} concentration is indeed required in every type of neurons, but this feature is even more crucial in PCs. These neurons with their extremely branched dendritic tree receiving mostly glutamatergic stimulation and, thus, massive Ca^{2+} influxes in post-synaptic dendrites, have intrinsic vulnerability to increased Ca^{2+} levels as demonstrated by many genetic forms of cerebellar ataxias showing alteration of Ca^{2+} homeostasis as pathogenetic mechanism[39 45 126]. In this scenario, a crucial role is assumed by mitochondria that not only support the energy requirements of the cells, but they exert themselves Ca^{2+} buffering accumulating Ca^{2+} into the matrix thus shaping Ca^{2+} signals cooperating with Ca^{2+}-binding proteins (e.g., calbindin and parvalbumin)[127]. In addition, they provide high levels of ATP to active Ca^{2+} clearance systems, represented by Ca^{2+} ATPases in the plasma membrane and ER.

We thus hypothesized that defective transport of mitochondria (and ER) in distal dendrites of PCs could cause pathological Ca^{2+} accumulation in *Sacs*$^{-/-}$ mice.

To explore Ca^{2+} homeostasis defects in ARSACS, we took advantage of two OMICS approaches. Firstly, performing LFQ proteomics on *Sacs*$^{-/-}$ cerebella and relative controls, at 5 months of age (post-symptomatic stage), we identified 364 proteins that were differentially expressed comparing two groups (246 upregulated and 118 downregulated). The following Gene Ontology (GO) enrichment analyses, using Gprofiler tool, revealed that, in addition to many proteins associated with cytoskeleton, in *Sacs*$^{-/-}$ samples also several classes of proteins linked to calmodulin and ion binding (GO: MF), cellular localization and transport, synaptic organization and signalling (GO: BP), mitochondrion and glutamatergic synapse (GO: CC) (Fig. 11A_Results) resulted deregulated. Among the most deregulated Ca^{2+}-related proteins, two

were particularly interesting: CaMKId (Calcium/calmodulin-dependent protein kinase type 1D, strongly upregulated) and IP3R1 (Inositol 1,4,5-trisphosphate receptor type 1, strongly downregulated). Proteins belonging to Ca^{2+}/calmodulin-dependent protein kineses (CaMKs), such as CaMKId, are involved in Ca^{2+} signalling. In fact, they are highly expressed in synaptic spines where sensitivity to Ca^{2+} concentrations is needed to handle the massive ion entry[128 129 130]. In resting condition, CaMKs are inactive, but upon Ca^{2+} influx they become active. The increase of Ca^{2+} concentration promotes Ca^{2+}-calmodulin (Ca^{2+}/CaM) binding and this complex binds CaMKs and relieves it from autoinhibition state favouring autophosphorylation. This results in the persistence of the kinase activity even beyond removal of Ca^{2+}/CaM complexes[131 132]. Moreover, the kinase activity leads to a signal cascade acting mostly on cytoskeletal structure of spines[133 134 135]. For this reason, the phosphorylation state of CaMKs can be considered an indirect way to monitor Ca^{2+} concentration in synapses and more generally in neuron cytosol.

On the other hand, the inositol 1,4,5-trisphosphate (IP3) receptors (IP3Rs) are a family of Ca^{2+} release channels localized predominately in the ER of all cell types[136 137]. Since ER is the major Ca^{2+} storage of the cell, IP3R1 co-works with ER Ca^{2+} ATPases (SERCA pumps) to maintain a proper balance of this ion in the cytosol. IP3Rs function to release Ca^{2+} into the cytoplasm in response to IP3 produced by diverse stimuli[137]. The channel gating is regulated not only by IP3, but by other ligands as well, in particular free cytosolic Ca^{2+} and ATP[138 139].

We then validated these findings by WB analysis. Although CaMKIIβ amount (the most expressed isoform in the cerebellum[140]) was unchanged in 5 months of age *Sacs*$^{-/-}$ cerebellar lysates in comparison to wild-type controls (Fig. 11B_Results), the phosphorylation levels of CaMKIIβ were drastically increased in *Sacs*$^{-/-}$ samples indicating an increase of cytosolic Ca^{2+} concentration (Fig. 11B_Results). A similar situation was also found at earlier stage of the disease. In fact, the upregulation of CaMKIIβ phosphorylation level in *Sacs*$^{-/-}$ cerebella compared to wild-type ones was already observed at 1 month of age (Fig. 11C_Results), correlating Ca^{2+} deregulation with NF cytoskeleton remodeling. In parallel, WB experiments highlighted a significant decrease of IP3R1 amount in *Sacs*$^{-/-}$ cerebella if compared with wild-type controls at 5 months of age (Fig. 11D_Results). All these data support the hypothesis of deregulated Ca^{2+} homeostasis when sacsin is absent.

A

Sacs$^{-/-}$ vs wild-type

source	term_name	term_id	Adjusted p_value	Intersection size
GO:MF	carbohydrate derivative binding	GO:0097367	2,27098E-06	31
GO:MF	ion binding	GO:0043167	0,000153113	47
GO:MF	structural molecule activity	GO:0005198	0,001020312	18
GO:MF	calmodulin binding	GO:0005516	0,001025302	9
GO:MF	anion binding	GO:0043168	0,002464518	34
GO:MF	identical protein binding	GO:0042802	0,004340161	42
GO:MF	purine ribonucleotide binding	GO:0032555	0,008426824	19
GO:MF	kinase binding	GO:0019900	0,008696425	23
GO:MF	ribonucleotide binding	GO:0032553	0,011864411	19
GO:MF	purine nucleotide binding	GO:0017076	0,012446289	19
GO:BP	establishment of localization in cell	GO:0051649	3,1211E-05	49
GO:BP	regulation of transport	GO:0051049	7,10873E-05	47
GO:BP	cell junction organization	GO:0034330	0,000202967	25
GO:BP	synapse organization	GO:0050808	0,000283201	20
GO:BP	positive regulation of transport	GO:0051050	0,000287644	32
GO:BP	regulation of cellular localization	GO:0060341	0,002542876	30
GO:BP	intracellular transport	GO:0046907	0,004011342	35
GO:BP	regulation of ion transport	GO:0043269	0,004548361	22
GO:BP	trans-synaptic signaling	GO:0099537	0,004739545	23
GO:BP	neuron projection development	GO:0031175	0,005870314	29
GO:CC	synapse	GO:0045202	1,52E-15	56
GO:CC	cell junction	GO:0030054	6,41E-14	64
GO:CC	mitochondrion	GO:0005739	4,90E-10	55
GO:CC	neuron projection	GO:0043005	1,29E-07	45
GO:CC	glutamatergic synapse	GO:0098978	5,88E-07	24
GO:CC	postsynapse	GO:0098794	1,07768E-06	28
GO:CC	somatodendritic compartment	GO:0036477	7,61732E-06	33
GO:CC	cell body	GO:0044297	1,62467E-05	28
GO:CC	cytosolic ribosome	GO:0022626	2,42388E-05	11
GO:CC	axon	GO:0030424	8,70353E-05	25

B

5 months of age cerebella

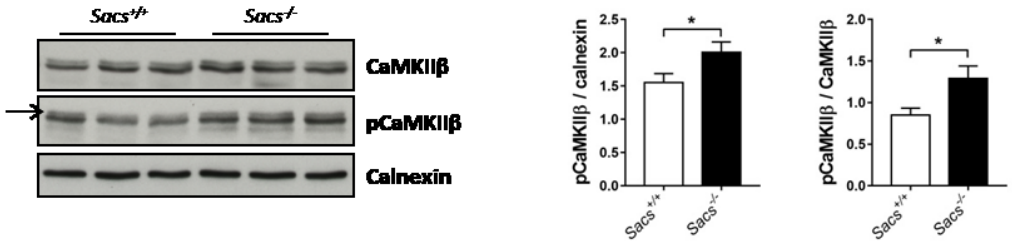

C

1 month of age cerebella

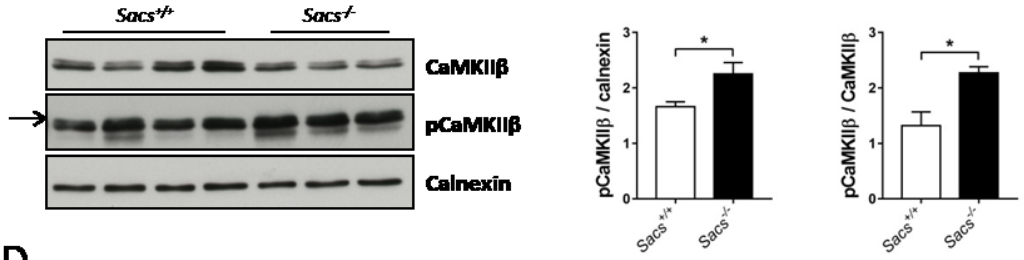

D

5 months of age cerebella

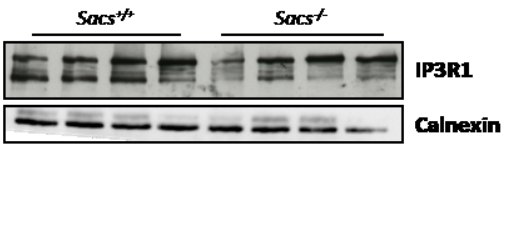

Figure 11_Results. *Sacs*$^{-/-}$ cerebella reveal Ca^{2+} deregulation. (A) Gprofiler enrichment of deregulated proteins comparing 5 months-old *Sacs*$^{-/-}$ and wild-type cerebella showing top 10 categories for each GO: molecular function (MF), biological process (BP) and cellular component (CC); (B) WB analysis showing levels of CaMKIIβ and pCaMKIIβ (upper band as indicated by the arrow) in *Sacs*$^{-/-}$ and wild-type control cerebella at 5 months of age with relative quantitation (normalized on calnexin). Bars represent mean±SEM; n=4; Welch's t-test: *p<0,05; (C) WB analysis showing levels of CaMKIIβ and pCaMKIIβ (upper band as indicated by the arrow) in *Sacs*$^{-/-}$ and wild-type control cerebella at 1 month of age with relative quantitation (normalized on calnexin). Bars represent mean±SEM; n=4; Welch's t-test: *p<0,05; (D) WB analysis showing levels of IP3R1 in *Sacs*$^{-/-}$ and wild-type control cerebella at 5 months of age with relative quantitation (normalized on calnexin). Bars represent mean±SEM; n=5; Welch's t-test: *p<0,05.

To further explore and dissect the key events in the pathophysiological cascade of ARSACS disease, we performed a second high-throughput approach. We conducted RNA sequencing (RNAseq) analysis on *Sacs*$^{-/-}$ cerebellar RNA extracts relative to age-matched wild-type controls at 5 months of age. This analysis revealed 136 deregulated genes in *Sacs*$^{-/-}$ cerebella (59 were upregulated and 77 were downregulated) (Fig. 12A_Results). GO analysis revealed different classes of genes involved in Ca^{2+} handling, ion transport and neuronal projections, but many of them were also linked to neuroinflammation (we will discuss this point in following paragraphs, Results 4.1). A detailed investigation highlighted that the majority of downregulated genes belong to ion channel transport and activity (GO: MF), neuronal projection and cation transport (GO: BP), and IF and dendrites/axons (GO:CC), as well as upregulation of genes involved into inflammatory response, glial cell development and cytokine production (GO: BP) (Fig. 12B_Results). This data supports our hypothesis of Ca^{2+} deregulation in synaptic terminal where this signal has important consequences also on the cyto-architecture of neuronal projections. Interestingly, *Itpr1* transcript was slightly downregulated in support to protein assay readouts. The RNAseq analysis revealed also the deregulation of some mitochondrial genes and, thanks to the ongoing collaboration with Bianca Habermann (Aix-Marseille Université CNRS), we submitted the transcriptomic output to MitoXplorer analysis, an online platform designed by her team[141]. MitoXplorer revealed several deregulated mitochondrial pathways in *Sacs*$^{-/-}$ cerebella respect to wild-type controls. The most enriched and deregulated mitochondrial categories were related to mitochondrial dynamics (all downregulated genes), Ca^{2+} signaling and transport, and amino acid metabolism (both up- and downregulated genes) (Fig. 12C_Results). These findings corroborate our idea of Ca^{2+} handling and homeostasis alterations in *Sacs*$^{-/-}$ cerebella.

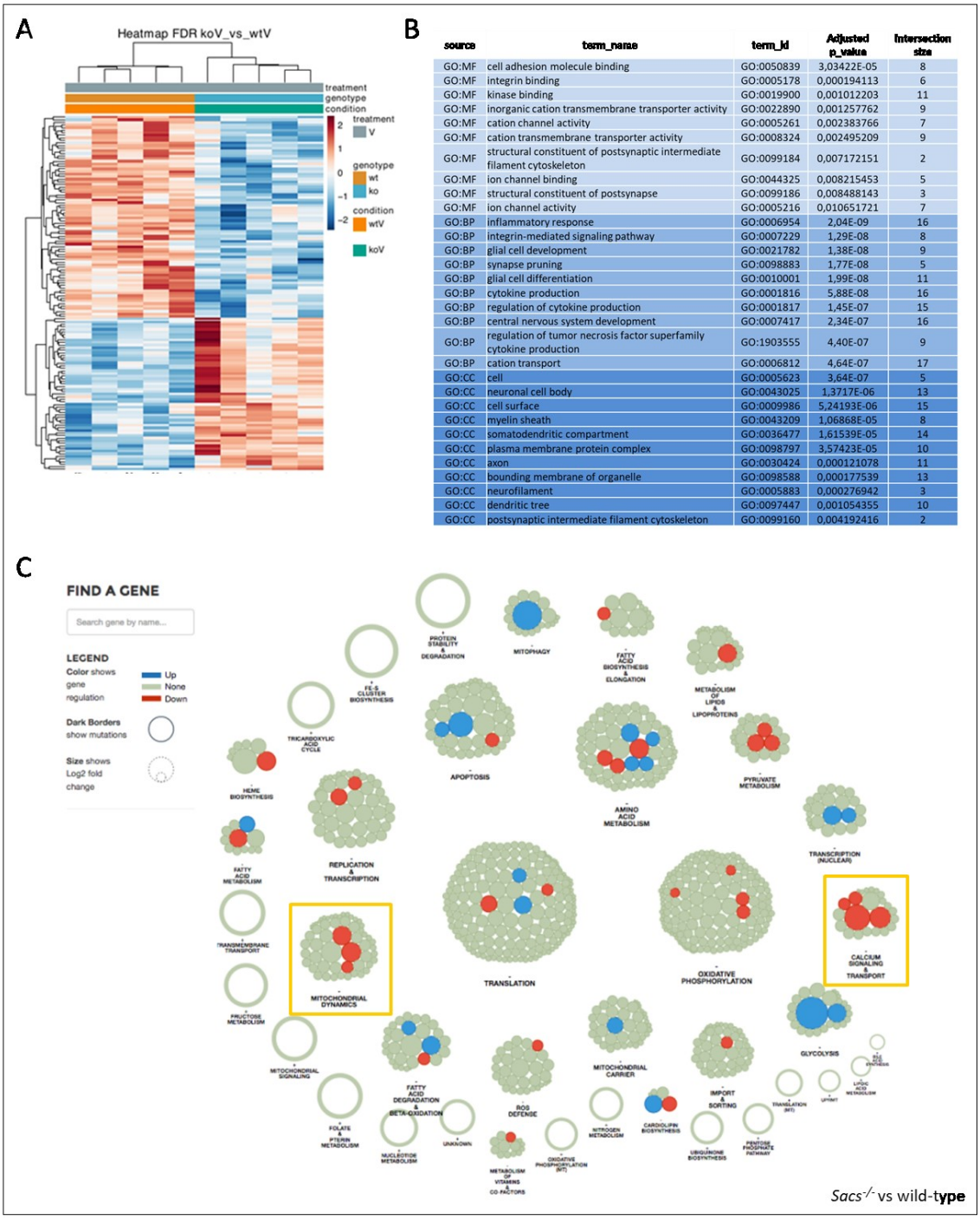

source	term_name	term_id	Adjusted p_value	Intersection size
GO:MF	cell adhesion molecule binding	GO:0050839	3,03422E-05	8
GO:MF	integrin binding	GO:0005178	0,000194113	6
GO:MF	kinase binding	GO:0019900	0,001012203	11
GO:MF	inorganic cation transmembrane transporter activity	GO:0022890	0,001257762	9
GO:MF	cation channel activity	GO:0005261	0,002383766	7
GO:MF	cation transmembrane transporter activity	GO:0008324	0,002495209	9
GO:MF	structural constituent of postsynaptic intermediate filament cytoskeleton	GO:0099184	0,007172151	2
GO:MF	ion channel binding	GO:0044325	0,008215453	5
GO:MF	structural constituent of postsynapse	GO:0099186	0,008488143	3
GO:MF	ion channel activity	GO:0005216	0,010651721	7
GO:BP	inflammatory response	GO:0006954	2,04E-09	16
GO:BP	integrin-mediated signaling pathway	GO:0007229	1,29E-08	8
GO:BP	glial cell development	GO:0021782	1,38E-08	9
GO:BP	synapse pruning	GO:0098883	1,77E-08	5
GO:BP	glial cell differentiation	GO:0010001	1,99E-08	11
GO:BP	cytokine production	GO:0001816	5,88E-08	16
GO:BP	regulation of cytokine production	GO:0001817	1,45E-07	15
GO:BP	central nervous system development	GO:0007417	2,34E-07	16
GO:BP	regulation of tumor necrosis factor superfamily cytokine production	GO:1903555	4,40E-07	9
GO:BP	cation transport	GO:0006812	4,64E-07	17
GO:CC	cell	GO:0005623	3,64E-07	5
GO:CC	neuronal cell body	GO:0043025	1,3717E-06	13
GO:CC	cell surface	GO:0009986	5,24193E-06	15
GO:CC	myelin sheath	GO:0043209	1,06868E-05	8
GO:CC	somatodendritic compartment	GO:0036477	1,61539E-05	14
GO:CC	plasma membrane protein complex	GO:0098797	3,57423E-05	10
GO:CC	axon	GO:0030424	0,000121078	11
GO:CC	bounding membrane of organelle	GO:0098588	0,000177539	13
GO:CC	neurofilament	GO:0005883	0,000276942	3
GO:CC	dendritic tree	GO:0097447	0,001054355	10
GO:CC	postsynaptic intermediate filament cytoskeleton	GO:0099160	0,004192416	2

Figure 12_Results. Transcriptomics analysis supports Ca^{2+} deregulation in *Sacs*$^{-/-}$ cerebella. (A) Heatmap of cerebellar gene profile comparing *Sacs*$^{-/-}$ and wild-type controls; (B) Gprofiler enrichment of deregulated genes comparing 5 months-old *Sacs*$^{-/-}$ and wild-type cerebella showing top 10 categories for each GO: molecular function (MF), biological process (BP), and cellular component (CC); (C) MitoXplorer output showing the clusters of deregulated mitochondrial-related genes.

2.2 *Sacs*$^{-/-}$ primary PCs show defective cytosolic Ca^{2+} handling

To investigate in depth the mechanism involved in the alteration of Ca^{2+} homeostasis in *Sacs*$^{-/-}$ PCs, we performed live Ca^{2+} imaging on primary PCs. At 15 DIV we tested basal cytosolic Ca^{2+} levels with fura-2 ratiometric measurements both in *Sacs*$^{-/-}$ and wild-type PCs. We found no differences in basal level of cytosolic Ca^{2+} concentration (340/380 ratio) between two genotypes (Fig. 13A_Results). To detect Ca^{2+}-evoked peaks, however, we took advantage of the highly sensitive Ca^{2+} probe Calbryte^{TM} 520. At the same timepoint (DIV15) we challenged primary PCs with 30 mM KCl, to promote Ca^{2+} entry by plasma membrane and to empty Ca^{2+} stores. The analysis of Ca^{2+}-evoked peaks ($\Delta F/F_0$) showed a significant increase in *Sacs*$^{-/-}$ compared to wild-type control PCs (Fig. 13B and C_Results). Moreover, the defective capacity to handle Ca^{2+} influxes of *Sacs*$^{-/-}$ cells was typical solely of PCs, as *Sacs*$^{-/-}$ granule cell Ca^{2+}-evoked responses were similar to wild-type ones (Fig. 13D_Results).

In summary, different approaches and techniques applied to *Sacs*$^{-/-}$ cerebella demonstrated Ca^{2+} deregulation as key aspect when sacsin is depleted. This is a downstream event that, based on our data, results from the derangement of NF structure affecting mitochondrial and ER trafficking in distal dendrites and, thus, leading to an inefficient handling of massive Ca^{2+} influxes typical of PC post-synapses.

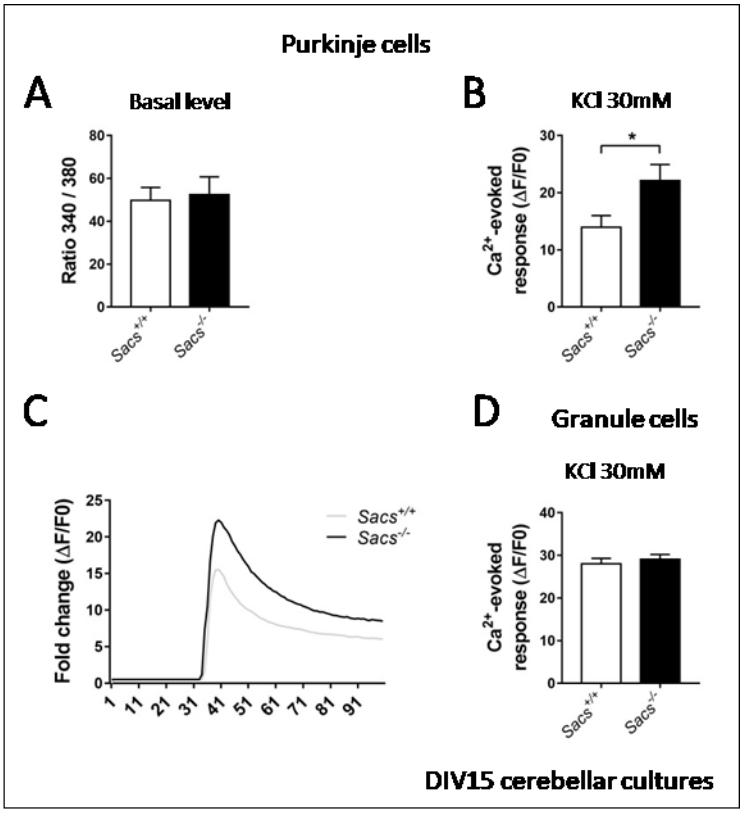

Figure 13_Results. Live Ca^{2+} imaging underlines defective Ca^{2+} handling in primary *Sacs*$^{-/-}$ PCs. (A) Basal values of cytosolic Ca^{2+} concentration evaluated by fura-2 fluorescence at 340/380 nm ratio. Bars represent mean±SEM; n=4; Welch's t-test: ns; (B) PC Ca^{2+}-evoked responses after stimulation with 30 mM KCl (normalized increase measured above the initial value). Bars represent mean±SEM; n= at least 10; Welch's t-test: *p<0,05; (C) Representative traces of cytosolic Ca^{2+} responses before and after KCl stimulation of *Sacs*$^{-/-}$ and wild-type control primary PCs; (D) Granule cell Ca^{2+}-evoked responses after stimulation with 30 mM KCl (normalized increase measured above the initial value). Bars represent mean±SEM; n=10; Welch's t-test: ns.

3. A pre-clinical pharmacological treatment with Ceftriaxone in ARSACS

3.1 Long-term Ceftriaxone treatment has no major toxic side effects in wild-type mice

Ceftriaxone is a β-lactam antibiotic that is usually engaged to inhibit bacterial synthetic pathways. In clinical routine, it is mostly administered to act against paediatric meningitis. Furthermore, there is evidence that Ceftriaxone exerts neuroprotection by several mechanisms in many preclinical models of neurodegeneration[142] [143]. Ceftriaxone is able to reduce glutamate concentration at inter-synaptic space increasing the expression and the activity of the astrocyte glutamate transporter EAAT2 (also known as GLT1) and it exerts neuroprotection[144] [145] [146], probably modulating transcription of targets acting via NF-kB[147]. In fact, Ceftriaxone was demonstrated to induce IkBα degradation and, thus, to promote p65

nuclear translocation, where it activates transcription of target genes, among them also GLT1[147] [148] [149]. In this way glutamatergic stimulation on post-synaptic PC dendrites, and following Ca^{2+} influx, is reduced[66] [144]. Studies have shown that neuroprotection is enhanced thanks to the upregulation of Nrf2 and GSH, two important factors in antioxidant response[145] [146]. Since our data support Ca^{2+} deregulation in *Sacs*$^{-/-}$ cerebellum, we decided to test this drug in the ARSACS pre-clinical model.

Before starting with Ceftriaxone administration in *Sacs*$^{-/-}$ mice, we designed a long-lasting administration protocol on wild-type mice to evaluate and exclude major side effects. The administration regimen consisted in intraperitoneal injection of Ceftriaxone at the dosage of 200mg/kg for 5 consecutive days, monthly. The wild-type mice were treated with Ceftriaxone or placebo (physiological solution - NaCl 0,9%), starting from the first month of age up to the age of 1-year (Fig. 14A_Results). This posology for Ceftriaxone administration was already used in other disease models targeting cerebellum[66] [150].

To monitor the general health state of treated mice of both experimental groups, we collected different data. Monthly, before every round of 5 days administration, we checked up the body weight of all mice involved in the study, both males and females, but we did not find any difference in this parameter (Fig. 14B_Results). Moreover, we tested the mice enrolled in this trial by rotarod test, to assess motor ability, and by Novel Object Recognition Test (NORT), to verify the cognitive functions. In this view, we planned to perform both tests at two different timepoints: at 8 months and 1 year of age. The analyses that revealed motor coordination and cognition were not negatively altered by drug administration both at 8 months (Fig. 14C_Results) and 1 year of age (Fig. 14D_Results). Rather, at 1 year of age Ceftriaxone treatment seems to slightly improve both motor and memory skills of treated mice respect to the untreated controls. Our data indicate Ceftriaxone administered with our posology has no major side effects on health status and quality of life of the mice.

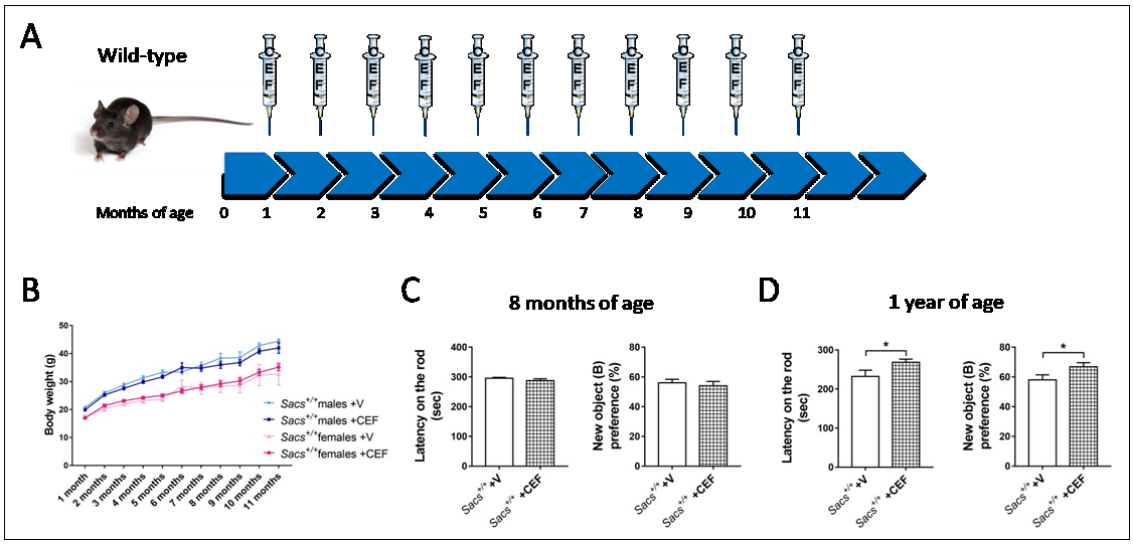

Figure 14_Results. Long-term Ceftriaxone treatment has no toxic effect on wild-type mice. (A) Schematic representation of Ceftriaxone administration protocol; (B) Monthly body weight check-up of both treated and untreated female/male mice. Dots represent mean±SEM; n= at least 5. (C-D) Rotarod (latency time on the rod) and NORT test (new object preference) readouts of Ceftriaxone-treated and untreated 8 months-old and 1 year-old wild-type mice. Bars represent mean±SEM; n= at least 8; Welch's t-test: *p<0,05.

3.2 Post-symptomatic Ceftriaxone administration in *Sacs*$^{-/-}$ mice ameliorates motor ability, delays PC loss and improves Ca^{2+} homeostasis

After testing the safety of Ceftriaxone administration at the dose of 200mg/kg in wild-type mice, we planned two different pre-clinical trials to evaluate Ceftriaxone efficacy in the ARSACS mouse model. In the post-symptomatic trial, mice were administered with the drug for the first time at 5 months of age, a stage at which PC loss is clearly assessed and motor symptoms are already evident[98]. Before the first dose of treatment motor incoordination of *Sacs*$^{-/-}$ mice was assessed by beam walking (BW) test. At this stage, we re-confirmed in our experimental settings that both *Sacs*$^{-/-}$ females and males took longer time to cross the beam compared to age- and sex-matched wild-type controls (Fig. 15A_Results). The same result was obtained counting the number of hindlimb missteps to perform the exercise (Fig. 15B_Results). Due to the striking difference between female and male performances, they were kept separated in our pre-clinical trials.

Mice were then treated with 200mg/kg of Ceftriaxone for 5 consecutive days. In this trial only two cycles of administration (5 days in a row, monthly) were performed (Fig. 15C_Results). One month later the last drug administration, motor balance and coordination of the mice were tested again. We appreciated a clear improvement of *Sacs*$^{-/-}$ mice motor ability upon Ceftriaxone treatment. The latency time to cross the beam (Fig. 15D_Results) and the number

of hindlimb missteps (Fig. 15E_Results) were remarkably reduced both in *Sacs*$^{-/-}$-treated females and males. Of note, *Sacs*$^{-/-}$ female performances were not completely rescued, as they were significantly different from age-matched wild-type controls. This data probably indicates the degeneration processes at 5 months of age were already ongoing. This post-symptomatic pharmacological treatment is thus able to delay disease progression without major side effects. In fact, comparing the data of mice with same sex and genotype, but different treatment, we did not detect any significant difference in terms of body-weight (Fig. 15F_Results).

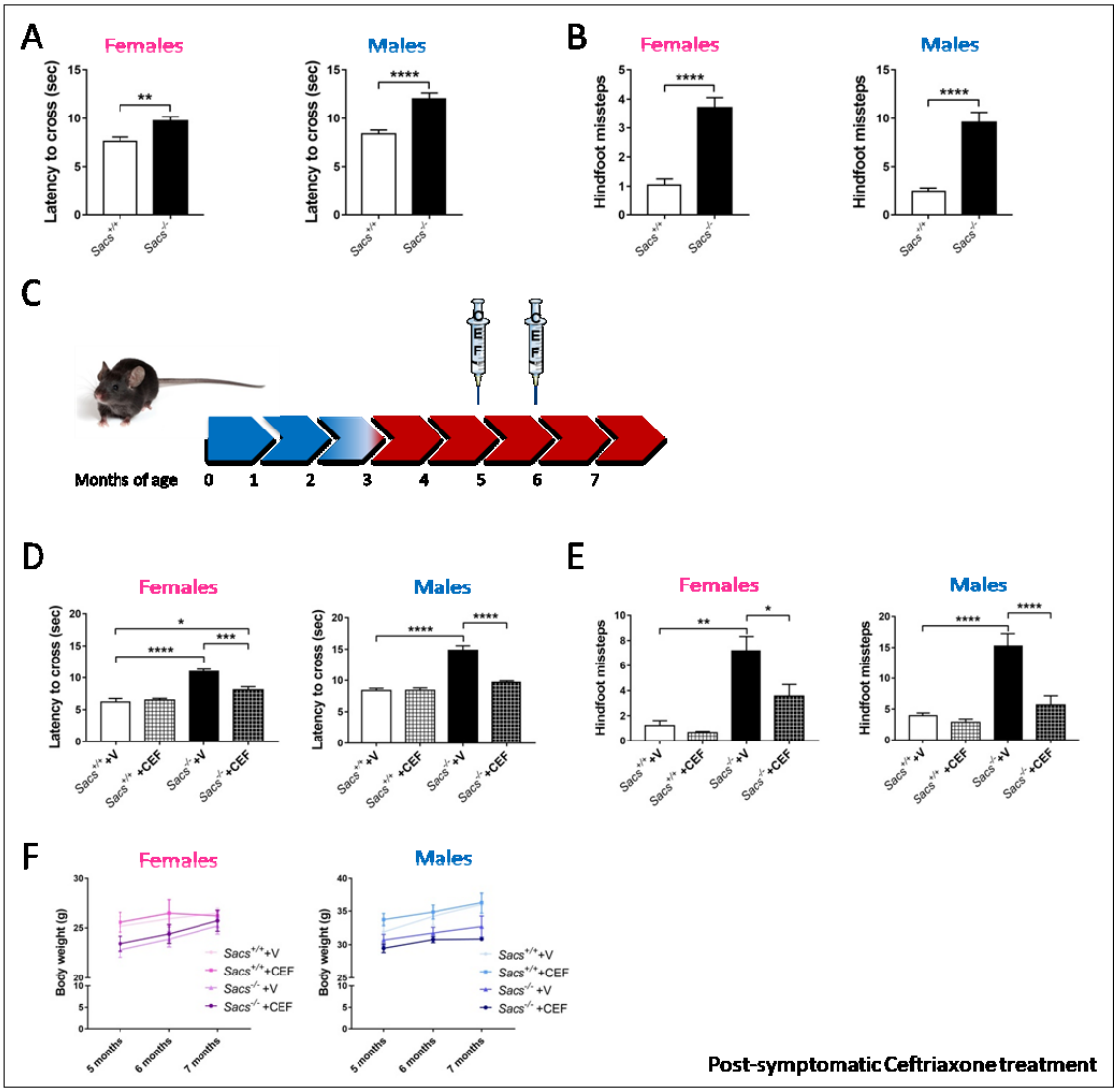

Figure 15_Results. Post-symptomatic Ceftriaxone treatment improves motor coordination of *Sacs*$^{-/-}$ mice. (A-B) Pre-treatment (5 month of age) motor assessment by BW test readouts of latency time to cross the beam (A) and number of hindfoot missteps (B) both in female and male mice. Bars represent mean±SEM; n= at least 10; Welch's t-test: *p<0,01, ****p<0,0001; (C) Schematic representation pre-clinical post-symptomatic Ceftriaxone administration protocol; (D-E) BW test performance in term of latency time to cross the beam (D) and number of hindfoot missteps (E) at 7 months of age both female and male Ceftriaxone- and vehicle-treated mice. Bars represent mean±SEM; n= at least 6; Two-way ANOVA with Tukey's correction: *p<0,05, **p<0,01, ***p<0,001,

****p<0,0001; (F) Monthly body weight check-up of both Ceftriaxone- and vehicle-treated female/male mice. Dots represent mean±SEM; n= at least 6.

We then correlated the motor improvement upon Ceftriaxone treatment with possible amelioration of histological and molecular parameters in *Sacs*$^{-/-}$ cerebella and controls. Semithin sections of anterior lobules of *Sacs*$^{-/-}$ Ceftriaxone-treated mice underlined an attenuation of PC degeneration when compared with placebo-treated *Sacs*$^{-/-}$ controls (Fig. 16A_Results). In fact, the PC density in these lobules was increased in the sample of mice treated with Ceftriaxone (Fig. 16A_Results). In addition, to investigate if Ca^{2+} deregulation observed in *Sacs*$^{-/-}$ cerebellum was rescued by Ceftriaxone administration, we evaluated the phosphorylation state of CaMKIIβ. Since Ceftriaxone acts reducing glutamatergic stimulation in post-synaptic dendrites, the phosphorylation levels of CaMKIIβ were found drastically reduced in *Sacs*$^{-/-}$ Ceftriaxone-treated cerebella compared with untreated ones (Fig. 16B_Results), despite unchanged level of total CaMKIIβ (Fig. 16B_Results). This result suggests that Ceftriaxone treatment was able to restore cytosolic Ca^{2+} homeostasis, while we found that it did not rescue the levels of npNFH (Fig. 16B_Results). Therefore, our data indicate this repurposed drug is able to ameliorate motor deficit, PC loss and Ca^{2+} deregulation.

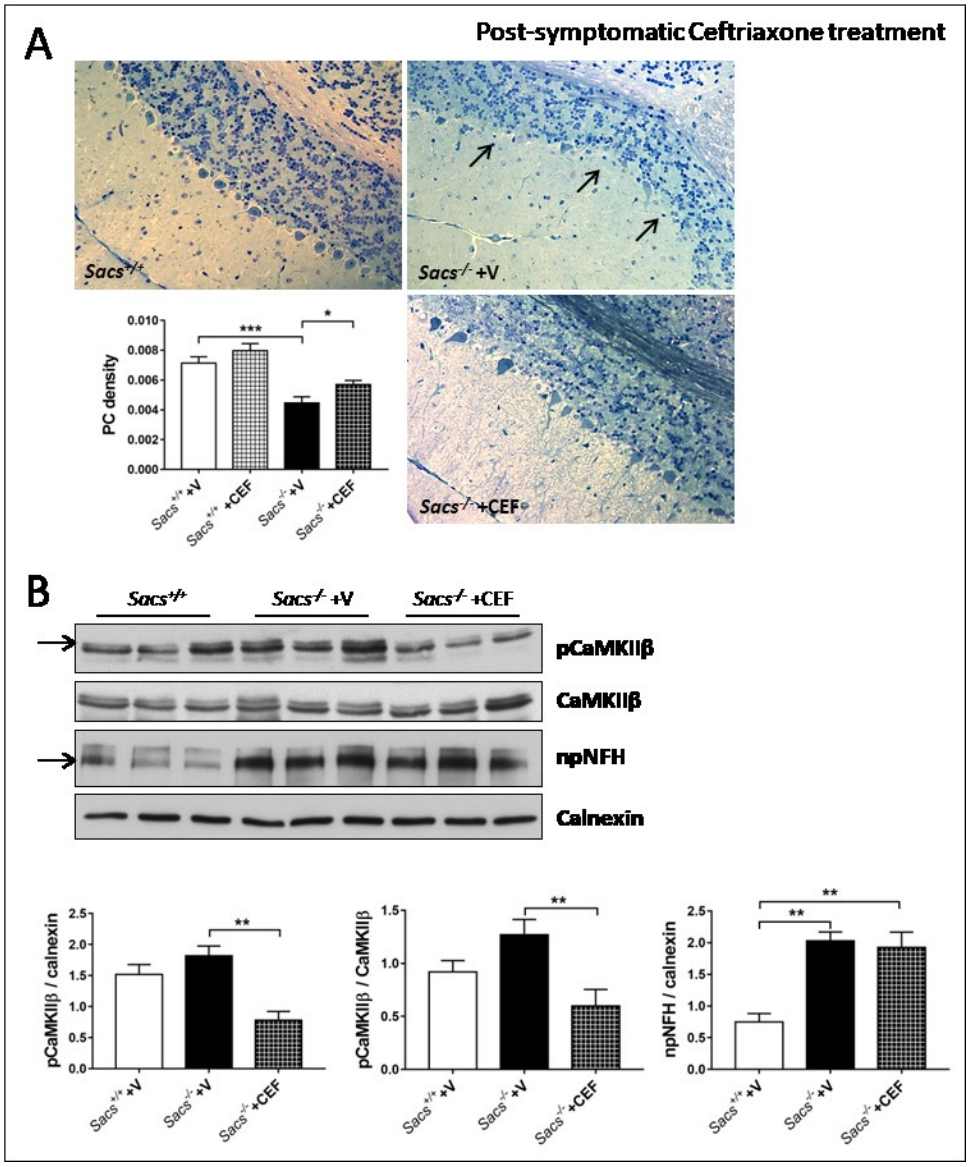

Figure 16_Results. Post-symptomatic Ceftriaxone treatment delays PC loss and mitigates Ca^{2+} deregulation in *Sacs*$^{-/-}$ cerebella. (A) Representative semithin section of cerebellum of Ceftriaxone- and vehicle-treated mice with relative quantitation of PC density. Bars represent mean±SEM; n= at least 4 (10 image analysed per sample); Two-way ANOVA with Tukey's correction: *p<0,01, ***p<0,001; (B) WB analysis showing levels of CaMKIIβ, pCaMKIIβ (upper band as indicated by the arrow) and npNFH (lower band as indicated by the arrow) in wild-type, vehicle- and Ceftriaxone-treated *Sacs*$^{-/-}$ cerebella at 7 months of age with relative quantitation (normalized on calnexin). Bars represent mean±SEM; n= at least 4; Two-way ANOVA with Tukey's correction: *p<0,5, **p<0,01.

3.3 *Sacs*$^{-/-}$ mice treated with Ceftriaxone at pre-symptomatic stage (1 month of age) show a delay in motor incoordination and PC degeneration

We also tested Ceftriaxone ability at pre-symptomatic stages, before the onset of disease symptoms. In this pre-clinical trial, the administration protocol consisted in the same posology: intraperitoneal injection of 200mg/kg of Ceftriaxone or placebo for 5 consecutive days

monthly, but the drug was administered earlier at 1 month of age and last 5 months (5 cycle of administration) till the age of 6-months. Also in this case, a month after the last Ceftriaxone administration, mice were evaluated for motor coordination by BW test and cerebella were used to investigate PC density (Fig. 17A_Results).

At 6 months of age motor assessment by BW test showed an evident improvement of *Sacs*$^{-/-}$ Ceftriaxone-treated mice both in latency time to cross the beam and in number of hindlimb missteps compared to placebo-treated age- and sex-matched controls (Fig. 17B_Results). Moreover, semithin section analysis underlined a reduced PC loss and, thus, increased PC density in *Sacs*$^{-/-}$ Ceftriaxone-treated cerebellar anterior lobules if compared to placebo-treated samples (Fig. 17C_Results).

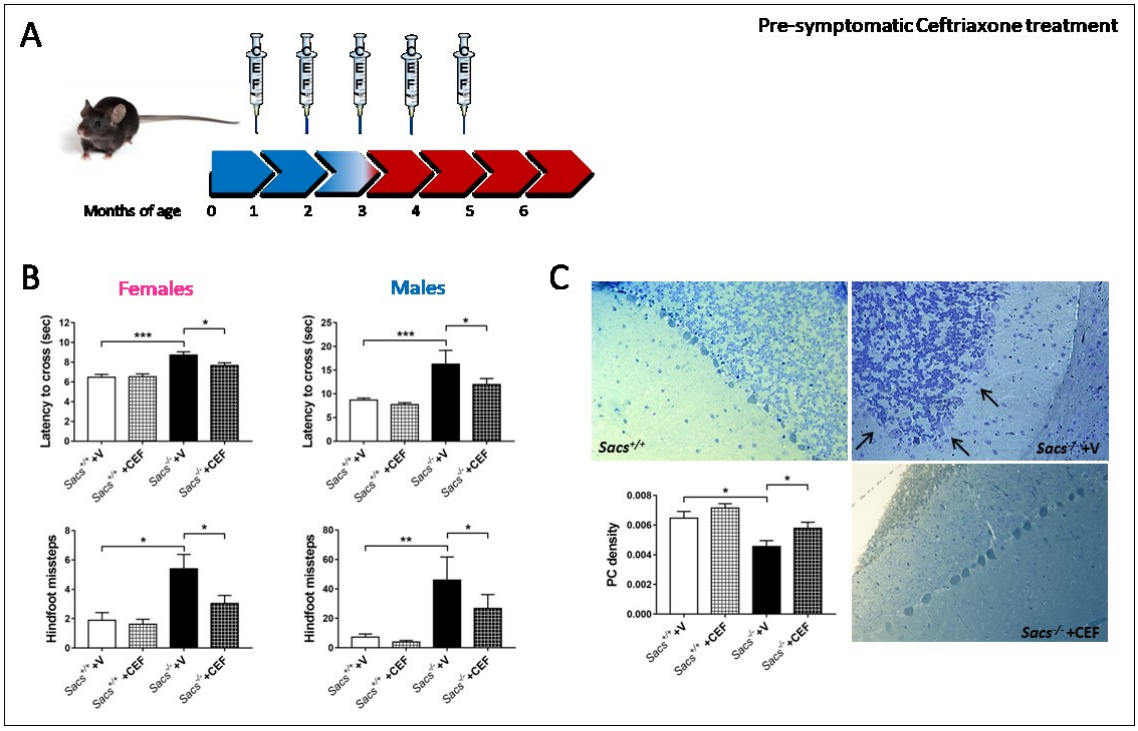

Figure 17_Results. Pre-symptomatic Ceftriaxone treatment ameliorates motor coordination of *Sacs*$^{-/-}$ mice delaying PC loss. (A) Schematic representation pre-clinical pre-symptomatic Ceftriaxone administration protocol; (B) BW test performance in term of latency time to cross the beam and number of hindfoot missteps at 6 months of age both female and male Ceftriaxone- and vehicle-treated mice. Bars represent mean±SEM; n= at least 4; Two-way ANOVA with Tukey's correction: *p<0,01, **p<0,01, ***p<0,001; (C) Representative semithin section of cerebellum of Ceftriaxone- and vehicle-treated mice with relative quantitation of PC density. Bars represent mean±SEM; n= at least 4 (10 image analysed per sample); Two-way ANOVA with Tukey's correction: *p<0,01.

As usual, during this trial we monitored body weight of treated and untreated mice and we found no significant differences between two groups (Fig. 18A_Results). To further explore the putative side effects of the drug, at the same stage of other analyses (6 months of age) we collected blood to perform general control of haematological parameters and some specific clinical chemistry analyses to assess kidney and liver functionality. The results of haematocrit

did not disclose any altered parameter (Fig. 18B_Results). Also, the values of blood urea and creatinine suggested that Ceftriaxone did not impact on kidney functionality. Likewise, albumin and transaminases ALT parameters indicated that liver works properly without any important alteration (Fig. 18B_Results).

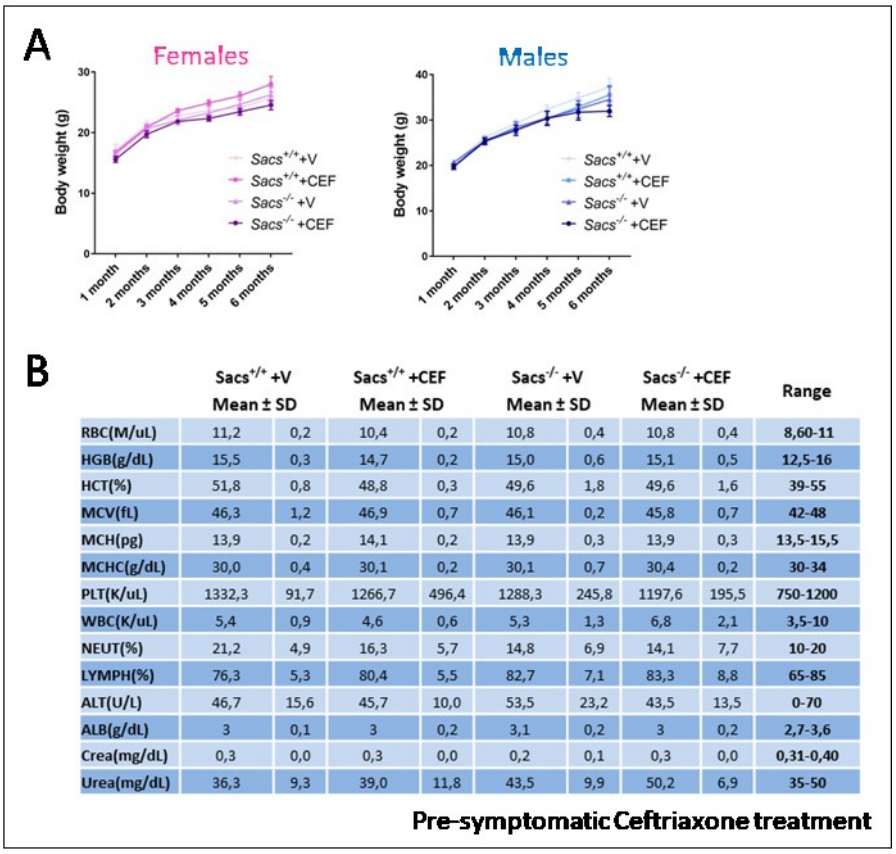

	Sacs$^{+/+}$ +V Mean ± SD		Sacs$^{+/+}$ +CEF Mean ± SD		Sacs$^{-/-}$ +V Mean ± SD		Sacs$^{-/-}$ +CEF Mean ± SD		Range
RBC(M/uL)	11,2	0,2	10,4	0,2	10,8	0,4	10,8	0,4	8,60-11
HGB(g/dL)	15,5	0,3	14,7	0,2	15,0	0,6	15,1	0,5	12,5-16
HCT(%)	51,8	0,8	48,8	0,3	49,6	1,8	49,6	1,6	39-55
MCV(fL)	46,3	1,2	46,9	0,7	46,1	0,2	45,8	0,7	42-48
MCH(pg)	13,9	0,2	14,1	0,2	13,9	0,3	13,9	0,3	13,5-15,5
MCHC(g/dL)	30,0	0,4	30,1	0,2	30,1	0,7	30,4	0,2	30-34
PLT(K/uL)	1332,3	91,7	1266,7	496,4	1288,3	245,8	1197,6	195,5	750-1200
WBC(K/uL)	5,4	0,9	4,6	0,6	5,3	1,3	6,8	2,1	3,5-10
NEUT(%)	21,2	4,9	16,3	5,7	14,8	6,9	14,1	7,7	10-20
LYMPH(%)	76,3	5,3	80,4	5,5	82,7	7,1	83,3	8,8	65-85
ALT(U/L)	46,7	15,6	45,7	10,0	53,5	23,2	43,5	13,5	0-70
ALB(g/dL)	3	0,1	3	0,2	3,1	0,2	3	0,2	2,7-3,6
Crea(mg/dL)	0,3	0,0	0,3	0,0	0,2	0,1	0,3	0,0	0,31-0,40
Urea(mg/dL)	36,3	9,3	39,0	11,8	43,5	9,9	50,2	6,9	35-50

Figure 18_Results. Toxicological analysis shows no altered blood parameters in pre-symptomatic Ceftriaxone-treated mice. (A) Monthly body weight check-up of both Ceftriaxone- and vehicle-treated female/male mice. Dots represent mean±SEM; n= at least 5; (B) Haematological and clinical chemistry parameters revealed by blood analysis in 6 month-old Ceftriaxone- and veihicle-treated mice.

Considering all these results, we can state that Ceftriaxone administration in the ARSACS mouse model with this posology is safe, and improves motor ability acting on regulation of cytosolic Ca^{2+} concentration and thus delaying PC death.

All these results represent the core components of a paper we will soon submit, in which I will be the first author. In fact, these data add new insights in the knowledge of ARSACS pathological mechanisms and provide suggestive perspectives in ARSACS treatments so far missing. Furthermore, recently, we obtained some intriguing findings that will be presented as preliminary data in the following chapter.

3.4 Ceftriaxone acts modulating transcription of genes related to synapse and neuroinflammation

In the laboratory, it was already demonstrated that Ceftriaxone administration improves ataxic phenotype in the SCA28 mouse model[66]. Anyway, Ceftriaxone mode of action and the mechanism through which the drug is able to delay the progression of neurodegenerative diseases, is missing to date. In order to understand how Ceftriaxone exerts beneficial effects in *Sacs*$^{-/-}$ mice, we decided to carry out a pilot experiment treating 5-months-old mice with Ceftriaxone in an acute way (5 consecutive days) and then perform RNAseq analysis on Ceftriaxone-treated and untreated cerebella (both wild-type and *Sacs*$^{-/-}$ mice) immediately after the treatment. In this way, we aimed at capturing the fastest transcriptional regulations mediated by the drug. The comparison of gene profile between wild-type untreated and Ceftriaxone-treated mice showed few significant changes in gene expression, and so we decided to focus on the modulation by Ceftriaxone in *Sacs*$^{-/-}$ mice. Also in this case Ceftriaxone was found to act on a limited number of targets, but we derived interesting hints. We first focused on genes that were significantly downregulated in *Sacs*$^{-/-}$ cerebella compared with wild-type controls, but upregulated by Ceftriaxone treatment (and thus "rescued"). We found 36 genes that cluster in specific categories (analysis performed by GProfiler tool) linked to synaptic signaling and anion transport, such as *Gabrq* and *Kcnj10* (Fig 19A and B_Results). On the other hand, we also analysed genes upregulated in *Sacs*$^{-/-}$ cerebellum versus wild-type, but downregulated ("rescued") by drug treatment. In this case we could not perform enrichment analysis due to the restricted number of genes (22 genes). Interestingly, this analysis underlined, in particular, two genes significantly upregulated in *Sacs*$^{-/-}$ cerebella versus wild-type that were downregulated by Ceftriaxone treatment (significant with $p<0,05$, but not significant with p adjusted). These genes are *Lcn2* and *Pycard*, two players of immune response[151] [152], that support with other genes neuroinflammation involvement in ARSACS pathogenesis, as described in the next paragraphs, Results 4.1 (Fig. 19C_Results). These results are of course preliminary and need more investigations, but they suggest that Ceftriaxone, in addition to the regulation of synapse and Ca^{2+} handling, may exert beneficial effects also on the neuroinflammatory response.

A

source	term_name	term_id	Adjusted p_value	Intersection size
GO:BP	anterograde trans-synaptic signaling	GO:0098916	0,004177458	6
GO:BP	chemical synaptic transmission	GO:0007268	0,004177458	6
GO:BP	trans-synaptic signaling	GO:0099537	0,004439002	6
GO:BP	synaptic signaling	GO:0099536	0,005439122	6
GO:BP	acidic amino acid transport	GO:0015800	0,010214277	3
GO:BP	anion transport	GO:0006820	0,017628574	5
GO:BP	dicarboxylic acid transport	GO:0006835	0,019234139	3

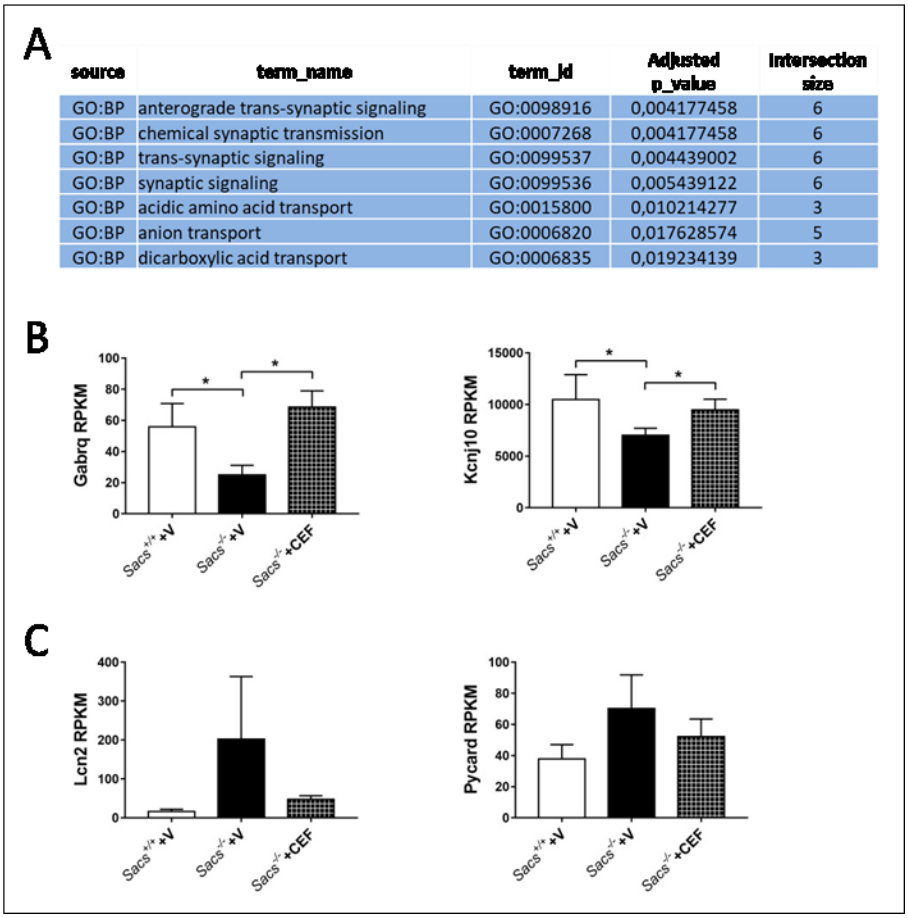

Figure 19_Results. Ceftriaxone treatment positively modulates synaptic signaling and neuroinflammation genes. (A) Gprofiler enrichment of deregulated genes comparing 5-months-old wild-type, *Sacs*$^{-/-}$ Ceftriaxone-treated and untreated cerebella showing top categories for GO biological process (BP); (B) RNAseq RPKM counts of *Gabrq* and *Kcnj10* genes in cerebellum of wild-type and *Sacs*$^{-/-}$ Ceftriaxone- and vehicle-treated mice. Bars represent mean±SEM; n=5; Two-way ANOVA with Tukey's correction: **p<0,01; (C) RNAseq RPKM counts of *Lcn2* and *Pycard* genes in cerebellum of wild-type and *Sacs*$^{-/-}$ Ceftriaxone- and vehicle-treated mice. Bars represent mean±SEM; n=5; Two-way ANOVA with Tukey's correction: ns.

4. *Sacs*$^{-/-}$ cerebellum manifests a strong neuroinflammatory response

4.1 Gene expression profile of *Sacs*$^{-/-}$ cerebellum underlines microglia and astrocyte activation

RNAseq analysis provided us not only evidence of Ca^{2+} deregulation, but also further interesting information. Besides the deregulation of genes related to Ca^{2+} handling (mostly downregulated), this experiment highlighted the upregulation of 59 genes in *Sacs*$^{-/-}$ cerebella compared to wild-type controls. The majority of these genes deals with the activation of neuroinflammatory response. In fact, genes with the highest fold-change (and significative p-

adjusted value) were linked to microglia and astrocyte activation, as underlined by GO enrichment analysis performed with GProfiler tool. This analysis revealed several deregulated classes of genes related to neuroinflammatory pathways and complement system activation (GO: BP, KEGG, REAC, WP) (Fig. 12B and 20A_Results). Microglia are brain-resident immune cells and play a pivotal role in the maintenance of brain homeostasis, but it is well assessed that they lose homeostatic function during neurodegenerative disorders[153 154 155]. Similarly, in response to brain insults, astroglia become reactive resulting in the activation of immune mediators and release of pro-inflammatory cytokines[156 157]. In this scenario, astrocyte- and microglia-mediated synapse pruning, a crucial process during normal brain development in forming precise synaptic circuits, is re-activated in order to phagocyte inactive synapses and degenerating neurons[158 159 160]. This process involves activation of the classical complement system, part of the brain-innate immune system, initiated by deposition of C1q on cellular components to be eliminated. The cascade converges on the central complement player C3, whose fragments (C3a and C3b) interact with their receptors (C3aR and CR3, respectively) to enact downstream immune effects such as phagocytosis[161 162 163]. Supporting this hypothesis, in depth analysis of deregulated genes in *Sacs*$^{-/-}$ cerebella (at 5 months of age) showed a strong upregulation of typical genes of Disease-Associated Microglia (DAM) signature such as *Lcn2*, *Itgax*, *Clec7a*, *Lpl*, *Pycard*, *Tyrobp* and *Trem2*[164 165] (Fig. 20B_Results). The same result was confirmed by qRT-PCR analysis, even if we did not reach statistical significance so far, probably because we have to improve the number of mice (Fig. 20C_Results). Investigating genes characterizing homeostatic microglia (e.g., *P2ry12*, *Cx3cr1*, *Tmem119*), we discovered they were unchanged comparing *Sacs*$^{-/-}$ cerebellar profile with wild-type control (Fig. 20D_Results). Interestingly, in *Sacs*$^{-/-}$ cerebella mRNA level of *Trem2*, a well-known master regulator of the second step of microglia activation (Trem2-dependent), was significantly upregulated (Fig. 20B_Results). No difference in microglial homeostatic genes and significant Trem2 activation at 5 months of age indicate that microglia phenotypic change has probably already reached the second stage (Trem2-dependent) of DAM, thus, suggesting an earlier involvement of neuroinflammation in ARSACS pathogenetic mechanism.

A

source	term_name	term_id	Adjusted p_value	Intersection size
KEGG	Complement and coagulation cascades	KEGG:04610	1,06E-07	7
KEGG	Staphylococcus aureus infection	KEGG:05150	3,10E-07	7
KEGG	Tuberculosis	KEGG:05152	9,74496E-06	7
KEGG	Systemic lupus erythematosus	KEGG:05322	0,000183273	5
KEGG	Amyotrophic lateral sclerosis (ALS)	KEGG:05014	0,000661419	4
KEGG	Phagosome	KEGG:04145	0,001888716	5
KEGG	Prion diseases	KEGG:05020	0,003958507	3
KEGG	Natural killer cell mediated cytotoxicity	KEGG:04650	0,005779213	4
KEGG	C-type lectin receptor signaling pathway	KEGG:04625	0,008448563	4
KEGG	Lysosome	KEGG:04142	0,011527126	4
REAC	Innate Immune System	REAC:R-MMU-168249	4,24E-15	24
REAC	Neutrophil degranulation	REAC:R-MMU-6798695	2,78E-12	17
REAC	Other semaphorin interactions	REAC:R-MMU-416700	7,73502E-06	4
REAC	Regulation of Complement cascade	REAC:R-MMU-977606	3,7708E-05	6
REAC	Complement cascade	REAC:R-MMU-166658	6,72076E-05	6
REAC	Hemostasis	REAC:R-MMU-109582	0,000293727	10
REAC	Initial triggering of complement	REAC:R-MMU-166663	0,000360552	5
REAC	Adaptive Immune System	REAC:R-MMU-1280218	0,000375087	11
REAC	Semaphorin interactions	REAC:R-MMU-373755	0,001410728	4
REAC	G alpha (i) signalling events	REAC:R-MMU-418594	0,005684551	7
WP	Microglia Pathogen Phagocytosis Pathway	WP:WP3626	9,63E-11	7
WP	TYROBP Causal Network	WP:WP3625	1,72E-09	7
WP	Complement Activation, Classical Pathway	WP:WP200	6,70E-09	5
WP	Oxidative Damage	WP:WP1496	1,37E-08	6
WP	Complement and Coagulation Cascades	WP:WP449	2,15E-07	6
WP	Spinal Cord Injury	WP:WP2432	0,002110175	4
WP	Macrophage markers	WP:WP2271	0,004783162	2
WP	Alpha6-Beta4 Integrin Signaling Pathway	WP:WP488	0,01535711	3
WP	Alzheimers Disease	WP:WP2075	0,020808796	3
WP	Focal Adhesion-PI3K-Akt-mTOR-signaling pathway	WP:WP2841	0,021673963	5

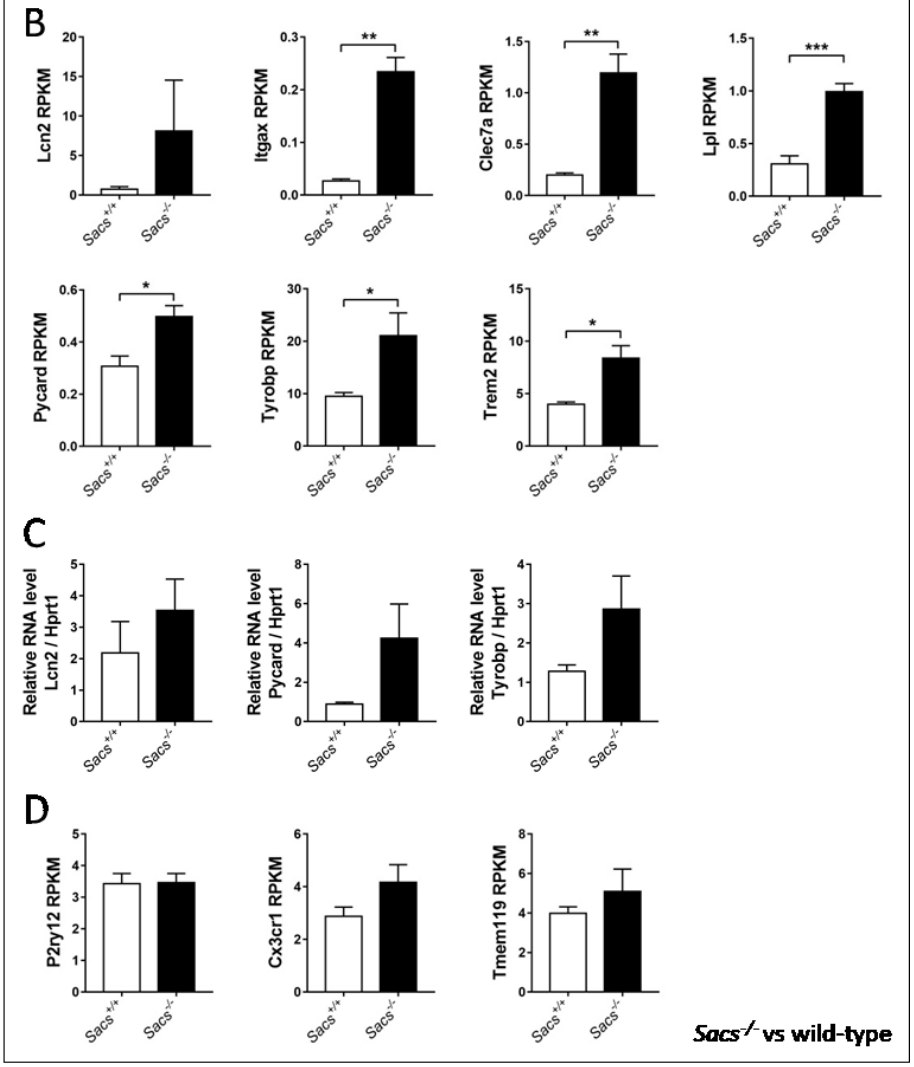

Figure 20_Results. Gene profiling of *Sacs*$^{-/-}$ cerebella shows activation of neuorinflammatory pathways. (A) Gprofiler enrichment showing top 10 categories for KEGG pathway (KEGG), Reactome (REACT) and WikiPathway (WP) database; (B) RNAseq RPKM counts of *Lcn2*, *Itgax*, *Clec7a*, *Lpl*, *Pycard*, *Tyrobp*, and *Trem2* genes in *Sacs*$^{-/-}$ and wild-type cerebella at 5 months of age. Bars represent mean±SEM; n=5; Welch's t-test : *p<0,05, **p<0,01, ***p<0,001; (C) qRT-PCR validation of levels of *Lcn2*, *Pycard* and *Tyrobp* mRNA (relative to *Hprt1* mRNA) in *Sacs*$^{-/-}$ and wild-type control cerebella at 5 months of age. Bars represent mean±SEM; n=5; Welch's t-test: ns; (D) RNAseq RPKM counts of *P2ry12*, *Cx3cr1*, and *Tmem119* genes in *Sacs*$^{-/-}$ and wild-type cerebella at 5 months of age. Bars represent mean±SEM; n=5; Welch's t-test: ns.

To further support neuroinflammation response in Sacs$^{-/-}$ cerebella, the analysis of RNAseq data showed, also, the activation of complement system in which C3 (with its receptors) together with C1q are the main players. In fact, we found striking upregulation of *C3*, *C3ar1*, *C4b*, *C1qa*, *C1qb* and *C1qc* genes in *Sacs*$^{-/-}$ cerebella compared to wild-type controls (Fig. 21A_Results).

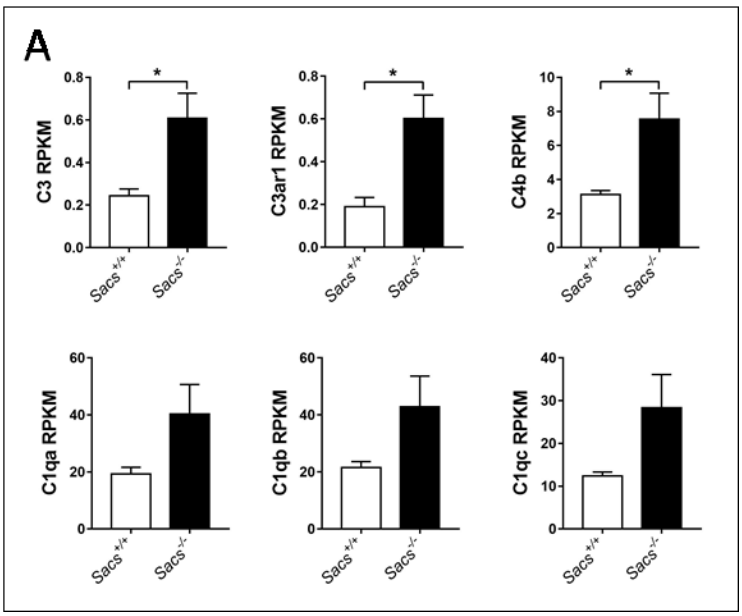

Figure 21_Results. Gene profiling of *Sacs*$^{-/-}$ cerebella highlights complement system activation. (A) RNAseq RPKM counts of *C3*, *C3ar1*, *C4b*, *C1qa*, *C1qb* and *C1qc* genes in *Sacs*$^{-/-}$ and wild-type cerebella at 5 months of age. Bars represent mean±SEM; n=5; Welch's t-test : *p<0,05.

4.2 Astrocytosis and microgliosis appear at early stages of disease in *Sacs*$^{-/-}$ mice

As a further confirmation of the activation of neuroinflammation process, we performed immunofluorescence assay to investigate the presence of GFAP-positive reactive astrocytes and putative morphological shift typical of phagocytic microglia. Double staining using anti-GFAP (astrocytic marker) and anti-Iba1 (microglial marker) antibodies documented a robust increase of GFAP signal underlying the activation of astrocytosis. In the more internal part of cerebellum where majority of glial cells resides, the increase of astrocyte cell number was prominent in *Sacs*$^{-/-}$ cerebella at 5 months of age (Fig. 22A_Results). Moreover, analysis of

Iba1-positive microglia disclosed the typical morphology of homeostatic state with small soma and quite branched processes in wild-type cerebella, while microglia in *Sacs*$^{-/-}$ slices assumed the amoeboid-phagocytic phenotype that characterizes the activation of DAM (Fig. 22A_Results). We did not detect lymphocyte ($CD3^+$ cells) and monocyte ($Ly6g^+$ cells) infiltration in *Sacs*$^{-/-}$ cerebella (data not shown).

Exploring these phenotypes earlier in disease progression (1 month of age), however, we appreciated increased number of reactive astrocytes in *Sacs*$^{-/-}$ cerebella (Fig. 22B_Results), indicating that astrocytosis is an early event in ARSACS pathogenesis. Likewise at the same timepoint, we observed morphological microglial shift in *Sacs*$^{-/-}$ cerebella (Fig. 22B_Results).

Altogether these findings suggest neuroinflammation could be involved in ARSACS disease progression.

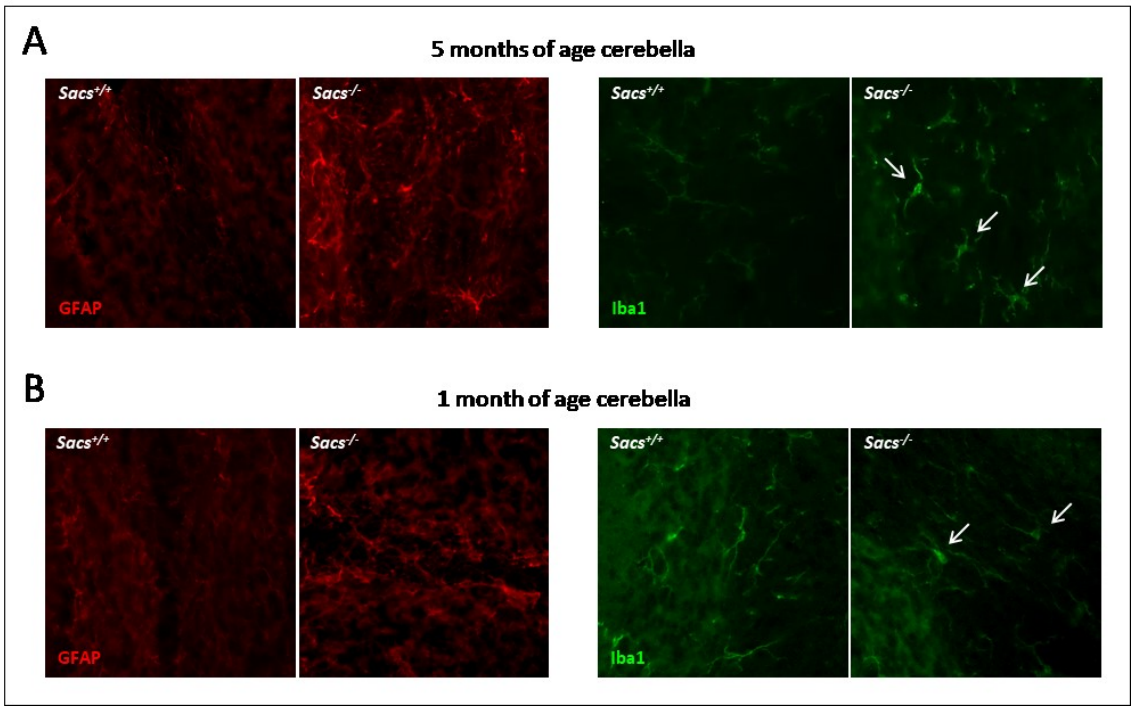

Figure 22_Results. *Sacs*$^{-/-}$ cerebella underline reactive astrocytes and phagocytic microglia as early as 1 month of age. (A-B) Representative images (40X) of immunofluorescence analysis showing astrocyte (GFAP, in red) and microglia (Iba1, in green) activation in *Sacs*$^{-/-}$ cerebella both at 5 months (A) and 1 month (B) of age compared with wild-type controls. Arrows indicate phagocytic microglia.

V. Discussion

In this work, we shed light on new molecular mechanisms involved in ARSACS pathogenesis, so far unexplored. The combination of complementary experimental strategies and different models (*in vitro*, *ex vivo* and *in vivo*), integrated with -omics approaches allowed us to better dissect the cascade of events downstream of sacsin absence/mutation, leading to PC degeneration. Namely, we established the consequences of aberrant npNFH accumulation specifically in PCs, i.e. defective transport of mitochondria (and ER) to distal dendrites and deregulation of Ca^{2+} homeostasis. We also identified NFs, plectin and myosin Va as specific interactors of sacsin. The latter two proteins may represent the missing connection between cytoskeleton and organelle alteration in ARSACS and for sure deserve further investigation.
As proof of concept of the proposed mechanism, targeting altered Ca^{2+} homeostasis with a pharmacological treatment reducing glutamate concentrations in inter-synaptic space, successfully delayed motor impairment and PC loss at both pre- and post-symptomatic stages in the ARSACS mouse model. Further, we disclosed a potential role for neuroinflammation in ARSACS pathogenesis, which appears to occur at early stages of disease in the *Sacs*$^{-/-}$ mouse.
Overall, the obtained data open new perspectives for the study and treatment of ARSACS.
The detailed discussion of each part of the thesis is reported below, subdivided in the same four chapters as the Results.

1. NFH accumulation is an early event in ARSACS pathogenesis and causes defective mitochondrial distribution in *Sacs*$^{-/-}$ PCs

In literature, it has been well assessed that loss of sacsin causes IF cytoskeleton derangement in different cell types, both proliferating cells and post-mitotic excitable neurons[95 88 98]. Anyway, the precise mechanism driving this phenotype and the molecular players involved are still missing. Lariviere and colleagues previously showed that only npNFH subunit accumulates both in post-mortem tissues of ARSACS patients and in several brain region of the ARSACS mouse models (cerebellum, cortex and hippocampus)[89 98]. However, among the different neuronal populations examined, only PCs were found degenerating, highlighting a peculiar susceptibility of these neurons in ARSACS [98].

Starting from this evidence, we wanted to understand how early NF remodelling appears in the *Sacs*$^{-/-}$ model and if it affects specific lobules of the cerebellum. By WB analysis, we found npNFH accumulation appearing as early as in 15-days-old *Sacs*$^{-/-}$ cerebella. This data support that npNFH accumulation precedes PC loss and motor incoordination, which manifest in *Sacs*$^{-/-}$ mice starting from 3 months of age. Furthermore, we demonstrated that npNFH accumulation strictly correlates with PC vulnerability, as it occurs mainly in the anterior lobules of the cerebellum. In these lobules, *Sacs*$^{-/-}$ PCs display altered firing properties[100] and later on degenerate[98]. This patterned sensitivity of anterior lobule-PCs was already observed in other mouse models of ataxia[166 167], anyway no clear association between ataxic spectrum and functional regionalization of PCs has been found to date. Cerebellar patterning is quite complex due to the presence of several topographical units based on anatomy, physiology or gene expression profile of PCs[18]. Although NFH expression PC patterning was described in cerebellum[168 169], hypothesizing a specific vulnerability of sacsin-depleted PCs based on molecular markers is quite difficult, since mediolateral gene expression codes so far identified are shared by all transverse zones even if with different organization. Therefore, we can speculate more likely about a susceptibility due to a specific combination of afferent fibers. This idea could be also supported by synaptic input changes that were recorded in *Sacs*$^{-/-}$ cerebella[100], even if the authors in this experiment did not specify the region in which they performed the electrophysiological measurements. Curiously, it is well established that the organization of parasagittal PC stripes is mirrored by the topography of mossy and climbing fibers afferent terminal fields[169].

We then decided to study in deep details the consequences of npNFH accumulation specifically in PCs. We worked *ex vivo*, by employing cerebellar cultures enriched in PCs, using a protocol developed in the lab. Time course analysis of *Sacs*$^{-/-}$ PCs in culture revealed that they degenerate over time, resulting a good tool to model ARSACS physiopathology. Our data show early and striking npNFH accumulation in proximal dendrites of *Sacs*$^{-/-}$ primary PCs. This phenotype has severe downstream consequences, which likely cause PC degeneration in ARSACS, i.e. altered mitochondrial and ER trafficking and Ca^{2+} deregulation. Indeed, our volumetric analysis of confocal stacks in primary PCs showed defective mitochondrial and ER distribution in distal processes of *Sacs*$^{-/-}$ cells. This faulty transport of mitochondria probably deprives the synapses of the primary source of energy (ATP) to activate Ca^{2+} clearance systems at plasma membrane and at the ER, but also of the Ca^{2+} buffering capacity of the mitochondria and ER themselves. The reduced transport of mitochondria to synapses in the absence of

sacsin is also supported by proteomics experiment performed on post-synaptic density (PSD) enrichments. This analysis showed a significant reduction of several mitochondrial structural proteins in *Sacs*$^{-/-}$ samples compared to wild-type controls (preliminary data, not shown).

Despite some studies in cell models proposed a direct effect of sacsin on mitochondrial functionality and morphology[96], our *ex vivo* and *in vivo* data in *Sacs*$^{-/-}$ cerebellum indicate that the alteration of mitochondrial trafficking is likely secondary to cytoskeleton remodelling and that mitochondrial functionality is preserved in the absence of sacsin.

Previous papers showed hyperfused mitochondrial morphology in ARSACS patient fibroblasts, MEFs and *SACS* knock-down SH-SY5Y cells[96]. This was proposed to occur through defective recruitment of fission machinery (DRP1) to mitochondria in the absence of sacsin[96]. Also, in the same cell models, it has been shown that the absence of sacsin impacts on mitochondrial bioenergetics, by reducing oxygen consumption rate of basal and maximal respiration, as well as of ATP production[96]. Our data, performed in primary PCs and cerebellum, which are mostly affected in ARSACS, however pinpoint concerns about studies performed in fibroblasts. Indeed, by EM we demonstrated that mitochondrial morphology was comparable between *Sacs*$^{-/-}$ mice and controls, with no signs of hyperfusion or cristae alteration. Accordingly, mitochondrial ATP production resulted unaltered in *Sacs*$^{-/-}$ cerebellum, both at baseline and upon pyruvate stimulation. These experiments were performed at 5 months of age, when neurodegeneration is overt in the ARSACS mouse model. One partial explanation to reconcile our *in vivo* bioenergetics data with previous studies in ARSACS cells could be the dilution effect, given that we measured total cerebellum and not specifically PCs. However, our preliminary data in primary *Sacs*$^{-/-}$ PCs show that $\Delta\Psi_{mito}$ is conserved, excluding major deficits in oxidative phosphorylation. Altogether, our findings show that mitochondria in *Sacs*$^{-/-}$ PCs are morphologically intact and metabolically active, allowing us to exclude that organelle dysfunction or hyper-elongation *per se* negatively affect mitochondrial transport.

On the contrary, in *Sacs*$^{-/-}$ mice the transport of mitochondria is likely disturbed by alterations in cytoskeletal tracks, on which they move towards distal dendrites. Although mitochondrial transport is known to occur mostly on microtubules and actin filaments, there is growing evidence that mitochondria can directly bind NFs[170].

Extensive dephosphorylation of NFH subunits affects their interaction with mitochondria leading to a reduced rate of mitochondrial motility[116]. This situation is more evident in the dendrites where the poorly phosphorylated NFs are prominent[171] and, thus, they form more rarely inter-NF crossbridges than phosphorylated ones[172]. This notion, associated with

experimental evidence of a specific npNFH accumulation in proximal dendrites of Sacs$^{-/-}$ PCs, enhances the idea of cytoskeleton involvement in defective distribution of mitochondria throughout all neuronal processes, till the most distant ones.

Another important evidence in support of the impact of IF cytoskeleton remodeling on organelle trafficking was provided by sacsin interactors identified in *SACS*$^{-/-}$ SH-SY5Y cells differentiated into neurons. We used this tool to increase the chances to efficiently immunoprecipitate sacsin and getting cleaner results, considering that in these cells we appreciated the same npNFH accumulation seen *ex vivo* and *in vivo*. The immunoprecipitation of sacsin and following LFQ/MS-MS revealed few proteins physically interacting with sacsin and the great majority of them were large cytoskeletal proteins, including NFL and NFM, while no mitochondrial proteins were detected as specific interactors. It is thus conceivable that the IF accumulation is directly and primarily related to the absence of sacsin, whereas the impaired mitochondrial distribution could be an indirect secondary effect.

In addition to NFs, two more sacsin interactors caught our attention: plectin and myosin Va. Plectin is a giant multifunctional protein (> 500 kDa) acting as a mechanical linker between IF network and other cytoskeletal structures, as well as mitochondria. Different plectin isoforms are differentially targeted to distinct cellular locations where they function as universal IF docking sites. The interaction of plectin with several cellular components, such as IF and mitochondria, is attributed to C-terminal region of the protein, but the specificity for plectin substrate is ascribable to N-terminal region that differentiates several plectin isoforms obtained by the activation of different promoters in a tissue and cell-specific manner[173]. Moreover, P1c isoform (mostly expressed in the brain) was found in post-synaptic dendrites and plectin deficiency was demonstrated to impact on mitochondrial shape and mostly its transport[121 122 174]. Interestingly, we uncovered reduced plectin amount in different sacsin-depleted cells (*SACS*$^{-/-}$ SH-SY5Y cells and ARSACS patient fibroblasts). However, plectin levels were found not significantly changed in *Sacs*$^{-/-}$ mouse cerebella versus wild-type by LFQ proteomics. The different results obtained in cells versus cerebellum could be ascribable to heterogeneity of cells in cerebellar preparations, in which we may have not appreciated plectin deficiency due to a dilution effect. Further experiments are necessary to strengthen these findings in *Sacs*$^{-/-}$ PCs (i.e. by imaging in primary PCs and WB *in vivo*). We think anyway that plectin could be the missing link between cytoskeleton remodeling and defective mitochondrial distribution, adding a crucial piece of the puzzle in ARSACS pathogenesis.

Class V myosins are actin-based motors that mediate the proper short-range intracellular transport of diverse organelles, mRNAs and proteins[175]. In particular, myosin Va (> 200 kDa protein) is expressed at high levels in PCs[176] and, indeed, its deletion causes severe ataxic phenotype[177]. Moreover, myosin Va-deficient PCs showed drastic organelle localization defects, as demonstrated by ER missing specifically from dendritic spines[178 123]. In these cellular districts ER is crucial to release Ca^{2+} locally through IP3R1 in response to IP3 produced after activation of the metabotropic glutamate receptor, but this process is strictly dependent on proper myosin Va-mediated ER transport in dendritic spines[123]. Our preliminary data showing alterations in ER distribution in distal part of dendrites in *Sacs*$^{-/-}$ primary PCs could support myosin Va involvement in ARSACS pathogenesis. As for plectin, further investigations are needed in this direction. Myosin Va levels in *Sacs*$^{-/-}$ cerebella are still unexplored, as it was not significantly detected in proteomics studies. Interestingly, myosin Va was also found to interact with NFs (selectively NFL subunit) influencing its density[179].

In summary, our data support the hypothesis that sacsin may function as chaperone (as suggested by the presence of hsp90 like domains) or co-chaperone (as suggested by the presence of SIRPT and J domains) for big size cytoskeletal proteins (e.g., NFs, plectin and myosin Va) modulating their folding and/or assembly. In this scenario, mutations in sacsin may lead to impaired sacsin function and, thus, to a severe cytoskeleton derangement. The synergism of these pathological events may then cause impaired mitochondrial (and ER) distribution and dynamics, leaving their ultrastructure and metabolism unaltered. Finally, dysfunctional cellular trafficking could drive deleterious downstream events as the deregulation of Ca^{2+} homeostasis (I will discuss later about this point).

Perspectives

To understand more about increased vulnerability of anterior lobule-PCs in the absence of sacsin, we want to explore in detail PC death patterning and try to correlate it with some specific cerebellar stripe distribution.

To address the intricate issue of sacsin function and its putative role as chaperone and hub protein for large cytoskeletal proteins, we want to explore if NFH and sacsin co-localized in the soma of primary PC by immunofluorescence experiment supporting a putative NFH folding defect, which oppose its entry in dendrites. Moreover, about plectin, we want to investigate deeper its localization and putative interaction with sacsin and NFs by immunofluorescence assay in primary PCs. We want, also, to discover if reduced amount of plectin is due to increase

degradation as consequence of misfolding event or misfolded plectin aggregates in insoluble complexes. Finally, about myosin Va, we are now analysing its levels in *Sacs*$^{-/-}$ cerebellar protein lysates to try to correlate this data with NFH and plectin amount.

Although cristae structure is conserved in *Sacs*$^{-/-}$ PCs, we want to perform histoenzymatic staining for different mitochondrial enzyme (e.g., SDH and CoxIV) in order to further evaluate mitochondrial functionality and exclude a dilution effect.

2. Alteration of mitochondrial trafficking due to cytoskeleton remodeling leads to the deregulation of Ca^{2+} homeostasis in PC distal dendrites

In the second chapter of the work, we focused our attention on downstream consequences of impaired mitochondrial and ER distribution. In fact, proper mitochondrial trafficking and its docking in precise sites allow to maintain the required number of stationary mitochondria in regions that particularly rely on energy production and Ca^{2+}-buffering capacity[64 170]. ATP has a limited diffusion capacity in the intracellular environment and particularly within long neuronal processes and, thus, mitochondria correctly distributed are needed to provide local sources of ATP, which is necessary to maintain the activity of Ca^{2+} ATPases, as well as fast spike propagation and synaptic transmission. Likewise mitochondria and ER, which can sequester intracellular Ca^{2+}, have an important role in maintaining Ca^{2+} homeostasis at synapses[64]. In this context, we demonstrated altered Ca^{2+} homeostasis in *Sacs*$^{-/-}$ cerebella highlighted both by proteomics and transcriptomics experiments, as well as by biochemical approaches. CaMKIIβ is a highly expressed protein in the brain (all CaMKII isoforms account for 1-2% of total brain proteins[133]) and a central coordinator of Ca^{2+} signals in synapse. We proved a specific increase of phosphorylation state of CaMKIIβ despite unaltered levels of CaMKIIβ in *Sacs*$^{-/-}$ cerebella, suggesting pathological Ca^{2+} elevations. Moreover, Ca^{2+} imaging experiments disclosed a higher cytosolic Ca^{2+} concentration in *Sacs*$^{-/-}$ PCs, and this resulted a peculiar feature of PCs, as *Sacs*$^{-/-}$ granule cells present normal Ca^{2+} handling upon KCl stimulation. We can explain increased Ca^{2+} sensitivity of PCs with their morphological and functional properties. In fact, PCs are highly polarized neurons with extremely ramified dendritic tree receiving mostly glutamatergic afferents inducing huge Ca^{2+} influxes in post-synapses. High glutamatergic inputs (typical of PCs) coupled to reduced mitochondrial and ER transport in distal dendrites, as we demonstrated, may lead to cytosolic Ca^{2+} dysregulation, ultimately causing degeneration of *Sacs*$^{-/-}$ PCs.

Ca^{2+} homeostasis at spines is locally modulated not only by mitochondria but also by ER. In response to precise cellular signals, ER either uptakes Ca^{2+} via SERCA pumps or release it through IP3R1 to maintain a proper Ca^{2+} concentration. Interestingly, we found IP3R1 downregulated in *Sacs*$^{-/-}$ cerebella, at both mRNA and protein level, at 5 months of age. We can speculate that IP3R1 reduced level can be a protective feedback response of the cell to prevent toxic consequences[138] [180] [181], avoiding further Ca^{2+} release into the cytoplasm. Interestingly, decreased IP3R1 levels or functionality was associated to several cerebellar ataxias. In fact, both heterozygous and homozygous mutations in *Itpr1* gene were reported to cause different type of ataxia (e.g., SCA15/SCA16/SCA29 and Gillespie Syndrome)[181]. In addition, in many other ataxic disorders it was described aberrant IP3R1-mediated Ca^{2+} signaling causing dysregulated Ca^{2+} mobilization from ER in PCs (e.g., SCA1, SCA2, SCA3, SCA5, SCA14, SCA41, ARCA2…)[181]. This evidence suggests that by targeting IP3R1 it could be possible to modulate and, possibly, to ameliorate a pathological mechanism common to many ataxias. IP3R1 is, indeed, highly expressed in cerebellar PCs and plays a critical role in the synaptic plasticity of the PF-PC synapse, dendritic development, spine maintenance in mature PCs, motor coordination, as well as learning in mice[182]. More studies are however needed to identify the precise role of IP3R1 in ARSACS pathogenesis.

Perspectives

Future perspectives aim to investigate Ca^{2+} currents in *Sacs*$^{-/-}$ PC post-synaptic dendrites. In fact, changes in fast glutamatergic synaptic transmission were already described in *Sacs*$^{-/-}$ PCs[100], however, no Ca^{2+} currents analysis were performed, as the authors focused their attention on Na^{+} and K^{+} conductance. Since we uncovered strong Ca^{2+} deregulation in *Sacs*$^{-/-}$ PCs, we want to dissect electrical PC membrane signals mediated by Ca^{2+}. For this purpose, we want to unravel synaptic plasticity mechanisms and PC firing properties such as complex spikes, which could provide more knowledge about Ca^{2+} currents so far missing in *Sacs*$^{-/-}$ cerebellum.

3. A pre-clinical pharmacological treatment with Ceftriaxone in ARSACS

Molecular and biochemical investigations suggesting Ca^{2+} deregulation in *Sacs*$^{-/-}$ cerebella provided us the rationale to test Ceftriaxone efficacy in the ARSACS mouse model. We decided

to administer Ceftriaxone intraperitoneally at the dosage of 200 mg/kg body weight for 5 consecutive days every month, a regimen already successfully proven to target cerebellum[66] [150]. Firstly, we decided to administer Ceftriaxone after the onset of motor incoordination (starting point fixed at 5 months of age). Drug treatment resulted highly successful in symptomatic *Sacs*$^{-/-}$ mice, as it restored Ca^{2+} levels and consequently delayed PC loss with striking improvement of motor performances. Similar results were obtained also with the pre-symptomatic Ceftriaxone treatment (starting at 1 month of age), where we tested the possibility to prevent or delay ARSACS disease progression. The outcomes obtained for pre-symptomatic Ceftriaxone administration seem not to be significantly different compared with post-symptomatic treatment, suggesting that they both delay PC loss and motor impairment. Two possible explanations could be that Ceftriaxone did not target the earliest upstream events of ARSACS pathogenesis (i.e. npNFH accumulation and/or other that we still undefined), and/or that maybe 1 month is already too late for treatment. In fact, although few papers showed that Ceftriaxone was able to rescue and prevent protein aggregation (also astrocyte intermediate filament, GFAP)[183] [184], we found in *Sacs*$^{-/-}$ mice Ceftriaxone failed to rescue the npNFH accumulation. On the other hand, we demonstrated that it restores normal phosphorylation state of CaMKIIβ, indicating that it acts mainly on Ca^{2+} regulation, as expected from previous studies[144]. Actually, the exact mode of action of Ceftriaxone is still poorly defined and it is supposed to occur by multiple mechanisms, including reduced excitotoxicity, increased antioxidant response and attenuated neuroinflammation[145] [146].

Ceftriaxone positive effects in neurodegenerative disorders were uncovered for the first time, in 2005 by Rothstein and colleagues, which found improvements upon Ceftriaxone administration in ALS mouse model, suggesting GLT1 upregulation as beneficial effector[144]. Some years later, two other papers came out supporting Ceftriaxone-mediated neuroprotection via Nrf2 induction and glutathione increased content, two well-known antioxidant response mechanisms, in ALS[145] and SMA[146] models. In the recent years Ceftriaxone was used to target cerebellum with good results both in GLT1 upregulation and in motor improvements in SCA28[66] and myotonic dystrophy[150] mouse models.

A first clinical trial in a cohort of ALS patients failed[185], but many explanations could be found behind this failure. First, in ALS Ceftriaxone was used because glutamate excitotoxicity may contribute to the pathophysiology, even if the precise molecular mechanisms was not elucidated. Second in the ALS trial Ceftriaxone was administered i.v., via a central venous catheter, chronically (at the dose of 4 g/day in 2 administrations in phase III) for several

months (in some cases up to 30 months). Also, most patients assumed Riluzole at the same time. This elicited toxic adverse reactions and many patients abandoned the study before its conclusion[185].

We thus believe that Ceftriaxone treatment failure in ALS does not imply the same for ARSACS or other cerebellar ataxias. The two diseases are different in terms of clinical features, disease progression and duration, neuronal populations involved and underlying molecular mechanisms. In the ARSACS model, Ceftriaxone was administered to specifically target post-synaptic Ca^{2+} deregulation in PCs, that we have documented. PCs possess an extremely branched dendritic tree receiving mostly glutamatergic stimulation, and thus massive Ca^{2+} influx. The intrinsic vulnerability of Purkinje cells to increased Ca^{2+} levels is indeed demonstrated by the many genetic forms of cerebellar ataxia showing alteration of Ca^{2+} as pathogenetic mechanism.

The chronic use of Ceftriaxone may be not necessary in a clinical trial in ARSACS. Our data show that a 5-days i.p. administration repeated monthly at the dose of 200 mg/kg is sufficient to ameliorate the ataxic phenotype of the *Sacs*$^{-/-}$ mice. Wild-type mice treated with this regimen (5-days/month at 200 mg/kg) for 1 year do not show any sign of major toxicity. Therefore, a marked reduction of the dosage combined with a pulsed treatment (tailored by following specific Ceftriaxone targets) could drastically reduce toxicity.

The pulsed administration may not imply the use of a central catheter, or Ceftriaxone maybe be also administered intramuscularly or subcutaneously. This strategy has been recently employed in a clinical trial for Parkinson's disease, where they are administering Ceftriaxone by intramuscular injection at 1 g with around 2 ml of lidocaine solvent per day for Day 1, 3, and 5 per cycle on a 2 weekly cycle (https://clinicaltrials.gov/ct2/show/NCT03413384?term=ceftriaxone&draw=2&rank=3).

A still open question relates to Ceftriaxone mode of action. The most widely accepted view is that it alters transcription of specific targets, acting via NF-kB pathway[147].

Before addressing this point, I need to discuss what described in the final chapter of the thesis, where we investigated a new and intriguing component of ARSACS pathogenesis. In fact, RNAseq analysis of 5 months-old Sacs$^{-/-}$ cerebella and relative wild-type controls revealed a strong upregulation of several genes involved in DAM signature[164] [165], suggesting the involvement of robust neuroinflammatory reaction in ARSACS progression. In support of transcriptomic data, we also confirmed astrocyte and microglia activation by immunofluorescence staining with GFAP and Iba1 in cerebellar slices both at 1 and 6 months

of age. In literature, it was described that DAM is generated through a precise modulation of microglia expression profile. In particular, it is a two-step process, in which the first phase is characterized mainly by downregulation of microglia homeostatic genes and a starting upregulation of specific markers of reactive microglia (e.g., ApoE, Tyrobp). Whereas the second part of this mechanism is mediated by activation of Trem2, a well-known master regulator of microglia activation (Trem2-dependent phase), that involves the upregulation of phagocytic and lipid metabolism genes (e.g., Lpl, Itgax, Clec7a)[165]. Since at post-symptomatic stage of ARSACS disease we detected no differences in microglia homeostatic genes and a significant upregulation of Trem2 in *Sacs*$^{-/-}$ cerebella, we hypothesized that at this stage (5 months of age) neuroinflammation reaches the second phase, supporting an earlier activation of neuroinflammatory response. This seems to be the case, as we observed typical signs of reactive astrocytosis and phagocytic microglia as early as in *Sacs*$^{-/-}$ cerebella at 1 month of age, suggesting that neuroinflammation could be an early component of ARSACS disease progression. This is also supported by strong upregulation of complement system players in *Sacs*$^{-/-}$ cerebella.

Innate immunity is increasingly recognized to contribute to the pathogenesis of neurodegenerative disorders. Although further investigations are needed, this insight provides us new piece of knowledge of ARSACS pathophysiological cascade and it could be also a good target for pharmacological treatment in order to stem disease progression.

In the view of these new results, to better assess Ceftriaxone mode of action, we performed preliminary RNAseq analysis of *Sacs*$^{-/-}$ mice treated for 5 days with Ceftraxone or vehicle. We choose this approach to increase the chances to see fast transcriptional regulations mediated by the drug. We focused on those genes that were highly deregulated in *Sacs*$^{-/-}$ mice compared to wild-type and significantly “rescued” by Ceftriaxone treatment. Among the downregulated genes by sacsin absence and upregulated by Ceftriaxone administration, GO enrichment underlined many genes involved in synaptic signaling and anion transport categories (e.g., *Gabrq* and *Kcnj10*). This supports our starting hypothesis that Ceftriaxone acts by improving synaptic functionality and by modulating Ca^{2+} homeostasis (and other signaling molecules). On the other hand, many of the upregulated genes in the absence of sacsin (which relate to neuroinflammation) show a trend towards the recovery upon Ceftriaxone treatment (even if many of them have no statistical significance yet). Among them, we identified two interesting genes, *Lcn2* and *Pycard*, which are two key players of the inflammatory response. *Lcn2* gene encodes for Lipocalin-2 (LCN2) a multifunctional protein synthesized and secreted as an

inducible factor from activated microglia, reactive astrocytes, neurons, and endothelial cells in response to inflammatory, infectious, or injurious insults. Moreover, Lipocalin-2 induces chemokine production in the CNS in response to inflammatory challenges, and actively participates in the innate immune response, and regulation of neuroinflammation and neurodegeneration[151]. Anyway, its specific role in pathophysiological events of CNS has not been completely elucidated yet, but it is emerging as a disease progression biomarker in frontotemporal dementia and AD[186]. Pycard is a key adaptor protein in the activation of inflammosome complex, a crucial step involved in cell death and in the release of inflammatory signals that amplify a damaging insult[152]. From the comparison of their expression profile in vehicle-treated *Sacs*$^{-/-}$ versus wild-type cerebella, *Lcn2* and *Pycard* displayed high $\log_2$FoldChange (3,44 and 1,13, respectively, p<0,01), thus resulting strongly upregulated. Conversely, Ceftriaxone administration downregulates their expression showing prominent negative $\log_2$FoldChange (-2,23 for *Lcn2* and -0,68 for *Pycard*, p<0,01:Ceftriaxone-treated *Sacs*$^{-/-}$ vs vehicle-treated *Sacs*$^{-/-}$ samples).

Altogether, this preliminary evidence suggests that Ceftriaxone could ameliorate ARSACS phenotype by acting on both ion transport/Ca^{2+} currents and neuroinflammation.

In this scenario, a crucial role in Ceftriaxone effectiveness could be assigned to NF-kB, a key regulator of neuroinflammation[187], whose activation was associated with various neurodegenerative condition (e.g., AD[188], PD[189], HD[190]). Anyway, in addition to neurotoxic role, also a neuroprotective effect was proposed for NF-kB, in which the outcome likely dependent on the timing, duration, and level of its activity[191]. In fact, upon degradation of IkB, NF-kB translocates to the nucleus where it activates expression of several targets, including its inhibitor IkBα, which form an autoinhibitory feedback loop that ensures proper silencing of NF-kB following each activation. Probably Ceftriaxone influences this timing control of NF-kB activation in order to promote GLT1 upregulation[147] and antioxidant response[145] [146], and modulating neuroinflammation.

Our data about pre-clinical pharmacological treatment with Ceftriaxone provide promising perspectives in the view of a therapy for ARSACS patients, so far missing. In particular, the post-symptomatic efficacy of drug administration is very encouraging because the majority of ARSACS patients are diagnosed only after the onset of gait abnormalities. Also, in the view of the recent findings, we may speculate a combined treatment with Ceftriaxone together another molecule repressing immune response.

Perspectives

To address the comprehension of the best Ceftriaxone administration protocol, we are going to test drug efficacy after longer time from the last dose in order to dilute pharmacological administration during time.

While in a translational view of Ceftriaxone administration in clinical settings, we want to screen and identify easy to measure with a non-invasive biomarkers that could help monitoring drug efficacy. In this scenario, we put our attention on RNFL thickness, which is peculiarly increased in ARSACS patients [76–85]. The RNFL is the most internal layer of the retina where axons of ganglion cells that are directed to optic nerve reside, and in this region ganglion cell axons are poorly myelinated. To verify if *Sacs*$^{-/-}$ mouse model recapitulates this feature, we are now performing OCT investigation at different timepoints and relative immunohistochemistry analysis of retinal layers.

In addition to OCT, we want also to explore bodily fluids biomarkers, such as plasma amount of specific protein that are well-known hallmarks of neurodegeneration. In fact, the recent implementation of ultrasensitive measurement technologies allowed us to test the proteins characterizing the cerebrospinal fluid (CSF) also in blood samples. These new approaches are of great importance to tackle diseases at such early stages and to follow, with non-invasive approach, biomarkers that reflect disease pathology and the impact of disease-modifying treatments understanding better the long-term effects. Among all of them, we are interested to test the plasma levels of NFs subunits, NFL and pNFH, by Single-Molecule Array (SiMoA). NFL is the most used blood biomarker to follow onset and progression of neurodegeneration processes and in some cases increase of NFL levels is already observed in asymptomatic/pre-symptomatic stages[192]. In fact, NFL presence in body fluids correlates with neuronal death realising this protein in the environment that flows in cerebrospinal fluid (CSF) and finally in blood. Moreover, NFL blood concentration is sensitive to experimental manipulations or targeted therapies of the proteopathic lesions. For these reasons, NFL is the main biomarker to monitor treatment response in pre-clinical research with potential clinical impact. NFL is, indeed, commonly used as biomarker in many disorders such as FA, MS and ALS, where it was found drastically increased and correlates with disease severity and progression[193 194 195]. Furthermore, in ALS also pNFH is a monitored biomarker. pNFH concentration is associated with faster disease progression and bulbar onset[193 194]. Finally, we may also test as biomarker some proteins that emerged from our original OMICS data, such as Lipocalin-2.

VI. Conclusions

With the results collected in this work, we improved the knowledge about ARSACS pathophysiological cascade, that now we can recapitulate as follows (Fig. 1_Conclusion):

1. Mutations in *Sacs* gene are loss-of-function and, when sacsin is mutated and so absent, we observe a series of pathological events. The primary well-studied consequence of sacsin loss is the remodeling of IF cytoskeleton, both in neurons[98] and non-neuronal cells[95 88]. We proved this is an early event appearing just after birth in anterior lobules of *Sacs*$^{-/-}$ cerebellum, the region where we later appreciate PC degeneration. Moreover, we disclosed that accumulation of npNFH in proximal dendrites of PCs cause alterations in organelle trafficking (mitochondria and ER). In particular, organellar defective distribution can be ascribed directly to IF remodeling (likely via plectin and/or myosin Va deificency). Mitochondria morphology and metabolism were instead normal, excluding a direct role of sacsin on mitochondrial physiology;
2. Mitochondrial deficiency in post-synaptic terminals disrupts Ca^{2+} homeostasis. This is highly relevant in PCs that are the biggest neurons in the CNS receiving mainly glutamatergic stimulations, and so they need a precise control of Ca^{2+} concentration. Our data suggest that the huge Ca^{2+} influx into *Sacs*$^{-/-}$ PCs is not properly handled due to missing mitochondrial and ER Ca^{2+} buffering capacity in these cellular districts. This defect, finally, leads to PC degeneration;
3. By targeting Ca^{2+} deregulation with Ceftriaxone treatment we were able to rescue molecular defects and improve ataxic phenotype in *Sacs*$^{-/-}$ mice, providing intriguing perspectives for pharmacological treatment in ARSACS patients;
4. Dissecting deregulated pathways found by comparison of *Sacs*$^{-/-}$ and wild-type cerebellar samples by OMICS approaches, we identified an early and prominent neuroinflammatory response that can concur in the progression of ARSACS pathogenesis. Some of these genes are rescued by Ceftriaxone treatment, opening to the possibility that Ceftriaxone exerts neuroprotection in ARSACS by a dual

mechanism: i.e. by improving synaptic functionality and by tempering neuroinflammation.

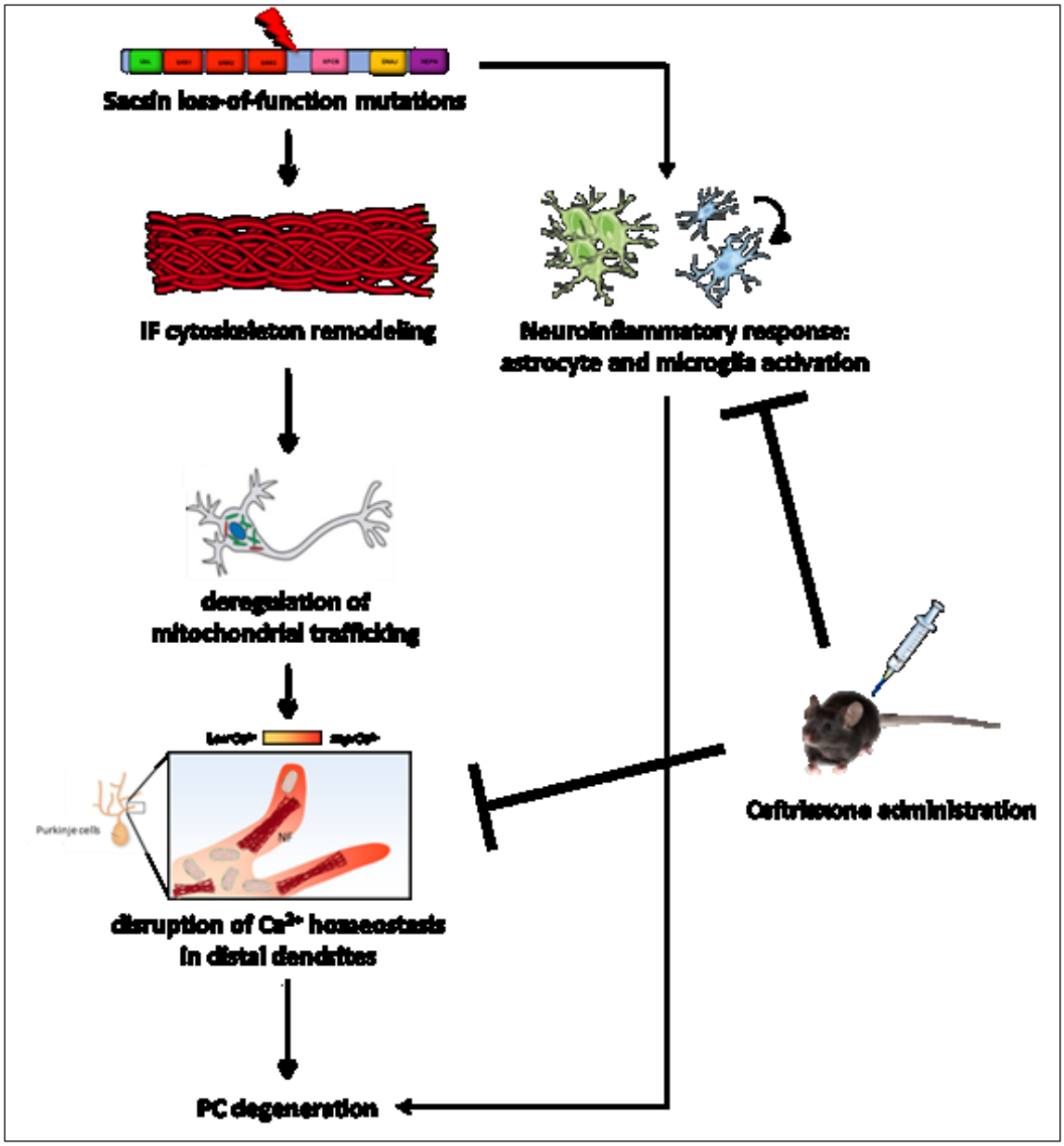

Figure 1_Conclusions. Hypothetical model of ARSACS pathogenesis.

References

1. Haug, H. History of neuromorphometry. *J. Neurosci. Methods* (1986). doi:10.1016/0165-0270(86)90110-X
2. Azevedo, F. A. C. *et al.* Equal numbers of neuronal and nonneuronal cells make the human brain an isometrically scaled-up primate brain. *J. Comp. Neurol.* (2009). doi:10.1002/cne.21974
3. Andrade-Moraes, C. H. *et al.* Cell number changes in Alzheimer's disease relate to dementia, not to plaques and tangles. *Brain* (2013). doi:10.1093/brain/awt273
4. Herculano-Houzel, S. Coordinated scaling of cortical and cerebellar numbers of neurons. *Front. Neuroanat.* **4**, 1–8 (2010).
5. Barton, R. A. & Venditti, C. Rapid evolution of the cerebellum in humans and other great apes. *Curr. Biol.* (2014). doi:10.1016/j.cub.2014.08.056
6. Andersen, B. B., Korbo, L. & Pakkenberg, B. A quantitative study of the human cerebellum with unbiased stereological techniques. *J. Comp. Neurol.* (1992). doi:10.1002/cne.903260405
7. Andersen, K., Andersen, B. B. & Pakkenberg, B. Stereological quantification of the cerebellum in patients with Alzheimer's disease. *Neurobiol. Aging* (2012). doi:10.1016/j.neurobiolaging.2010.06.013
8. von Bartheld, C. S., Bahney, J. & Herculano-Houzel, S. The search for true numbers of neurons and glial cells in the human brain: A review of 150 years of cell counting. *Journal of Comparative Neurology* (2016). doi:10.1002/cne.24040
9. Galliano, E., Mazzarello, P. & D'Angelo, E. Discovery and rediscoveries of Golgi cells. *J. Physiol.* **588**, 3639–3655 (2010).
10. D'Angelo, E. *et al.* The cerebellar network: From structure to function and dynamics. *Brain Research Reviews* (2011). doi:10.1016/j.brainresrev.2010.10.002
11. Kandel, E.; Schwartz, J.; Jessel, T. M., Kandel, E. R. & Kandel, E.; Schwartz, J.; Jessel, T. M. *Principles of Neural Science, Fifth Edition | AccessNeurology | McGraw-Hill Medical*. *Elsevier,* (1991).
12. D'Angelo, E. *Physiology of the cerebellum*. *Handbook of Clinical Neurology* **154**, (Elsevier B.V., 2018).
13. Roostaei, T., Nazeri, A., Sahraian, M. A. & Minagar, A. The human cerebellum: A review of physiologic neuroanatomy. *Neurol. Clin.* **32**, 859–869 (2014).
14. Stoodley, C. J. & Schmahmann, J. D. Functional topography of the human cerebellum. in *Handbook of Clinical Neurology* (2018). doi:10.1016/B978-0-444-63956-1.00004-7
15. Sillitoe, R. V. & Joyner, A. L. Morphology, molecular codes, and circuitry produce the three-dimensional complexity of the cerebellum. *Annual Review of Cell and Developmental Biology* (2007). doi:10.1146/annurev.cellbio.23.090506.123237
16. Voogd, J. & Glickstein, M. The anatomy of the cerebellum. *Trends Neurosci.* (1998). doi:10.1016/S0166-2236(98)01318-6
17. Apps, R. & Garwicz, M. Anatomical and physiological foundations of cerebellar information processing. *Nature Reviews Neuroscience* (2005). doi:10.1038/nrn1646
18. Apps, R. & Hawkes, R. Cerebellar cortical organization: A one-map hypothesis. *Nature Reviews Neuroscience* (2009). doi:10.1038/nrn2698

19. Kano, M., Watanabe, T., Uesaka, N. & Watanabe, M. Multiple Phases of Climbing Fiber Synapse Elimination in the Developing Cerebellum. *Cerebellum* (2018). doi:10.1007/s12311-018-0964-z
20. Sillitoe, R. V. *et al.* Conservation of the architecture of the anterior lobe vermis of the cerebellum across mammalian species. *Progress in Brain Research* (2005). doi:10.1016/S0079-6123(04)48022-4
21. Fine, E. J., Ionita, C. C. & Lohr, L. The history of the development of the cerebellar examination. *Seminars in Neurology* (2002). doi:10.1055/s-2002-36759
22. Buckner, R. L. The cerebellum and cognitive function: 25 years of insight from anatomy and neuroimaging. *Neuron* (2013). doi:10.1016/j.neuron.2013.10.044
23. Schmahmann, J. D. Disorders of the cerebellum: Ataxia, dysmetria of thought, and the cerebellar cognitive affective syndrome. *Journal of Neuropsychiatry and Clinical Neurosciences* (2004). doi:10.1176/jnp.16.3.367
24. Tada, M., Nishizawa, M. & Onodera, O. Redefining cerebellar ataxia in degenerative ataxias: Lessons from recent research on cerebellar systems. *Journal of Neurology, Neurosurgery and Psychiatry* (2015). doi:10.1136/jnnp-2013-307225
25. van de Warrenburg, B. P. C., Steijns, J. A. G., Munneke, M., Kremer, B. P. H. & Bloem, B. R. Falls in degenerative cerebellar ataxias. *Mov. Disord.* (2005). doi:10.1002/mds.20375
26. Fonteyn, E. M. R. *et al.* Falls in spinocerebellar ataxias: Results of the EuroSCA fall study. *Cerebellum* (2010). doi:10.1007/s12311-010-0155-z
27. Sullivan, R., Yau, W. Y., O'Connor, E. & Houlden, H. Spinocerebellar ataxia: an update. *J. Neurol.* (2019). doi:10.1007/s00415-018-9076-4
28. Klockgether, T., Mariotti, C. & Paulson, H. L. Spinocerebellar ataxia. *Nat. Rev. Dis. Prim.* (2019). doi:10.1038/s41572-019-0074-3
29. Soong, B. W. & Morrison, P. J. Spinocerebellar ataxias. in *Handbook of Clinical Neurology* (2018). doi:10.1016/B978-0-444-64189-2.00010-X
30. Mundwiler, A. & Shakkottai, V. G. Autosomal-dominant cerebellar ataxias. in *Handbook of Clinical Neurology* (2018). doi:10.1016/B978-0-444-63233-3.00012-9
31. Beaudin, M. *et al.* The Classification of Autosomal Recessive Cerebellar Ataxias: a Consensus Statement from the Society for Research on the Cerebellum and Ataxias Task Force. *Cerebellum* (2019). doi:10.1007/s12311-019-01052-2
32. Noreau, A., Dupré, N., Bouchard, J. P., Dion, P. A. & Rouleau, G. A. Autosomal recessive cerebellar Ataxias. in *Handbook of the Cerebellum and Cerebellar Disorders* (2013). doi:10.1007/978-94-007-1333-8_100
33. Fogel, B. L. Autosomal-recessive cerebellar ataxias. in *Handbook of Clinical Neurology* (2018). doi:10.1016/B978-0-444-63233-3.00013-0
34. Eidhof, I., Van De Warrenburg, B. P. & Schenck, A. Integrative network and brain expression analysis reveals mechanistic modules in ataxia. *J. Med. Genet.* (2019). doi:10.1136/jmedgenet-2018-105703
35. Bettencourt, C. *et al.* Insights from cerebellar transcriptomic analysis into the pathogenesis of ataxia. *JAMA Neurol.* (2014). doi:10.1001/jamaneurol.2014.756
36. Lim, J. *et al.* A Protein-Protein Interaction Network for Human Inherited Ataxias and Disorders of Purkinje Cell Degeneration. *Cell* (2006). doi:10.1016/j.cell.2006.03.032
37. Meera, P., Pulst, S. M. & Otis, T. S. Cellular and circuit mechanisms underlying spinocerebellar ataxias. *Journal of Physiology* (2016). doi:10.1113/JP271897
38. Person, A. L. & Raman, I. M. Purkinje neuron synchrony elicits time-locked spiking in the cerebellar nuclei. *Nature* (2012). doi:10.1038/nature10732
39. Giorgi, C., Marchi, S. & Pinton, P. The machineries, regulation and cellular functions of mitochondrial calcium. *Nature Reviews Molecular Cell Biology* (2018). doi:10.1038/s41580-018-0052-8

40. Simms, B. A. & Zamponi, G. W. Neuronal voltage-gated calcium channels: Structure, function, and dysfunction. *Neuron* (2014). doi:10.1016/j.neuron.2014.03.016
41. Jeppesen, D. K., Bohr, V. A. & Stevnsner, T. DNA repair deficiency in neurodegeneration. *Progress in Neurobiology* (2011). doi:10.1016/j.pneurobio.2011.04.013
42. Rass, U., Ahel, I. & West, S. C. Defective DNA Repair and Neurodegenerative Disease. *Cell* (2007). doi:10.1016/j.cell.2007.08.043
43. Humbert, S. & Saudou, F. The Ataxia-ome: Connecting Disease Proteins of the Cerebellum. *Cell* (2006). doi:10.1016/j.cell.2006.05.007
44. Nelson, D. L., Orr, H. T. & Warren, S. T. The unstable repeats-Three evolving faces of neurological disease. *Neuron* (2013). doi:10.1016/j.neuron.2013.02.022
45. Synofzik, M. & Németh, A. H. Recessive ataxias. in *Handbook of Clinical Neurology* (2018). doi:10.1016/B978-0-444-64189-2.00005-6
46. Synofzik, M., Puccio, H., Mochel, F. & Schöls, L. Autosomal Recessive Cerebellar Ataxias: Paving the Way toward Targeted Molecular Therapies. *Neuron* (2019). doi:10.1016/j.neuron.2019.01.049
47. Rossi, M. *et al.* The genetic nomenclature of recessive cerebellar ataxias. *Movement Disorders* (2018). doi:10.1002/mds.27415
48. Vernon, H. J. & Bindoff, L. A. Mitochondrial ataxias. in *Handbook of Clinical Neurology* (2018). doi:10.1016/B978-0-444-64189-2.00009-3
49. Dodge, J. C. Lipid involvement in neurodegenerative diseases of the motor system: Insights from lysosomal storage diseases. *Frontiers in Molecular Neuroscience* (2017). doi:10.3389/fnmol.2017.00356
50. Shimobayashi, E. & Kapfhammer, J. P. Calcium Signaling, PKC Gamma, IP3R1 and CAR8 Link Spinocerebellar Ataxias and Purkinje Cell Dendritic Development. *Curr. Neuropharmacol.* (2017). doi:10.2174/1570159x15666170529104000
51. Kasumu, A. & Bezprozvanny, I. Deranged calcium signaling in purkinje cells and pathogenesis in spinocerebellar ataxia 2 (SCA2) and other ataxias. *Cerebellum* (2012). doi:10.1007/s12311-010-0182-9
52. Ureshino, R. P. *et al.* The interplay between ca2+ signaling pathways and neurodegeneration. *International Journal of Molecular Sciences* (2019). doi:10.3390/ijms20236004
53. Hajnóczky, G., Robb-Gaspers, L. D., Seitz, M. B. & Thomas, A. P. Decoding of cytosolic calcium oscillations in the mitochondria. *Cell* (1995). doi:10.1016/0092-8674(95)90430-1
54. Rizzuto, R., De Stefani, D., Raffaello, A. & Mammucari, C. Mitochondria as sensors and regulators of calcium signalling. *Nature Reviews Molecular Cell Biology* (2012). doi:10.1038/nrm3412
55. Greer, P. L. & Greenberg, M. E. From Synapse to Nucleus: Calcium-Dependent Gene Transcription in the Control of Synapse Development and Function. *Neuron* (2008). doi:10.1016/j.neuron.2008.09.002
56. Neher, E. & Sakaba, T. Multiple Roles of Calcium Ions in the Regulation of Neurotransmitter Release. *Neuron* (2008). doi:10.1016/j.neuron.2008.08.019
57. Mark, M. D., Schwitalla, J. C., Groemmke, M. & Herlitze, S. Keeping Our Calcium in Balance to Maintain Our Balance. *Biochemical and Biophysical Research Communications* (2017). doi:10.1016/j.bbrc.2016.07.020
58. Bezprozvanny, I. Calcium signaling and neurodegenerative diseases. *Trends Mol. Med.* (2009). doi:10.1016/j.molmed.2009.01.001
59. Prestori, F., Moccia, F. & D'angelo, E. Disrupted calcium signaling in animal models of human spinocerebellar ataxia (SCA). *International Journal of Molecular Sciences* (2020). doi:10.3390/ijms21010216

60. Berridge, M. J., Bootman, M. D. & Roderick, H. L. Calcium signalling: Dynamics, homeostasis and remodelling. *Nature Reviews Molecular Cell Biology* (2003). doi:10.1038/nrm1155
61. MacAskill, A. F. *et al.* Miro1 Is a Calcium Sensor for Glutamate Receptor-Dependent Localization of Mitochondria at Synapses. *Neuron* (2009). doi:10.1016/j.neuron.2009.01.030
62. Chang, K. T., Niescier, R. F. & Min, K. T. Mitochondrial matrix Ca 2+ as an intrinsic signal regulating mitochondrial motility in axons. *Proc. Natl. Acad. Sci. U. S. A.* (2011). doi:10.1073/pnas.1106862108
63. Kang, J. S. *et al.* Docking of Axonal Mitochondria by Syntaphilin Controls Their Mobility and Affects Short-Term Facilitation. *Cell* (2008). doi:10.1016/j.cell.2007.11.024
64. Sheng, Z. H. & Cai, Q. Mitochondrial transport in neurons: Impact on synaptic homeostasis and neurodegeneration. *Nature Reviews Neuroscience* (2012). doi:10.1038/nrn3156
65. Patron, M., Sprenger, H. G. & Langer, T. M-AAA proteases, mitochondrial calcium homeostasis and neurodegeneration. *Cell Research* (2018). doi:10.1038/cr.2018.17
66. Maltecca, F. *et al.* Purkinje neuron Ca2+ influx reduction rescues ataxia in SCA28 model. *J. Clin. Invest.* (2015). doi:10.1172/JCI74770
67. Tulli, S. *et al.* Pathogenic variants in the AFG3L2 proteolytic domain cause SCA28 through haploinsufficiency and proteostatic stress-driven OMA1 activation. *J. Med. Genet.* (2019). doi:10.1136/jmedgenet-2018-105766
68. Maltecca, F. *et al.* Haploinsufficiency of AFG3L2, the gene responsible for spinocerebellar ataxia type 28, causes mitochondria-mediated Purkinje cell dark degeneration. *J. Neurosci.* (2009). doi:10.1523/JNEUROSCI.1532-09.2009
69. Engert, J. C. *et al.* ARSACS, a spastic ataxia common in northeastern Quebec, is caused by mutations in a new gene encoding an 11.5-kb ORF. *Nat. Genet.* (2000). doi:10.1038/72769
70. Bouhlal, Y., Amouri, R., El Euch-Fayeche, G. & Hentati, F. Autosomal recessive spastic ataxia of Charlevoix-Saguenay: An overview. *Parkinsonism and Related Disorders* (2011). doi:10.1016/j.parkreldis.2011.03.005
71. Bouchard, J. P., Barbeau, A., Bouchard, R. & Bouchard, R. W. Electromyography and Nerve Conduction Studies in Friedreich's Ataxia and Autosomal Recessive Spastic Ataxia of Charlevoix-Saguenay (ARSACS). *Can. J. Neurol. Sci. / J. Can. des Sci. Neurol.* (1979). doi:10.1017/S0317167100119614
72. Synofzik, M. *et al.* Autosomal recessive spastic ataxia of Charlevoix Saguenay (ARSACS): Expanding the genetic, clinical and imaging spectrum. *Orphanet J. Rare Dis.* (2013). doi:10.1186/1750-1172-8-41
73. Xiromerisiou, G. *et al.* A novel homozygous SACS mutation identified by whole exome sequencing-genotype phenotype correlations of all published cases. *J. Mol. Neurosci.* (2020). doi:10.1007/s12031-019-01410-z
74. Romano, A. *et al.* Comparative Analysis and Functional Mapping of SACS Mutations Reveal Novel Insights into Sacsin Repeated Architecture. *Hum. Mutat.* (2013). doi:10.1002/humu.22269
75. Baets, J. *et al.* Mutations in SACS cause atypical and late-onset forms of ARSACS. *Neurology* (2010). doi:10.1212/WNL.0b013e3181f4d86c
76. Parkinson, M. H. *et al.* Optical coherence tomography in autosomal recessive spastic ataxia of charlevoix-Saguenay. *Brain* (2018). doi:10.1093/brain/awy028
77. van Lint, M., Hoornaert, K. & ten Tusscher, M. P. M. Retinal nerve fiber layer thickening in ARSACS carriers. *J. Neurol. Sci.* (2016). doi:10.1016/j.jns.2016.09.023
78. Ricca, I. *et al.* Clinical and molecular studies in two new cases of ARSACS. *Neurogenetics*

(2019). doi:10.1007/s10048-019-00564-7
79. Borruat, F. X., Holder, G. E. & Bremner, F. Inner retinal dysfunction in the autosomal recessive spastic ataxia of Charlevoix-Saguenay. *Front. Neurol.* (2017). doi:10.3389/fneur.2017.00523
80. Desserre, J. *et al.* Thickening of peripapillar retinal fibers for the diagnosis of autosomal recessive spastic ataxia of Charlevoix-Saguenay. *Cerebellum* (2011). doi:10.1007/s12311-011-0286-x
81. Nethisinghe, S. *et al.* Retinal imaging in autosomal recessive spastic ataxia of charlevoix-saguenay. *Neuro-Ophthalmology* (2011). doi:10.3109/01658107.2011.595043
82. Pablo, L. E. *et al.* Retinal nerve fiber hypertrophy in ataxia of Charlevoix-Saguenay patients. *Mol. Vis.* (2011).
83. Vingolo, E. M. *et al.* Myelinated retinal fibers in autosomal recessive spastic ataxia of Charlevoix-Saguenay. *Eur. J. Neurol.* (2011). doi:10.1111/j.1468-1331.2010.03335.x
84. Garcia-Martin, E. *et al.* Retinal segmentation as noninvasive technique to demonstrate hyperplasia in ataxia of Charlevoix-Saguenay. *Invest. Ophthalmol. Vis. Sci.* (2013). doi:10.1167/iovs.13-12726
85. Yu-Wai-Man, P. *et al.* Abnormal retinal thickening is a common feature among patients with ARSACS-related phenotypes. *British Journal of Ophthalmology* (2014). doi:10.1136/bjophthalmol-2013-304534
86. Silvestri, G., Masciullo, M. & Santorelli, F. M. Autosomal recessive spastic ataxia of Charlevoix-Saguenay in the time of next-generation sequencing. *Archives of Neurology* (2012). doi:10.1001/2013.jamaneurol.70
87. Parfitt, D. A. *et al.* The ataxia protein sacsin is a functional co-chaperone that protects against polyglutamine-expanded ataxin-1. *Hum. Mol. Genet.* (2009). doi:10.1093/hmg/ddp067
88. Gentil, B. J. *et al.* Sacsin, mutated in the ataxia ARSACS, regulates intermediate filament assembly and dynamics. *FASEB J.* (2019). doi:10.1096/fj.201801556R
89. Larivière, R. *et al.* Sacs R272C missense homozygous mice develop an ataxia phenotype. *Mol. Brain* (2019). doi:10.1186/s13041-019-0438-3
90. Girard, M. *et al.* Mitochondrial dysfunction and Purkinje cell loss in autosomal recessive spastic ataxia of Charlevoix-Saguenay (ARSACS). *Proc. Natl. Acad. Sci. U. S. A.* (2012). doi:10.1073/pnas.1113166109
91. Tilokani, L., Nagashima, S., Paupe, V. & Prudent, J. Mitochondrial dynamics: Overview of molecular mechanisms. *Essays in Biochemistry* (2018). doi:10.1042/EBC20170104
92. Anderson, J. F., Siller, E. & Barral, J. M. The Sacsin Repeating Region (SRR): A Novel Hsp90-Related Supra-Domain Associated with Neurodegeneration. *J. Mol. Biol.* **400**, 665–674 (2010).
93. Kamionka, M. & Feigon, J. Structure of the XPC binding domain of hHR23A reveals hydrophobic patches for protein interaction. *Protein Sci.* (2004). doi:10.1110/ps.04824304
94. Grynberg, M., Erlandsen, H. & Godzik, A. HEPN: A common domain in bacterial drug resistance and human neurodegenerative proteins. *Trends in Biochemical Sciences* (2003). doi:10.1016/S0968-0004(03)00060-4
95. Duncan, E. J. *et al.* Altered organization of the intermediate filament cytoskeleton and relocalization of proteostasis modulators in cells lacking the ataxia protein sacsin. *Hum. Mol. Genet.* (2017). doi:10.1093/hmg/ddx197
96. Bradshaw, T. Y. *et al.* A reduction in Drp1-mediated fission compromises mitochondrial health in autosomal recessive spastic ataxia of Charlevoix Saguenay. *Hum. Mol. Genet.* (2016). doi:10.1093/hmg/ddw173
97. Chen, H. & Chan, D. C. Mitochondrial dynamics-fusion, fission, movement, and

mitophagy-in neurodegenerative diseases. *Hum. Mol. Genet.* (2009). doi:10.1093/hmg/ddp326
98. Larivière, R. *et al.* Sacs knockout mice present pathophysiological defects underlying autosomal recessive spastic ataxia of charlevoix-saguenay. *Hum. Mol. Genet.* (2015). doi:10.1093/hmg/ddu491
99. Lowery, J., Kuczmarski, E. R., Herrmann, H. & Goldma, R. D. Intermediate filaments play a pivotal role in regulating cell architecture and function. *J. Biol. Chem.* (2015). doi:10.1074/jbc.R115.640359
100. Ady, V. *et al.* Altered synaptic and firing properties of cerebellar Purkinje cells in a mouse model of ARSACS. *J. Physiol.* (2018). doi:10.1113/JP275902
101. Thiffault, I. *et al.* Diversity of ARSACS mutations in french-canadians. *Can. J. Neurol. Sci.* (2013). doi:10.1017/S0317167100012968
102. Brooks, S. P. & Dunnett, S. B. Tests to assess motor phenotype in mice: A user's guide. *Nat. Rev. Neurosci.* **10**, 519–529 (2009).
103. Valenza, M. *et al.* Disruption of astrocyte-neuron cholesterol cross talk affects neuronal function in Huntington's disease. *Cell Death Differ.* (2015). doi:10.1038/cdd.2014.162
104. Cox, J. *et al.* Accurate proteome-wide label-free quantification by delayed normalization and maximal peptide ratio extraction, termed MaxLFQ. *Mol. Cell. Proteomics* **13**, 2513–2526 (2014).
105. Raudvere, U. *et al.* G:Profiler: A web server for functional enrichment analysis and conversions of gene lists (2019 update). *Nucleic Acids Res.* (2019). doi:10.1093/nar/gkz369
106. Tabata, T. *et al.* A reliable method for culture of dissociated mouse cerebellar cells enriched for Purkinje neurons. *J. Neurosci. Methods* (2000). doi:10.1016/S0165-0270(00)00323-X
107. Codazzi, F. *et al.* Synergistic control of protein kinase Cγ activity by ionotropic and metabotropic glutamate receptor inputs in hippocampal neurons. *J. Neurosci.* (2006). doi:10.1523/JNEUROSCI.0478-06.2006
108. Maltecca, F. *et al.* The mitochondrial protease AFG3L2 is essential for axonal development. *J. Neurosci.* (2008). doi:10.1523/JNEUROSCI.4677-07.2008
109. Al-Chalabi, A. & Miller, C. C. J. Neurofilaments and neurological disease. *BioEssays* (2003). doi:10.1002/bies.10251
110. Perrot, R., Berges, R., Bocquet, A. & Eyer, J. Review of the multiple aspects of neurofilament functions, and their possible contribution to neurodegeneration. *Molecular Neurobiology* (2008). doi:10.1007/s12035-008-8033-0
111. Yuan, A., Rao, M. V., Veeranna & Nixon, R. A. Neurofilaments and neurofilament proteins in health and disease. *Cold Spring Harb. Perspect. Biol.* (2017). doi:10.1101/cshperspect.a018309
112. Holmgren, A., Bouhy, D. & Timmerman, V. Neurofilament phosphorylation and their proline-directed kinases in health and disease. *Journal of the Peripheral Nervous System* (2012). doi:10.1111/j.1529-8027.2012.00434.x
113. Shea, T. B. & Chan, W. K. H. Regulation of neurofilament dynamics by phosphorylation. *European Journal of Neuroscience* (2008). doi:10.1111/j.1460-9568.2008.06165.x
114. Agholme, L., Lindström, T., Kgedal, K., Marcusson, J. & Hallbeck, M. An in vitro model for neuroscience: Differentiation of SH-SY5Y cells into cells with morphological and biochemical characteristics of mature neurons. *J. Alzheimer's Dis.* (2010). doi:10.3233/JAD-2010-091363
115. Coulombe, P. A., Ma, L., Yamada, S. & Wawersik, M. Intermediate filaments at a glance. *J. Cell Sci.* (2001).
116. Wagner, O. I. *et al.* Mechanisms of mitochondria-neurofilament interactions. *J.*

Neurosci. (2003). doi:10.1523/jneurosci.23-27-09046.2003
117. Straube-West, K., Loomis, P. A., Opal, P. & Goldman, R. D. Alterations in neural intermediate filament organization: Functional implications and the induction of pathological changes related to motor neuron disease. *J. Cell Sci.* (1996).
118. Itoh, K., Nakamura, K., Iijima, M. & Sesaki, H. Mitochondrial dynamics in neurodegeneration. *Trends in Cell Biology* (2013). doi:10.1016/j.tcb.2012.10.006
119. Barnhart, E. L. Mechanics of mitochondrial motility in neurons. *Current Opinion in Cell Biology* (2016). doi:10.1016/j.ceb.2016.02.022
120. Wiche, G. Role of plectin in cytoskeleton organization and dynamics. *Journal of Cell Science* (1998).
121. Winter, L., Abrahamsberg, C. & Wiche, G. Plectin isoform 1b mediates mitochondrion - Intermediate filament network linkage and controls organelle shape. *J. Cell Biol.* (2008). doi:10.1083/jcb.200710151
122. Valencia, R. G. *et al.* Plectin dysfunction in neurons leads to tau accumulation on microtubules affecting neuritogenesis, organelle trafficking, pain sensitivity and memory. *Neuropathol. Appl. Neurobiol.* (2020). doi:10.1111/nan.12635
123. Wagner, W., Brenowitz, S. D. & Hammer, J. A. Myosin-Va transports the endoplasmic reticulum into the dendritic spines of Purkinje neurons. *Nat. Cell Biol.* (2011). doi:10.1038/ncb2132
124. Berridge, M. J. Dysregulation of neural calcium signaling in Alzheimer disease, bipolar disorder and schizophrenia. in *Prion* (2013). doi:10.4161/pri.21767
125. Tong, B. C. K., Wu, A. J., Li, M. & Cheung, K. H. Calcium signaling in Alzheimer's disease & therapies. *Biochimica et Biophysica Acta - Molecular Cell Research* (2018). doi:10.1016/j.bbamcr.2018.07.018
126. Duchen, M. R. Mitochondria, calcium-dependent neuronal death and neurodegenerative disease. *Pflugers Archiv European Journal of Physiology* (2012). doi:10.1007/s00424-012-1112-0
127. Hartmann, J. & Konnerth, A. Determinants of postsynaptic Ca2+ signaling in Purkinje neurons. *Cell Calcium* (2005). doi:10.1016/j.ceca.2005.01.014
128. Merrill, M. A., Chen, Y., Strack, S. & Hell, J. W. Activity-driven postsynaptic translocation of CaMKII. *Trends in Pharmacological Sciences* (2005). doi:10.1016/j.tips.2005.10.003
129. Strack, S. & Hell, J. W. Postsynaptic targeting of protein kinases and phosphatases. in *Structural And Functional Organization Of The Synapse* (2008). doi:10.1007/978-0-387-77232-5_16
130. Feng, B., Raghavachari, S. & Lisman, J. Quantitative estimates of the cytoplasmic, PSD, and NMDAR-bound pools of CaMKII in dendritic spines. *Brain Res.* (2011). doi:10.1016/j.brainres.2011.08.051
131. Hudmon, A. & Schulman, H. Structure-function of the multifunctional Ca 2+ /calmodulin-dependent protein kinase II. *Biochemical Journal* (2002). doi:10.1042/BJ20020228
132. Hudmon, A. & Schulman, H. Neuronal Ca2+/calmodulin-dependent protein kinase II: The role of structure and autoregulation in cellular function. *Annual Review of Biochemistry* (2002). doi:10.1146/annurev.biochem.71.110601.135410
133. Hell, J. W. CaMKII: Claiming center stage in postsynaptic function and organization. *Neuron* (2014). doi:10.1016/j.neuron.2013.12.024
134. Kim, K. *et al.* A Temporary Gating of Actin Remodeling during Synaptic Plasticity Consists of the Interplay between the Kinase and Structural Functions of CaMKII. *Neuron* (2015). doi:10.1016/j.neuron.2015.07.023
135. Wang, Q. *et al.* Assemblies of calcium/calmodulin-dependent kinase II with actin and their dynamic regulation by calmodulin in dendritic spines. *Proc. Natl. Acad. Sci. U. S. A.*

(2019). doi:10.1073/pnas.1911452116
136. Banerjee, S. & Hasan, G. The InsP3 receptor: Its role in neuronal physiology and neurodegeneration. *BioEssays* (2005). doi:10.1002/bies.20298
137. Foskett, J. K., White, C., Cheung, K. H. & Mak, D. O. D. Inositol trisphosphate receptor Ca2+ release channels. *Physiological Reviews* (2007). doi:10.1152/physrev.00035.2006
138. Egorova, P. A. & Bezprozvanny, I. B. Inositol 1,4,5-trisphosphate receptors and neurodegenerative disorders. *FEBS Journal* (2018). doi:10.1111/febs.14366
139. Ivanova, H. *et al.* Inositol 1,4,5-trisphosphate receptor-isoform diversity in cell death and survival. *Biochimica et Biophysica Acta - Molecular Cell Research* (2014). doi:10.1016/j.bbamcr.2014.03.007
140. Miller, S. G. & Kennedy, M. B. Distinct forebrain and cerebellar isozymes of type II Ca2+/calmodulin-dependent protein kinase associate differently with the postsynaptic density fraction. *J. Biol. Chem.* (1985). doi:10.1016/s0021-9258(17)39454-1
141. Yim, A. *et al.* MitoXplorer, a visual data mining platform to systematically analyze and visualize mitochondrial expression dynamics and mutations. *Nucleic Acids Res.* (2020). doi:10.1093/nar/gkz1128
142. Yimer, E. M., Hishe, H. Z. & Tuem, K. B. Repurposing of the β-lactam antibiotic, ceftriaxone for neurological disorders: A review. *Frontiers in Neuroscience* (2019). doi:10.3389/fnins.2019.00236
143. Tai, C. H. *et al.* A new avenue for treating neuronal diseases: Ceftriaxone, an old antibiotic demonstrating behavioral neuronal effects. *Behavioural Brain Research* (2019). doi:10.1016/j.bbr.2019.02.020
144. Rothstein, J. D. *et al.* β-Lactam antibiotics offer neuroprotection by increasing glutamate transporter expression. *Nature* (2005). doi:10.1038/nature03180
145. Lewerenz, J. *et al.* Induction of Nrf2 and xCT are involved in the action of the neuroprotective antibiotic ceftriaxone in vitro. *J. Neurochem.* (2009). doi:10.1111/j.1471-4159.2009.06347.x
146. Nizzardo, M. *et al.* Beta-lactam antibiotic offers neuroprotection in a spinal muscular atrophy model by multiple mechanisms. *Exp. Neurol.* (2011). doi:10.1016/j.expneurol.2011.01.017
147. Lee, S. G. *et al.* Mechanism of ceftriaxone induction of excitatory amino acid transporter-2 expression and glutamate uptake in primary human astrocytes. *J. Biol. Chem.* (2008). doi:10.1074/jbc.M707697200
148. Karin, M. Nuclear factor-κB in cancer development and progression. *Nature* (2006). doi:10.1038/nature04870
149. Sitcheran, R., Gupta, P., Fisher, P. B. & Baldwin, A. S. Positive and negative regulation of EAAT2 by NF-κB: A role for N-myc in TNFα-controlled repression. *EMBO J.* (2005). doi:10.1038/sj.emboj.7600555
150. Sicot, G. *et al.* Downregulation of the Glial GLT1 Glutamate Transporter and Purkinje Cell Dysfunction in a Mouse Model of Myotonic Dystrophy. *Cell Rep.* (2017). doi:10.1016/j.celrep.2017.06.006
151. Jha, M. K. *et al.* Diverse functional roles of lipocalin-2 in the central nervous system. *Neuroscience and Biobehavioral Reviews* (2015). doi:10.1016/j.neubiorev.2014.12.006
152. Weber, A. N. R. *et al.* Recent insights into the regulatory networks of NLRP3 inflammasome activation. *Journal of cell science* (2020). doi:10.1242/jcs.248344
153. Veerhuis, R., Nielsen, H. M. & Tenner, A. J. Complement in the brain. *Molecular Immunology* (2011). doi:10.1016/j.molimm.2011.04.003
154. Song, W. M. & Colonna, M. The identity and function of microglia in neurodegeneration. *Nature Immunology* (2018). doi:10.1038/s41590-018-0212-1
155. Subhramanyam, C. S., Wang, C., Hu, Q. & Dheen, S. T. Microglia-mediated

neuroinflammation in neurodegenerative diseases. *Seminars in Cell and Developmental Biology* (2019). doi:10.1016/j.semcdb.2019.05.004
156. Kyritsis, N., Kizil, C. & Brand, M. Neuroinflammation and central nervous system regeneration in vertebrates. *Trends in Cell Biology* (2014). doi:10.1016/j.tcb.2013.08.004
157. Yang, Q. qiao & Zhou, J. wei. Neuroinflammation in the central nervous system: Symphony of glial cells. *GLIA* (2019). doi:10.1002/glia.23571
158. Lian, H. *et al.* Astrocyte-microglia cross talk through complement activation modulates amyloid pathology in mouse models of alzheimer's disease. *J. Neurosci.* (2016). doi:10.1523/JNEUROSCI.2117-15.2016
159. Zhang, K. *et al.* Complement and microglia mediate early synapse loss in Alzheimer mouse models. *Science (80-.).* (2016).
160. Vasek, M. J. *et al.* A complement-microglial axis drives synapse loss during virus-induced memory impairment. *Nature* (2016). doi:10.1038/nature18283
161. Litvinchuk, A. *et al.* Complement C3aR Inactivation Attenuates Tau Pathology and Reverses an Immune Network Deregulated in Tauopathy Models and Alzheimer's Disease. *Neuron* (2018). doi:10.1016/j.neuron.2018.10.031
162. Dejanovic, B. *et al.* Changes in the Synaptic Proteome in Tauopathy and Rescue of Tau-Induced Synapse Loss by C1q Antibodies. *Neuron* (2018). doi:10.1016/j.neuron.2018.10.014
163. Hong, S. *et al.* Complement and microglia mediate early synapse loss in Alzheimer mouse models. *Science (80-.).* (2016). doi:10.1126/science.aad8373
164. Krasemann, S. *et al.* The TREM2-APOE Pathway Drives the Transcriptional Phenotype of Dysfunctional Microglia in Neurodegenerative Diseases. *Immunity* (2017). doi:10.1016/j.immuni.2017.08.008
165. Keren-Shaul, H. *et al.* A Unique Microglia Type Associated with Restricting Development of Alzheimer's Disease. *Cell* (2017). doi:10.1016/j.cell.2017.05.018
166. Sawada, K. *et al.* Striking pattern of Purkinje cell loss in cerebellum of an ataxic mutant mouse, tottering. *Acta Neurobiol. Exp. (Wars).* (2009).
167. Sarna, J. R. & Hawkes, R. Patterned Purkinje cell loss in the ataxic sticky mouse. *Eur. J. Neurosci.* (2011). doi:10.1111/j.1460-9568.2011.07725.x
168. White, J. J. & Sillitoe, R. V. Postnatal development of cerebellar zones revealed by neurofilament heavy chain protein expression. *Front. Neuroanat.* (2013). doi:10.3389/fnana.2013.00009
169. Demilly, A., Reeber, S. L., Gebre, S. A. & Sillitoe, R. V. Neurofilament heavy chain expression reveals a unique parasagittal stripe topography in the mouse cerebellum. *Cerebellum* (2011). doi:10.1007/s12311-010-0156-y
170. Schwarz, T. L. Mitochondrial trafficking in neurons. *Cold Spring Harb. Perspect. Biol.* (2013). doi:10.1101/cshperspect.a011304
171. Brown, A. Contiguous phosphorylated and non-phosphorylated domains along axonal neurofilaments. *J. Cell Sci.* (1998).
172. Gotow, T. & Tanaka, J. Phosphorylation of neurofilament H subunit as related to arrangement of neurofilaments. *J. Neurosci. Res.* (1994). doi:10.1002/jnr.490370604
173. Winter, L. & Wiche, G. The many faces of plectin and plectinopathies: Pathology and mechanisms. *Acta Neuropathologica* (2013). doi:10.1007/s00401-012-1026-0
174. Winter, L. *et al.* Plectin isoform P1b and P1d deficiencies differentially affect mitochondrial morphology and function in skeletal muscle. *Hum. Mol. Genet.* (2015). doi:10.1093/hmg/ddv184
175. Hammer, J. A. & Wagner, W. Functions of class v myosins in neurons. *Journal of Biological Chemistry* (2013). doi:10.1074/jbc.R113.514497

176. Miyata, M. *et al.* Local calcium release in dendritic spines required for long-term synaptic depression. *Neuron* (2000). doi:10.1016/S0896-6273(00)00099-4
177. Moore, K. J. *et al.* Dilute suppressor dsu acts semidominantly to suppress the coat color phenotype of a deletion mutation, d(l20J), of the murine dilute locus. *Proc. Natl. Acad. Sci. U. S. A.* (1988). doi:10.1073/pnas.85.21.8131
178. Takagishi, Y. *et al.* The dilute-lethal (d(l)) gene attacks a Ca2+ store in the dendritic spine of Purkinje cells in mice. *Neurosci. Lett.* (1996). doi:10.1016/0304-3940(96)12967-0
179. Rao, M. V. *et al.* Myosin Va binding to neurofilaments is essential for correct myosin Va distribution and transport and neurofilament density. *J. Cell Biol.* (2002). doi:10.1083/jcb.200205062
180. Sugawara, T. *et al.* Type 1 inositol trisphosphate receptor regulates cerebellar circuits by maintaining the spine morphology of purkinje cells in adult mice. *J. Neurosci.* (2013). doi:10.1523/JNEUROSCI.0545-13.2013
181. Hisatsune, C., Hamada, K. & Mikoshiba, K. Ca 2+ signaling and spinocerebellar ataxia. *Biochimica et Biophysica Acta - Molecular Cell Research* (2018). doi:10.1016/j.bbamcr.2018.05.009
182. Alba, A. *et al.* Deficient cerebellar long-term depression and impaired motor learning in mGluR1 mutant mice. *Cell* (1994). doi:10.1016/0092-8674(94)90205-4
183. Bachetti, T. *et al.* In vitro treatments with ceftriaxone promote elimination of mutant glial fibrillary acidic protein and transcription down-regulation. *Exp. Cell Res.* (2010). doi:10.1016/j.yexcr.2010.05.005
184. Ho, Y. J. *et al.* Use of ceftriaxone in treating cognitive and neuronal deficits associated with dementia with lewy bodies. *Front. Neurosci.* (2019). doi:10.3389/fnins.2019.00507
185. Cudkowicz, M. E. *et al.* Safety and efficacy of ceftriaxone for amyotrophic lateral sclerosis: A multi-stage, randomised, double-blind, placebo-controlled trial. *Lancet Neurol.* (2014). doi:10.1016/S1474-4422(14)70222-4
186. Song, J. & Kim, O. Y. Perspectives in Lipocalin-2: Emerging Biomarker for Medical Diagnosis and Prognosis for Alzheimer's Disease. *Clin. Nutr. Res.* (2018). doi:10.7762/cnr.2018.7.1.1
187. Baltimore, D. NF-κB is 25. *Nature Immunology* (2011). doi:10.1038/ni.2072
188. Lian, H. *et al.* NFκB-Activated Astroglial Release of Complement C3 Compromises Neuronal Morphology and Function Associated with Alzheimer's Disease. *Neuron* (2015). doi:10.1016/j.neuron.2014.11.018
189. Mattson, M. P. & Meffert, M. K. Roles for NF-κB in nerve cell survival, plasticity, and disease. *Cell Death and Differentiation* (2006). doi:10.1038/sj.cdd.4401837
190. Hsiao, H. Y., Chen, Y. C., Chen, H. M., Tu, P. H. & Chern, Y. A critical role of astrocyte-mediated nuclear factor-κB-dependent inflammation in huntington's disease. *Hum. Mol. Genet.* (2013). doi:10.1093/hmg/ddt036
191. Pizzi, M. & Spano, P. F. Distinct roles of diverse nuclear factor-κB complexes in neuropathological mechanisms. *European Journal of Pharmacology* (2006). doi:10.1016/j.ejphar.2006.06.027
192. Bacioglu, M. *et al.* Neurofilament Light Chain in Blood and CSF as Marker of Disease Progression in Mouse Models and in Neurodegenerative Diseases. *Neuron* (2016). doi:10.1016/j.neuron.2016.05.018
193. Khalil, M. *et al.* Neurofilaments as biomarkers in neurological disorders. *Nature Reviews Neurology* (2018). doi:10.1038/s41582-018-0058-z
194. Boylan, K. B. *et al.* Phosphorylated neurofilament heavy subunit (pNF-H) in peripheral blood and CSF as a potential prognostic biomarker in Amyotrophic Lateral Sclerosis. *J. Neurol. Neurosurg. Psychiatry* (2013). doi:10.1136/jnnp-2012-303768

195. Zetterberg, H. & Blennow, K. From Cerebrospinal Fluid to Blood: The Third Wave of Fluid Biomarkers for Alzheimer's Disease. *Journal of Alzheimer's Disease* (2018). doi:10.3233/JAD-179926

Appendix

Publications

- *U-fibers leukoencephalopathy due to a novel mutation in TACO1 gene.*
  Sferruzza G, **Del Bondio A**, Citterio A, Vezzulli P, Guerrieri S, Radaelli M, Martinelli Boneschi F, Filippi M, Maltecca F, Bassi MT, Scarlato M.
  Neurology Genetics, in press

- *The WRB subunit of the Get3 receptor is required for the correct integration of its partner CAML into the ER.*
  Carvalho HJF, **Del Bondio A**, Maltecca F, Colombo SF, Borgese N.Sci Rep. 2019 Aug 15;9(1):11887. doi: 10.1038/s41598-019-48363-2.PMID: 31417168

- *Pathogenic variants in the AFG3L2 proteolytic domain cause SCA28 through haploinsufficiency and proteostatic stress-driven OMA1 activation.*
  Tulli S, **Del Bondio A** (co-first author), Baderna V, Mazza D, Codazzi F, Pierson TM, Ambrosi A, Nolte D, Goizet C, Toro C, Baets J, Deconinck T, DeJonghe P, Mandich P, Casari G, Maltecca F.
  J Med Genet. 2019 Aug;56(8):499-511. doi: 10.1136/jmedgenet-2018-105766. Epub 2019 Mar 25.PMID: 30910913